QCD analysis of deep inelastic lepton-hadron scattering in the region of small values of the bjorken parameter x

Staśto, Anna

QCD analysis of deep inelastic lepton-hadron scattering in the region of small values of the Bjorken parameter x

A thesis presented for the degree of
Doctor of Philosophy
by

Anna Staśto

H. Niewodniczański Institute of Nuclear Physics
Kraków
June 1999

Abstract

We present the new framework based on BFKL and DGLAP evolution equations in which the leading $\ln(Q^2)$ and $\ln(1/x)$ terms are treated on equal footing. We introduce a pair of coupled integro-differential equations for the quark singlet and the unintegrated gluon distribution. The observable structure functions are calculated using high energy factorisation approach. We also include the sub-leading $\ln(1/x)$ effects via consistency constraint. We argue that the use of this constraint leads to more stable solution to the Pomeron intercept than that based on the NLO calculation of the BFKL equation alone and generates resummation to all orders of the major part of the subleading $\ln(1/x)$ effects. The global fit to all available deep inelastic data is performed using a simple parametrisation of the non-perturbative region. We also present the results for the longitudinal structure function and the charm component of the F_2 structure function.

Next, we extend this approach to the low Q^2 domain. At small distances we use the perturbative approach based on the unified BFKL/DGLAP equations and for large distances we use Vector Meson Dominance Model and, for the higher mass $q\bar{q}$ states, the additive quark approach. We show the results for the total cross section and for the ratio of the longitudinal and transverse structure functions.

Finally, we calculate the dijet production and consider the decorrelation effects in the azimuthal distributions caused by the diffusion in the transverse momentum k_T of the exchanged gluon. Using the gluon distribution which is fixed by the fit to the DIS data we are able to make absolute predictions. We show the results for the $dF_T/d\phi$, the total cross section and also the distributions in Q^2 as well as in the longitudinal momentum fraction of the gluon. Our theoretical predictions are confronted with the measurements made using ZEUS detector at HERA.

Declaration

I declare that no material in this thesis has previously been submitted for a degree at this or any other institution.

The work in this thesis has been carried out in collaboration with Professors J. Kwieciński, A.D. Martin and M.G. Ryskin. The material in chapter 1 is meant to be introductory and is not original. The contents of chapters 2, 3 and 4 are based on the following publications:

- "A UNIFIED BFKL AND GLAP DESCRIPTION OF F_2 DATA",
  J. Kwieciński, A.D. Martin and A.M. Staśto, *Phys. Rev.* **D56** (1997) 3991.
- "A UNIFIED BFKL AND DGLAP EVOLUTION EQUATIONS" FOR QUARKS AND GLUONS",
  J. Kwieciński, A.D. Martin and A.M. Staśto,
  Acta Physica Polonica B, vol. 28, (1997), 2577.
- "THE DESCRIPTION OF F_2 AT LOW Q^2",
  A.D. Martin, M.G. Ryskin and A.M. Staśto, *Eur.Phys.J.* **C7** (1999) 643.
- "F_2 AT LOW Q^2",
  A.D. Martin, M.G. Ryskin and A.M. Staśto, *Nucl. Phys.* **B74** (Proc. Suppl.) (1999) 121.
- "PREDICTIONS FOR DIJET PRODUCTION IN DIS USING SMALL X DYNAMICS",
  J. Kwieciński, A.D. Martin and A.M. Staśto, `hep-ph/9904402` (to be published in *Phys. Lett. B*).

Acknowledgements

First of all I would like to thank my supervisor Professor Jan Kwieciński for his guidance throughout my PhD study, for being so patient and kind every day.

I am very grateful to Professor Alan Martin for many interesting collaborations and illuminating discussions on physics. I am also very grateful for organising my stay in Durham.

Many thanks to Krzysztof for discussions which helped me enormously to understand the small x physics. And also for the suggestions and ideas not always concerning physics.

Special thanks to Grażyna, Ryszard and Michał for their support during most difficult days.

I am very grateful to my parents and two sisters Barbara and Marta for their love, patience and help throughout this study. Without them this thesis wouldn't be possible.

I thank Foundation for Polish Science for financial support.

Kraków,
June 1999.

Contents

1 Introduction **3**

1.1 Deep Inelastic Scattering 5

1.2 Bjorken scaling 8

1.3 Operator product expansion 9

1.4 Renormalisation group equations 14

1.5 Dokshitzer-Gribov-Lipatov-Altarelli-Parisi evolution equations 17

1.6 BFKL equation and the high energy limit 23

1.7 Unitarization and saturation at large rapidities 32

2 Towards the unified BFKL and DGLAP description **33**

2.1 Introduction 33

2.1.1 k_T versus collinear factorisation and the anomalous dimension of the gluon 34

2.2 Unified BFKL and DGLAP equation for the gluon 39

2.2.1 Solution of the generalised BFKL-DGLAP equation for the gluon 43

2.3 The equation for the quark distribution 48

2.3.1 The light quark component of the sea 49

2.3.2 The charm component 50

2.3.3 The equation for the quark singlet distribution 51

2.4 Numerical analysis and the description of F_2 52

2.4.1 The optimum description of the F_2 data at small x 53

2.4.2 The effect of the $\ln(1/x)$ resummation on the gluon 58

2.4.3 Effect of $\ln(1/x)$ resummation on the structure function F_2 . . 61

2.4.4 Predictions for F_2^c and F_L 63

2.5 Summary 67

3 The description of F_2 at low Q^2 **69**

3.1 Short and long distance contributions and the description of F_2 at low Q^2 69

3.2 The $\gamma^* p$ cross section 71

3.2.1 The $\gamma^* p$ in the perturbative domain 72

3.2.2 The $\gamma^* p$ cross section in the non-perturbative domain 75

3.3 Final formulae 76

3.4 The quark mass 77

3.5 The description of the data for F_2 at low Q^2 78

3.6 Discussion 79

4 Dijet production as a probe of BFKL dynamics **88**

5 Summary and outlook **95**

A Formulae for the strong ordering approximation **97**

B Method of solution to the unifed system **99**

Chapter 1

Introduction

The more the wise person thinks about the simple (that there can be any question of a longer preoccupation with it already shows that it is not so easy after all), the more difficult it becomes for him.

- S.Kierkegaard

Preamble

Deep inelastic experiments allow us to probe the structure of matter. The non-composite particle like electron when scattering off the nucleon can provide us with lot of information on the structure of hadronic matter. The four-momentum squared of the exchanged vector boson in this process determines the resolving power. The higher the momentum, the smaller wavelengths are involved and hence the smaller distances within the nucleon can be probed. The deep inelastic experiment at SLAC in 1960s (see for example [1]) at large Q^2 exhibited scaling in the Bjorken x variable. Due to Feynman we now know how to explain scaling within the parton model. Thus scaling behaviour was a proof of the existence of pointlike particles $\rightarrow$ *partons* within a nucleon. Further experiments showed that scaling is violated by logarithmic corrections. This effect could be explained within a framework of Quantum Chromodymamics and it was due to the emission of gluons. Thus the QCD theory was able to predict the existence of gluons which are important constituents of the nucleonic structure.

Next phenomenon was a striking rise of the structure function F_2 at HERA [2], a collider of electrons and protons at DESY. This rise could be explained in two ways, first it could be reproduced by ordinary renormalisation group equations starting from a valence-like input parton distributions at very low scale. Then by large scaling violations the rise of structure function is generated. This approach is based on the Dokshitzer-Gribov-Lipatov-Altarelli evolution equations [3] for the partons which are just renormalisation group equations known from quantum field theory. This approach effectively resums the $\log(Q^2)$ terms, where Q^2 is the exchanged vector boson four-momentum. However there is also an alternative approach which

is based on the resummation of large terms $\ln(1/x)$. This framework known as the Balitskij-Fadin-Kuraev-Lipatov evolution equation [4] predicts naturally the strong rise of the gluon distribution and since the quark sea is being driven by the gluon, also the $x^{-\lambda}$ behaviour for the observable structure functions.

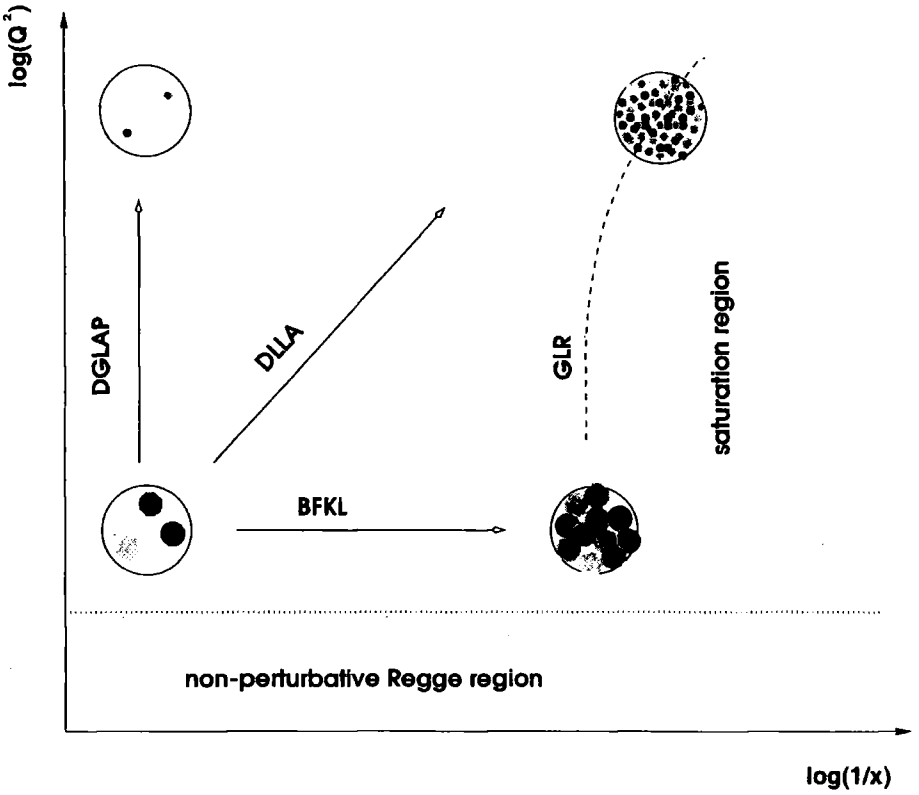

Figure 1.1: Schematic representation of parton densities and the theoretical evolution directions in the (x, Q^2) phase space.

The region of applicability of the two evolution schemes is shown in Figure 1.1 . Both these approaches have distinctive regions of validity. If one goes to asymptotic limit where $x \to 0$ and $Q^2 \to \infty$ then the DGLAP equations determine completely the behaviour of the structure functions from the input. One then speaks about the DLLA where only $\ln(Q^2)\ln(1/x)$ terms are retained. It would be however desirable to have a calculation which would cover the entire or at least most of the (x, Q^2) phase space. With few free parameters one would be able then to determine structure functions in the whole region of the (x, Q^2) space.
When x becomes very small, then the parton densities inside the nucleon become very large. One eventually hits the saturation region and the unitarity bound can be violated. The Gribov-Levin-Ryskin (GLR) equation (see Fig. 1.1) is able to describe the evolution of the gluon distribution including the shadowing corrections which become important in this regime of phase space.

Main aim of this thesis is to present such an approach which unifies the renormalisation group approach and the BFKL equation. Large $\ln(Q^2)$ and $\ln(1/x)$ terms

are resummed and treated on equal footing. Although the whole approach is done at leading order it also enables to estimate the subleading $\ln(1/x)$ corrections and leads to a very stable and reliable predictions for the total cross section and the structure functions.
The content of this thesis is as follows:
First chapter containts introductory material about the deep inelastic scattering, DGLAP evolution equations, operator product expansion and the high energy limit of QCD which follows the BFKL equation . In the second chapter the whole framework of coupled unified equations is presented together with the results for the structure functions F_2, F_L and F_C. In the third chapter we discuss the extension of these equations to the region of very low values of Q^2. Finally, in chapter 4 we apply this formalism to dijet production in deep inelastic scattering and make the predictions for the angular distributions as well as the total cross-section. We also make the predictions for the dijet distributions in Q^2 and in the longitudinal moemntum fraction of the gluon.

1.1 Deep Inelastic Scattering

In this section we will introduce useful variables and quantities needed for description of deep inelastic processes, see for example [1, 5, 6, 7]. To this aim let us consider the scattering of a pointlike particle like a lepton off the composite nucleon, see Figure 1.2 .

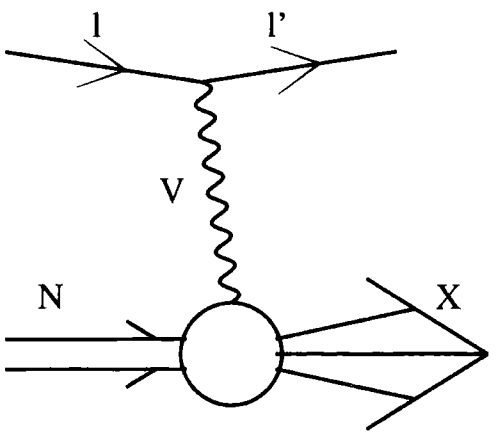

Figure 1.2: Diagrammatic representation of deep inelastic scattering.

Here l and l' are the incoming and outgoing lepton correspondingly, V is the exchanged vector boson, N is the probed nucleon and X an arbitrary hadronic final state. We introduce the following four-momenta,

$k^\mu = (E, 0, 0, E)_{LAB}$	incoming lepton
$k'^\mu = (E', 0, 0, E')_{LAB}$	outgoing lepton
$p^\mu = (M, 0, 0, 0)_{LAB}$	target nucleon
$q^\mu = (\nu, 0, 0, \sqrt{\nu^2 - q^2})_{LAB}$	exchanged vector boson

and the Lorentz invariants,

$Q^2 = -q^2$	squared four-momentum of the vector boson
$s = (p + k)^2$	total energy of the lepton - nucleon system
$W^2 = (p + q)^2$	total energy of the vector boson - nucleon system.

It is also convenient to introduce the following scaling variables,

$$x = \frac{Q^2}{2p \cdot q} \text{ Bjorken scaling variable}$$
$$y = \frac{p \cdot q}{p \cdot k} \text{ inelasticity}$$

We have defined the four-momenta in the laboratory frame, that is the one where nucleon is at rest. We also neglect the lepton masses as compared to their momenta. In the above process the exchanged vector boson could be a photon, Z^0 or W boson if the process involves charged current interaction. In the latter case if the incoming lepton is charged then we do not observe the outgoing neutrino in the detector. The scattering amplitude for this process (in electromagnetic case) can be expressed in the following way,

$$\mathcal{M} = e^2 \bar{u}(k', \lambda') \gamma^\mu u(k, \lambda) \frac{1}{q^2} < X | J_\mu^{em}(0) | N, \sigma >, \tag{1.1}$$

where $< X|$ is a hadronic final state and $|N, \sigma >$ is a nucleon state of polarisation σ. λ and λ' are the polarisation of the incoming and outgoing leptons correspondingly. $J_\mu^{em}(0)$ is the electromagnetic current.

The total cross section can be evaluated in the standard way,

$$d\sigma = \frac{1}{F} \frac{d^3k'}{2E'(2\pi)^3} \frac{1}{4} \sum_{\sigma\lambda\lambda'} |\mathcal{M}|^2, \tag{1.2}$$

where F denotes the flux factor and is equal to,

$$F = 4p \cdot k, \tag{1.3}$$

and the sum is performed over all possible polarisation states. One can factorise the cross section in the following way:

$$\frac{d^2\sigma}{dE' d\Omega} = \frac{\alpha^2}{Q^4} \frac{E'}{E} L_{\mu\nu}^{em} W^{\mu\nu} \tag{1.4}$$

where $\alpha = \frac{e^2}{4\pi}$ is fine structure constant. The $L^{em}_{\mu\nu}$ term entirely depends on the lepton vertex, and $W_{\mu\nu}$ contains all the information about the hadron involved in the process. We consider here the electromagnetic case. The formulae for the weak interaction case can be derived in the similiar way although they are more complicated.

$L^{em}_{\mu\nu}$ can be evaluated exactly in a strightforward way and reads:

$$\begin{aligned} L^{\mu\nu}_{em} &= \frac{1}{2}\sum_{s'} \bar{u}^{(s')}_{\alpha}(k')\gamma^{\mu}_{\alpha\beta}\sum_{s} u^{(s)}_{\beta}(k)\bar{u}^{(s)}_{\gamma}(k)\gamma^{\nu}_{\gamma\delta}u^{(s')}_{\delta}(k') = \\ &= \frac{1}{2}Tr(\not{k}'\gamma^{\mu}\not{k}\gamma^{\nu}) = 2(k^{\mu}k'^{\nu} + k'^{\mu}k^{\nu} - \frac{1}{2}Q^2 g^{\mu\nu}). \end{aligned} \tag{1.5}$$

The hadronic tensor $W_{\mu\nu}$ is given by the expression:

$$\begin{aligned} W_{\mu\nu}(p,q) &= \frac{1}{4M}\sum_{\sigma}\sum_{X}(2\pi)^4\delta^4(p_x - p - q) < N\sigma|J^{em}_{\mu}(0)|X >< X|J^{em}_{\nu}(0)|N\sigma > = \\ &= \frac{1}{4M}\sum_{\sigma}\sum_{X}\int d^4x e^{i(p-p_x+q)x} < N\sigma|J^{em}_{\mu}(0)|X >< X|J^{em}_{\nu}(0)|N\sigma > = \\ &= \frac{1}{4M}\sum_{\sigma}\int \frac{d^4x}{2\pi}e^{iqx} < N\sigma|J^{em}_{\mu}(x)J^{em}_{\nu}(0)|N\sigma > = \\ &= \frac{1}{4M}\sum_{\sigma}\int \frac{d^4x}{2\pi}e^{iqx} < N\sigma|[J^{em}_{\mu}(x), J^{em}_{\nu}(0)]|N\sigma > . \end{aligned} \tag{1.6}$$

Last line of (1.6) can be easily derived when we consider the fact that there are no intermediate states with momentum $p_x = p - q$ and energy $E_x = M - \nu \leq M$ which can contribute. Since the electromagnetic current is conserved we have $\partial^{\mu}J^{em}_{\mu} = 0$ and correspondingly $q_{\mu}W^{\mu\nu} = q_{\nu}W^{\mu\nu} = 0$. From this fact and the knowledge that $W_{\mu\nu}$ is a second rank tensor we can perform the following decomposition in terms of two independent structure functions W_1 and W_2 [1]:

$$W_{\mu\nu}(p,q) = -W_1(g_{\mu\nu} - \frac{q_{\mu}q_{\nu}}{q^2}) + \frac{W_2}{M^2}(p_{\mu} - \frac{p\cdot q}{q^2}q_{\mu})\cdot(p_{\nu} - \frac{p\cdot q}{q^2}q_{\nu}). \tag{1.7}$$

Using (1.7) and the explicit expression for $L^{\mu\nu}$ (1.5) one can derive the following expression for the cross-section:

$$\frac{d^2\sigma}{d\Omega dE'} = \frac{\alpha^2}{4E^2\sin^4\frac{\Theta}{2}}(2W_1\sin^2\frac{\Theta}{2} + W_2\cos^2\frac{\Theta}{2}) \tag{1.8}$$

where Θ denotes the electron scattering angle in the hadron rest frame. The structure functions W_1 and W_2 contain all the information about the hadron involved in

[1] In the case of weak interactions we would have three instead of two independent structure functions. This is due to the V-A structure of the weak current and the presence of the additional VA (AV) interference terms in the product of two currents. We would also loose the symmetry of the hadronic tensor.

the process. In principle they depend on two variables: ν and q^2. What kind of information can we get about the hadron from the behaviour of these functions? The first observation was that in the so called deep inelastic limit when $Q^2 \to \infty$, $\nu \to \infty$ and $Q^2/2M\nu = x$ is fixed, the two functions obey the *Bjorken scaling* which is a direct consequence of the fact that nucleon consists of the pointlike components. In the next paragraph we will derive the Bjorken scaling pattern from the naive parton model picture, see for example [6].

1.2 Bjorken scaling

If the proton consists of the components that are pointlike particles then at sufficiently high energies (and thus at very small wavelengths) the scattering off the proton will become just an incoherent scattering off these pointlike objects. By comparing the cross section (1.8) with the formula for electron-muon scattering ,

$$\frac{d^2\sigma^{e\mu\to e\mu}}{d\Omega dE'} = \frac{\alpha^2}{4E^2\sin^4\frac{\Theta}{2}}[\cos^2\frac{\Theta}{2} - \frac{q^2}{2m^2}\sin^2\frac{\Theta}{2}]\delta(\nu + \frac{q^2}{2m}) \tag{1.9}$$

we can immediately read out the forumale for the structure functions for one parton,

$$\begin{aligned} 2mW_1^p(\nu, Q^2) &= \frac{Q^2}{2m\nu}\delta(1 - \frac{Q^2}{2m\nu}) \\ \nu W_2^p(\nu, Q^2) &= \delta(1 - \frac{Q^2}{2m\nu}). \end{aligned} \tag{1.10}$$

We now observe that at sufficiently high values of the photon four-momentum Q^2 we will have Bjorken scaling, i.e. the structure functions will depend only on one variable $\omega = \frac{2m\nu}{Q^2}$,

$$\begin{aligned} mW_1^p(\nu, Q^2) &\to F_1^p(\omega) \\ \nu W_2^p(\nu, Q^2) &\to F_2^p(\omega) \end{aligned} \tag{1.11}$$

where F_1 and F_2 are now dimensionless quantities. To get the results for the whole nucleon we should convolute (1.10) with the *parton distributions* inside the nucleon which tell us about the probability $f_i(x)$ of finding a parton of type i and with a longitudinal momentum xp, where p is the momentum of the nucleon. Here, we adopted the assumption that we are working in the frame of proton's infinite momentum. Our final prescription for the structure functions is just:

$$\begin{aligned} F_2(\omega) &= \sum_i \int_0^1 dx\, e_i^2\, x f_i(x)\delta(x - \frac{1}{\omega}) \\ F_1(\omega) &= \frac{\omega}{2}F_2(\omega) \end{aligned} \tag{1.12}$$

or more formally,

$$F_2(x) = \sum_i e_i^2 x f_i(x) \tag{1.13}$$

$$F_1(x) = \frac{1}{2x}F_2(x) \tag{1.14}$$

where $x = \frac{Q^2}{2M\nu} = \frac{1}{\omega}$.
Formulae (1.13) and (1.14) summarise the Bjorken scaling phenomenon in the naive parton model. We have to stress the two basic assumptions which we have made in order to get the Bjorken scaling pattern:

- the photon scatters incoherently off the pointlike particles inside the nucleon.
- the transverse momentum of the interacting parton is **limited**

We also have to underline that the relation (1.14) is a consequence of the fact that the partons are spin 1/2 particles. It is called *Callan-Gross* relation and implies that the part of the cross section which corresponds to the exchange of longitudinally polarized virtual photon has to vanish in the scaling limit. The parton model picture can also be formulated in a covariant way by means of field theoretical apparatus [8]. In this picture partons can acquire transverse momenta but we assume that the amplitude for scattering a parton on a nucleon is strongly damped as the transverse momentum of the parton grows to become large [8] (see also [9]).
The Bjorken scaling is an approximation and it is violated in QCD by the logarithmic terms of the form $\ln(Q^2/\mu^2)$, where μ is factorisation scale. Within a QCD theory a quark can emit a gluon and thus acquire a large transverse momentum which eventually leads to the scaling violations. We shall now present the theoretical framework which will give us the factorisation of the stucture functions in terms of coefficient functions and the local operators. We will see that the coefficient functions satisfy the renormalisation group equations which will lead to the scaling violations.

1.3 Operator product expansion

The method we will present here (following [7, 10]) is useful when one considers the product of the fields at the same space-time point. Such product is called a *composite operator*. The operator product expansion procedure enables us to factorise such composite operators into a c-numbers containing all the singularities and the regular local operator. To see where the singularities come from, we can consider a single example of the vacuum expectation value of the time ordered product of two scalar fields, see [10],

$$< 0|T[\Phi(x)\Phi(y)]|0 >= -i\Delta(x-y) = -i\int \frac{d^4p}{(2\pi)^4}\frac{e^{-ip(x-y)}}{m^2-p^2-i\epsilon} \tag{1.15}$$

The above expression can be calculated explicitly and it has the form,

$$\Delta(x-y) = \frac{1}{4\pi^2 i}\frac{1}{(x-y)^2-i\epsilon} + \text{less singular terms} \tag{1.16}$$

and it is obviously divergent when $x \to y$. To obtain a meaningful definition of such operator we have to perform the *operator-product expansion.* We will consider here two ways of expansion depending on the character of singularity:

- **short distance expansion**

$$\hat{A}(x)\hat{B}(y) = \sum_i C_i(x-y)\hat{O}_i(\frac{x+y}{2}) \; ; \quad x-y \to 0 \tag{1.17}$$

  $\hat{A}$, $\hat{B}$ are arbitrary local operators. The singularity at $x \to y$ of the composite operator $\hat{A}(x)\hat{B}(y)$ is now fully contained in the functions $C_i(x-y)$ (which are just c-numbers) and are called *coefficient functions.* The operators $\hat{O}_i$ are well defined regular quantities, and they have the same quantum numbers as $\hat{A}(x)\hat{B}(y)$.

- **light-cone expansion**
  In the case of deep inelastic scattering we need however the expansion near the light cone $x^2 \sim 0$, rather than near $x \sim 0$. In case of $-q^2 \to \infty$ and with $\frac{-q^2}{2M\nu}$ fixed, the dominant contribution to tensor $W_{\mu\nu}$ (1.6) comes from the region near the light cone:

$$0 \leq x^2 \leq \frac{\text{const}}{-q^2} \tag{1.18}$$

In the rest of the section we will only consider light cone expansion. We will now expand the operators $\hat{O}_i(x)$ in the Taylor series and substitute into equation (1.17). The expansion near the light cone can then be written as:

$$j(x)j(0) = \sum_i C_i(x)\hat{O}_i(\frac{x}{2}) = \sum_{i,n} C_i^{(n)}(x^2)x^{\mu_1}\ldots x^{\mu_n}\mathcal{O}^{(i,n)}_{\mu_1\ldots\mu_n} \tag{1.19}$$

(here we consider two currents instead of the arbitrary operators $\hat{A}$ and $\hat{B}$). The operators $\mathcal{O}^{(i,n)}_{\mu_1\ldots\mu_n}$ are symmetric in the indices μ_n and they correspond to the operators of spin n. We can naively count the dimensions of all the terms in the operator-product expansion as in (1.19) and determine the light-cone singularity of the coefficient function $C_i^{(n)}(x^2)$,

$$C_i^{(n)}(x^2) \; \sim \; (x^2)^{-d_j - \frac{n}{2} + \frac{d_{(i,n)}}{2}} \tag{1.20}$$

where d_j and $d_{(i,n)}$ are the canonical dimensions of the current $j(x)$ and the operator $\mathcal{O}^{(i,n)}$ respectively. The leading term in the above expansion is determined by the most singular element $C_i^{(n)}$. Its singularity is controlled by the number $\tau = d_{(i,n)} - n$ (dimension - spin) and it is called *twist* of the operator $\mathcal{O}^{(i,j)}_{\mu_1\ldots\mu_j}$. The lowest value of twist will give us the leading term in the expansion (1.19).
We will now apply this formalism to the deep inelastic scattering case and see how the scaling violations can be obtained within the QCD theory.

In the case of deep inelastic lepton-hadron scattering we are concerned with the time-ordered product of two electromagnetic currents:

$$T[J_\mu(x)J_\nu(x')] \tag{1.21}$$

We can write down the most general form for this expression in the following way [10],

$$\begin{aligned} T[J_\mu(x)J_\nu(x')] &= (\partial_\mu\partial'_\nu - g_{\mu\nu}\partial\cdot\partial')\hat{O}_L(x,x') \\ &+ (g_{\mu\lambda}\partial_\rho\partial'_\nu + g_{\rho\nu}\partial_\mu\partial'_\lambda - g_{\mu\lambda}g_{\rho\nu}\partial\cdot\partial' - g_{\mu\nu}\partial_\lambda\partial'_\rho)\hat{O}_2^{\lambda\rho}(x,x') \\ &+ \text{antisymmetric part} \end{aligned} \tag{1.22}$$

This form[2] is very closely related (via Fourier transform) to the general expression for $W_{\mu\nu}$, see eqns. (1.6) and (1.7). We will drop the antisymmetric part because it will vanish when contracted with the symmetric tensor $L^{\mu\nu}$ (in the unpolarised case of deep inelastic scattering).
We can perform now the light cone expansion for the two bilocal operators $\hat{O}_L(x,x')$ and $\hat{O}_2^{\lambda\rho}(x,x')$,

$$\begin{aligned} \hat{O}_L(x,x') &= \sum_{i,n} C_{L,i}^{(n)}(y^2)y^{\mu_1}\ldots y^{\mu_n}\mathcal{O}_{L,\mu_1\ldots\mu_n}^{(i,n)}\left(\frac{x+x'}{2}\right) \\ \hat{O}_2^{\lambda\rho}(x,x') &= \sum_{i,n} C_{2,i}^{(n)}(y^2)y^{\mu_1}\ldots y^{\mu_n}\mathcal{O}_{2,\mu_1\ldots\mu_n}^{(i,n)\lambda\rho}\left(\frac{x+x'}{2}\right) \end{aligned} \tag{1.23}$$

where $y = x - x'$. We can construct three kinds of twist 2 operators in QCD. For the flavour non-singlet case we have,

$$\mathcal{O}_{NS}^{\mu_1\ldots\mu_n} \propto \bar{\Psi}(x)t^a\gamma^{\mu_1}D^{\mu_2}\ldots D^{\mu_n}\Psi(x) \;+\; \text{permutations} \tag{1.24}$$

where t^a are the generators of the **flavour** SU(N_f) group and D^{μ_n} are the covariant derivatives. Additionally we have a flavour-singlet operators:
the quark operator,

$$\mathcal{O}_q^{\mu_1\ldots\mu_n} \propto \bar{\Psi}(x)\gamma^{\mu_1}D^{\mu_2}\ldots D^{\mu_n}\Psi(x) \;+\; \text{permutations} \tag{1.25}$$

and the gluon operator,

$$\mathcal{O}_G^{\mu_1\ldots\mu_n} \propto Tr[F^{\mu_1\nu}D^{\mu_2}\ldots D^{\mu_n-1}F_\nu^{\mu_n}] \;+\; \text{permutations} \tag{1.26}$$

$F^{\mu\nu}$ is the standard gauge field strength in the Yang Mills theory. In the renormalisation group equations, the two operators $\mathcal{O}_q$ and $\mathcal{O}_G$ will mix beacuse they have identical quantum numbers.
Having done the expansion for the operators we can now calculate the forward

[2]We have introduced here an operator $\hat{O}_L$ which corresponds to the longitudinal structure function $F_L \equiv F_2 - 2xF_1$.

Compton scattering amplitude which is related to the hadronic tensor in DIS in the following way,

$$\begin{aligned} T_{\mu\nu}(p,q) &= \int d^4x e^{iqx} < p|T[J_\mu(x)J_\nu(0)]|p> = \\ &= (q_\mu q_\nu - q^2 g_{\mu\nu}) \sum_{i,n} < p|\mathcal{O}^{(i,n)}_{L,\mu_1\ldots\mu_n}(0)|p> \cdot \\ &\quad \cdot \int d^4x e^{iqx} x^{\mu_1}\ldots x^{\mu_n} C^{(n)}_{L,i}(x^2) \; + \\ &+ (g_{\mu\lambda}q_\rho q_\nu + g_{\rho\nu}q_\mu q_\lambda - q^2 g_{\mu\lambda}g_{\rho\nu} - g_{\mu\nu}q_\lambda q_\rho) \sum_{i,n} < p|\mathcal{O}^{(i,n)\lambda\rho}_{2,\mu_1\ldots\mu_n}(0)|p> \cdot \\ &\quad \cdot \int d^4x e^{iqx} x^{\mu_1}\ldots x^{\mu_n} C^{(n)}_{2,i}(x^2) \end{aligned} \tag{1.27}$$

We define now Fourier transforms of the Wilson coefficient functions,

$$\begin{aligned} -i\tilde{C}^{(n)}_{L,i}(-q^2)\left(\frac{-q^2}{2}\right)^{-n-1} q^{\mu_1}\ldots q^{\mu_n} &= \int d^4x\, e^{iqx} x^{\mu_1}\ldots x^{\mu_n}\, C^{(n)}_{L,i}(x^2) \\ -2i\tilde{C}^{(n+2)}_{2,i}(-q^2)\left(\frac{-q^2}{2}\right)^{-n-2} q^{\mu_1}\ldots q^{\mu_n} &= \int d^4x\, e^{iqx} x^{\mu_1}\ldots x^{\mu_n}\, C^{(n)}_{2,i}(x^2) \end{aligned} \tag{1.28}$$

Next, we express the matrix elements of the operators $\mathcal{O}^{(i,n)}$ in the following way,

$$\begin{aligned} < p|\mathcal{O}^{(i,n)}_{L,\mu_1\ldots\mu_n}(0)|p> &= A^{(n)}_{L,i} p_{\mu_1}\ldots p_{\mu_n} \; + \; \ldots \\ < p|\mathcal{O}^{(i,n)\lambda\rho}_{2,\mu_1\ldots\mu_n}(0)|p> &= A^{(n)}_{2,i} p^\lambda p^\rho p_{\mu_1}\ldots p_{\mu_n} \; + \; \ldots \end{aligned} \tag{1.29}$$

The dots in the above expansion denote the trace terms containing $g_{\mu_i\nu_j}$. These terms will have lower powers of $p\cdot q$ than the written ones and hence they can be safely neglected in the scaling limit. To derive (1.29) we have used the assumption that these expressions are symmetric in the indices $\mu_1\ldots\mu_n$ and that they should depend on p^μ. If we now use (1.28) and (1.29) and put into (1.27) then we get the following results for the forward virtual Compton scattering amplitude.

$$\begin{aligned} T_{\mu\nu}(p,q) &= 2\sum_{i,n}\left[(g_{\mu\nu} - \frac{q_\mu q_\nu}{q^2}) A^{(n)}_{L,i}\tilde{C}^{(n)}_{L,i}(-q^2) + \right. \\ &+ \left. \left(-g_{\mu\nu} - \frac{p_\mu p_\nu q^2}{(p\cdot q)^2} + \frac{p_\mu q_\nu + p_\nu q_\mu}{(p\cdot q)}\right) A^{(n)}_{2,i}\tilde{C}^{(n)}_{2,i}(-q^2)\right]\left(\frac{2p\cdot q}{-q^2}\right)^n \end{aligned} \tag{1.30}$$

We would like to have eventually the results for the structure functions W_1 and W_2. We recall that the hadronic tensor $W_{\mu\nu}$ is the absorptive part of the virtual forward Compoton scattering amplitude $T_{\mu\nu}$. By absorptive part we mean here:

$$\mathrm{Abs}\, T_{\mu\nu} = \frac{1}{2i}[T_{\mu\nu}(q_0 + i\epsilon) - T_{\mu\nu}(q_0 - i\epsilon)] \tag{1.31}$$

To get the expressions for the measured structure functions we can perform integration over the contour C shown on figure 1.3.

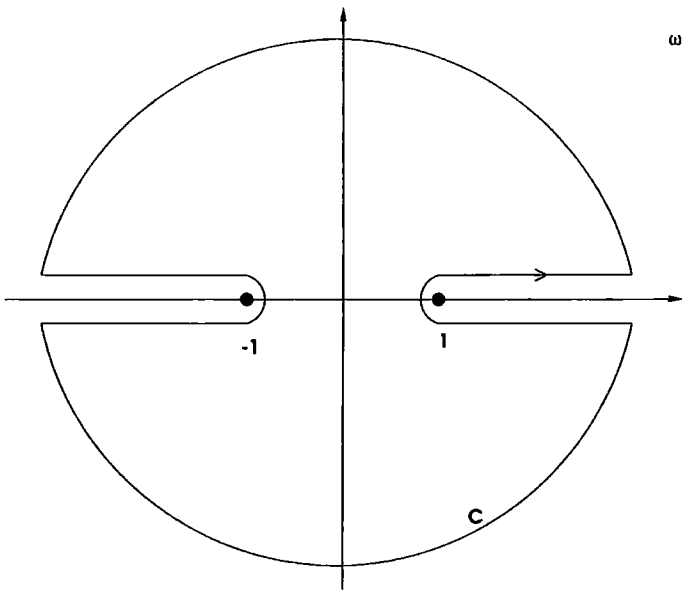

Figure 1.3: Contour of integration in ω plane for the hadronic tensor.

$$\begin{aligned} \frac{1}{2\pi i}\oint d\omega\,\frac{T_{\mu\nu}}{\omega^n} &= 2\int_1^\infty \frac{d\omega}{\omega^n}\,\mathrm{Abs}\;\mathrm{T}_{\mu\nu} \\ &= 2\int_0^1 d\xi\xi^{n-2}W_{\mu\nu} \end{aligned} \tag{1.32}$$

where $\omega = \frac{2p\cdot q}{-q^2}$ and $\xi = 1/\omega$.

Using (1.30) and the fact that

$$\frac{1}{2\pi i}\oint d\omega\omega^{m-n} = \delta_{m,n-1} \tag{1.33}$$

we get from (1.32) and the expansion for $W_{\mu\nu}$,

$$\begin{aligned} \int_0^1 dx\; x^{n-2}\; F_L(x,Q^2) &= \sum_i A_{L,i}^{(n)}\;\tilde{C}_{L,i}^{(n)}(Q^2) \\ \int_0^1 dx\; x^{n-2}\; F_2(x,Q^2) &= \sum_i A_{2,i}^{(n)}\;\tilde{C}_{2,i}^{(n)}(Q^2) \end{aligned} \tag{1.34}$$

We should recall here that the two structure functions have the following form:

$$\begin{aligned} F_2 &= \nu W_2 \\ F_L &= -W_1 + (1+\nu^2/Q^2)W_2 \end{aligned} \tag{1.35}$$

where F_L is the longitudinal structure function since it corresponds to the exchange of the longitudinally polarized virtual photon in deep inelastic scattering. We shall note here that now F_2 and F_L depend on two variables x, Q^2. We have factorized the expression for the moments of the structure functions into two terms:

- $\tilde{C}_{2,i}^{(n)}(Q^2)$, $\tilde{C}_{L,i}^{(n)}(Q^2)$ the Wilson coefficient functions which contain the information about the short distance dynamics and can be calculated perturbatively within the framework of the QCD.
- $A_{2,i}^{(n)}$, $A_{L,i}^{(n)}$ are related to the matrix elements of the local operators and which contain the long-distance part of the process. They cannot be calculated in the perturbative theory.

In the practical calculations the matrix elements $A_{2,i}^{(n)}$, $A_{L,i}^{(n)}$ have to be determined experimentally whereas the coefficient functions $\tilde{C}_{2,i}^{(n)}(Q^2)$, $\tilde{C}_{L,i}^{(n)}(Q^2)$ obey the renormalisation group equations.

1.4 Renormalisation group equations

In this subsection we will show how the coefficient functions obey the renormalisation group equations. Let us recall the general formula for the operator product expansion:

$$j(x)j(0) = \sum_i C_i(x)\, \hat{O}_i(0) \tag{1.36}$$

To get the renormalisation group equations we should rather consider matrix elements than the operators. We therefore define,

$$\begin{aligned} \mathcal{G}_j^{(n)} &= < 0|T[j(x)j(0)\Phi(x_1)\ldots\Phi(x_n)]|0 > \\ \mathcal{G}_i^{(n)} &= < 0|T[\hat{O}_i(0)\Phi(x_1)\ldots\Phi(x_n)]|0 > \end{aligned} \tag{1.37}$$

These are just the n-point Green's functions with insertions of the current product $j(x)j(0)$ and the local operator $\hat{O}_i$. $\Phi(x_k)$ is the scalar field. Taking the appropriate matrix element of (1.36) we have,

$$\mathcal{G}_j^{(n)} = \sum_i C_i(x)\mathcal{G}_i^{(n)} \tag{1.38}$$

We now know from the field theory that Green functions $\mathcal{G}_j^{(n)}$ and $\mathcal{G}_i^{(n)}$ satisfy separately the renormalisation group equations,

$$\begin{aligned} [\mathcal{D} + n\gamma_\Phi(g) - 2\gamma_j(g)]\, \mathcal{G}_j^{(n)} &= 0 \\ [\mathcal{D} + n\gamma_\Phi(g) - \gamma_i(g)]\, \mathcal{G}_i^{(n)} &= 0 \end{aligned} \tag{1.39}$$

where we have defined the derivative $\mathcal{D}$,

$$\mathcal{D} = \mu \frac{\partial}{\partial \mu} + \beta(g) \frac{\partial}{\partial g} \tag{1.40}$$

The derivative $\mathcal{D}$ is taken over the renormalisation scale μ. γ_Φ,γ_j, γ_i are the anomalous dimensions of the field Φ, current $j(x)$ and the operator $\hat{O}_i$ respectively. From

these equations (1.39) and the operator product expansion (1.36) we can easily derive the evolution equations for the Wilson coefficient functions,

$$[\mathcal{D} + 2\gamma_j(g) - \gamma_i(g)]\, C_i(g) = 0 \tag{1.41}$$

In deep inelastic case we have the light cone expansion of the form (1.19) with the local operators $\mathcal{O}^{(i,n)}_{\mu_1\cdots\mu_n}$ of spin n. In this case similiar renormalisation group equation can be derived for the Fourier transform, (1.28) of the coefficient $C_i(g)$,

$$[\mathcal{D} + 2\gamma_j(g) - \gamma_i^{(n)}(g)]\, \tilde{C}_i^{(n)}(-q^2) = 0 \tag{1.42}$$

where now $\gamma_i^{(n)}(g)$ is the anomalous dimension of the operator $\mathcal{O}^{(i,n)}_{\mu_1\cdots\mu_n}$. We can solve this equation as it is usually done for the renormalisation group equations and the solution reads,

$$\tilde{C}_i^{(n)}(g, -q^2/\mu^2) = \tilde{C}_i^{(n)}(\bar{g}(t), 1)\, \exp\,[\int_0^t dt'\, [2\gamma_j(\bar{g}(t')) - \gamma_i^{(n)}(\bar{g}(t'))] \tag{1.43}$$

where $t = \frac{1}{2}\ln\frac{Q^2}{\mu^2}$ and we have the condition $\bar{g}(0) = g$.

We can now apply this formalism to the deep inelastic scattering case. We shall concentrate ourselves on the flavour singlet operators (the results for the non-singlet operator can be obtained in a similiar manner). In this case we have a mixing between the two operators $\mathcal{O}_q^{\mu_1\cdots\mu_n}$ and $\mathcal{O}_G^{\mu_1\cdots\mu_n}$, see eqns. (1.25) and (1.26) and the renormalisation group equation can be recast into the 2x2 matrix form,

$$[\mathcal{D}\delta_{jk} - \gamma_{jk}^{(n)}]\, \tilde{C}_{\alpha,k}^{(n)}(-q^2, g, \mu) = 0\ ,\ \alpha = \mathrm{L}, 2 \tag{1.44}$$

where $\gamma_{jk}^{(n)}$ is the two dimensional anomalous dimension matrix for the flavour singlet operators. Note, that we do not have the anomalous dimension γ_j as in eq.(1.41) because of conservation of the electromagnetic current $j(x)$. The solution to (1.44) is the following,

$$\tilde{C}_{\alpha,i}^{(n)}(-q^2/\mu^2, g) = \sum_j \tilde{C}_{\alpha,j}^{(n)}(1, \bar{g}(t))\, \exp\,[-\int_0^t dt'\, \gamma_{ji}^{(n)}(\bar{g}(t'))]. \tag{1.45}$$

Using the relation between $\bar{g}(t)$ and the Beta function $\beta(g)$ we can rewrite (1.45) in the corresponding way,

$$\tilde{C}_{\alpha,i}^{(n)}(-q^2/\mu^2, g) = \sum_j \tilde{C}_{\alpha,j}^{(n)}(1, \bar{g}(t))\, \exp\,[-\int_g^{\bar{g}} d\lambda\, \frac{\gamma_{ji}^{(n)}(\lambda)}{\beta(\lambda)}] \tag{1.46}$$

where $\beta = \partial\bar{g}(t)/\partial t$. The quantities $\gamma_{ij}^{(n)}$ can be calculated in perturbative QCD according to appropriate diagrams shown on Figure 1.4. We can thus write the following perturbative expansions for the anomalous dimensions $\gamma_{ij}^{(n)}(\lambda)$ and the beta function $\beta(\lambda)$,

$$\begin{aligned} \gamma_{ij}^{(n)}(\lambda) &= \gamma_{ij}^{(n)0}\lambda^2 + \gamma_{ij}^{(n)1}\lambda^4 + \ldots \\ \beta(\lambda) &= -\beta_0\lambda^3 + \beta_1\lambda^5 + \ldots \end{aligned} \tag{1.47}$$

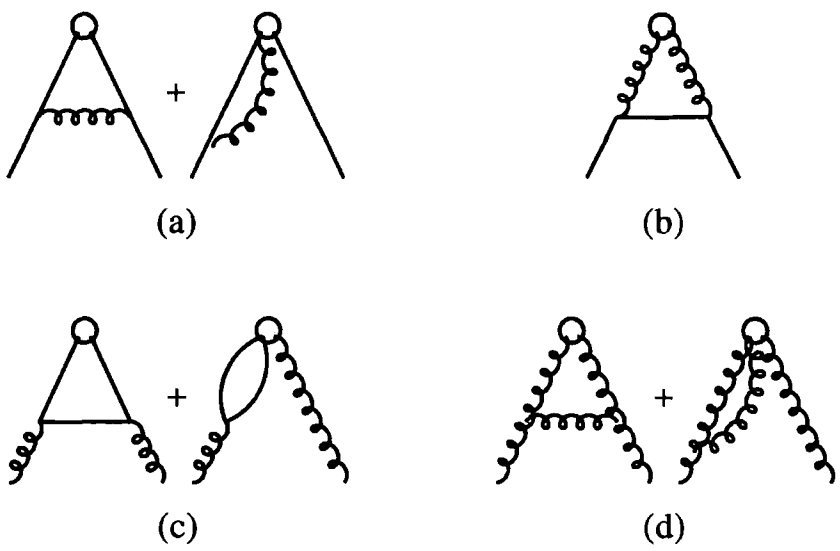

Figure 1.4: Diagrams corresponding to different anomalous dimensions; a)γ_{qq}, b) γ_{gq}, c) γ_{qg}, d) γ_{gg}.

Taking only the lowest order terms we obtain the following formula for the coefficient function,

$$\begin{aligned}
\tilde{C}^{(n)}_{\alpha,i}(-q^2/\mu^2, g) &= \sum_j \tilde{C}^{(n)}_{\alpha,j}(1, \bar{g}(t)) \exp[\int_g^{\bar{g}} d\lambda \frac{\gamma^{(n)0}_{ji}}{\beta_0 \lambda}] = \\
&= \sum_j \tilde{C}^{(n)}_{\alpha,j}(1, \bar{g}(t)) \exp[\ln \frac{\bar{g}}{g} \frac{\gamma^{(n)0}_{ji}}{\beta_0}] = \\
&= \sum_j \tilde{C}^{(n)}_{\alpha,j}(1, \bar{g}(t)) \left(\frac{\bar{g}}{g}\right)^{\frac{\gamma^{(n)0}_{ji}}{\beta_0}}
\end{aligned} \tag{1.48}$$

We can now express $\bar{g}$ in terms of g,

$$\bar{g}^2 = \frac{g^2}{1 + 2\beta_0 g^2 t} = \frac{1}{\beta_0 \ln \frac{-q^2}{\Lambda^2}} \tag{1.49}$$

where we have defined the Λ_{QCD} parameter to be: $\Lambda = \mu \exp[-1/2\beta_0 g^2]$. Inserting (1.49) into (1.48) we get the final solution,

$$\tilde{C}^{(n)}_{\alpha,i}(-q^2/\mu^2, g) \sim \sum_j \tilde{C}^{(n)}_{\alpha,j}(1, 0) \left(\ln \frac{Q^2}{\Lambda^2}\right)^{-\frac{\gamma^{(n)0}_{ji}}{2\beta_0}} \tag{1.50}$$

where now $\tilde{C}^{(n)}_{\alpha,i}(1,0)$ are the Wilson coefficient functions in the free field theory. The result (1.50) completes our calculation for the coeficient functions in deep inelastic scattering. We can now use these results and calculate the apropriate expressions for the moments of the structure functions. We define Mellin moments to be,

$$M^{(n)}_{\alpha}(Q^2) \equiv \int_0^1 dx\, x^{n-2} F_{\alpha}(x,Q^2) \tag{1.51}$$

and get the final results for these expressions by inserting (1.50) into (1.34),

$$M^{(n)}_{\alpha}(Q^2) = \sum_{ij} A^{(n)}_{\alpha,i} \tilde{C}^{(n)}_{\alpha,i}(1,0) \left(\ln \frac{Q^2}{\Lambda^2}\right)^{-\frac{\gamma^{(n),0}_{ij}}{2\beta_0}} \tag{1.52}$$

These results show that perturbative QCD predicts weak, logarithmic violations of the Bjorken scaling. We have obtained these important results by means of operator product expansion. We have factored out the local operator which is independent of the external momentum q_μ and the coefficient functions which obey the renormalisation group equations and can be calculated perturbatively. On the other hand the local operators $A^{(n)}_{\alpha,i}$ cannot be obtained from perturbative QCD because they contain information about the long distance part of the theory. We have used very formal approach of operator product expansion to obtain the formulae for the scaling violations. It can be also derived within more practical perturbative calculation as we shall see in the next following paragraphs.

1.5 Dokshitzer-Gribov-Lipatov-Altarelli-Parisi evolution equations

Scaling violations can also be easily obtained in a QCD improved parton picture, see for example [5, 7]. When the virtuality of the probe (i.e. photon) increases, the resolving power is increased too, because the resolving length goes roughly as $\sim \frac{1}{\sqrt{Q^2}}$. Since the coupling constant does't vanish fast enough with $Q^2 \to \infty$ there will be still some residual interactions at these virtualities and the multiple emission of gluons from the quarks will change the distribution in their transverse momenta. This will eventually lead to a breaking of scaling violations. All this can be nicely described by the Dokshitzer-Gribov-Lipatov-Altarelli-Parisi (DGLAP) [3] evolution equations and we shall see below that they are totally compatible with the renormalisation group equations obtained in Sec. 1.4 from the operator product expansion. Following [7] let us first look at Figure 1.5 : the quark i emits the gluon and travels further as quark j. We can introduce two quantities $q(x,Q^2)$ and $P_{qq}(z)$. The first, $q(x,Q^2)$ describes a probability of finding a quark within a hadron carrying a fraction x of nucleon's momentum at the given photon virtuality Q^2. It is the same quantity as $f_i(x)$ introduced before in eqns. (1.12). Second object, $P_{qq}(z)$, is a perturbative quantity, called *splitting function* which describes a probability

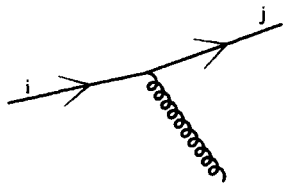

Figure 1.5: Splitting of the quark i into gluon and quark j.

of finding a quark with momentum x within a quark of momentum y ($z = x/y$). The DGLAP equation describes then an evolution of the parton density with the external scale Q^2,

$$Q^2 \frac{dq(x,Q^2)}{dQ^2} = \frac{\alpha_s(Q^2)}{2\pi} \int_x^1 \frac{dy}{y} P_{qq}(\frac{x}{y})\, q(y,Q^2) \tag{1.53}$$

This equation can be easily solved by means of Mellin transform technique introduced already before, see eq. (1.51),

$$M_q^{(n)}(Q^2) = \int_0^1 dx\, x^n\, q(x,Q^2) \tag{1.54}$$

(we have used here slightly different definition than before in eq. (1.51)). Using (1.54) equation (1.53) reads,

$$Q^2 \frac{dM^{(n)}(Q^2)}{dQ^2} = \frac{\alpha_s(Q^2)}{2\pi} M_q^{(n)}(Q^2)\, \tilde{P}_{qq}^{(n)} \tag{1.55}$$

where $\tilde{P}_{qq}^{(n)} = \int_0^1 dz\, z^n\, P_{qq}(z)$. We can solve (1.55) immediately,

$$M_q^{(n)}(Q^2) = M_q^{(n)}(Q_0^2) \left(\frac{\alpha_s(Q^2)}{\alpha_s(Q_0^2)} \right)^{\frac{-\tilde{P}_{qq}^{(n)}}{2\beta_0}} \tag{1.56}$$

We see that the DGLAP equation is completely compatible with the renormalisation group equations (1.52) if we identify $\tilde{P}_{ij}^{(n)} = -\gamma_{ij}^{(0)}$. Equation (1.56) describes only quark $\rightarrow$ quark transition. In the flavour singlet case however we have the set of evolution equations as already mentioned before. They describe all possible transitions: quark $\rightarrow$ gluon, gluon $\rightarrow$ quark and gluon $\rightarrow$ gluon transitions. The general structure of these evolution equations can be recast into the following 2x2 matrix form,

$$Q^2 \frac{d}{dQ^2} \begin{bmatrix} M_q^{(n)}(Q^2) \\ M_g^{(n)}(Q^2) \end{bmatrix} = \frac{\alpha_s(Q^2)}{2\pi} \begin{bmatrix} \tilde{P}_{qq}^{(n)} & \tilde{P}_{qg}^{(n)} \\ \tilde{P}_{gq}^{(n)} & \tilde{P}_{gg}^{(n)} \end{bmatrix} \begin{bmatrix} M_q^{(n)}(Q^2) \\ M_g^{(n)}(Q^2) \end{bmatrix}$$

The splitting functions $\tilde{P}_{ij}$ are perturbative quantities and are currently available up to NNLO accuracy. We shall note one important point here: in principle these

equations are valid for the parton densities $q(x,Q^2)$, $g(x,Q^2)$ and the equation (1.52) for the structure functions. We cannot identify these two objects because the structure functions are directly observable quantities measured in experiments whereas the parton densities can be dependent on a additional factorisation scale μ and therefore they are not observables. They are however connected via so called *collinear factorisation* to the structure functions:

$$F_i(x,Q^2) \;=\; \sum_j \int_x^1 dy\; C_{ij}(x/y, Q^2/\mu^2)\; q_j(y, Q^2/\mu^2) \tag{1.57}$$

where C_{ij} are coefficient functions and can be calculated in the perturbative way. We will come back to the problem of collinear factorisation in chapter 2.

We shall now sketch the derivation of the DGLAP equations by following the method in [5, 7]. First of all we have to identify the diagrams which contain the mass singularities. In the case of deep inelastic scattering we will have the collinear singularities coming from the particles being parallel in the final state.
Thus we will have to consider only the diagrams of the form shown on Figure 1.6.a

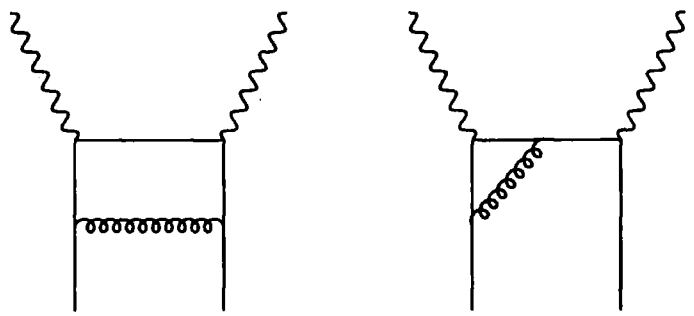

Figure 1.6: Left diagram (a) contains mass singularities; right diagram (b) is finite.

but not on Figure 1.6.b because the first has the collinear singularity and the latter is finite. In order to calculate the contribution to the hadron structure functions we have to take the absorptive part of the forward Compton scattering amplitude shown on Figure 1.7. We shall work in the axial gauge since there are no ghosts in that case,

$$\eta_\mu\, A^\mu \;=\; 0 \tag{1.58}$$

where η_μ is an arbitrary four-vector. The gluon propagator has then the following form,

$$\frac{d_{\mu\nu}(k)}{k^2 + i\epsilon} \tag{1.59}$$

with the polarisation tensor

$$d_{\mu\nu}(k) \;=\; g_{\mu\nu} \;-\; \frac{k_\mu \eta_\nu + k_\nu \eta_\mu}{k\cdot\eta} \;+\; \eta^2\, \frac{k_\mu k_\nu}{(k\cdot\eta)^2} \tag{1.60}$$

The contribution of the diagram 1.7 to the hadronic tensor $W_{\mu\nu}$ is then the following,

$$W_{\mu\nu} = \frac{g^2 C_F}{2M} \int \frac{d^4k}{(2\pi)^4} \frac{\pi\delta((p-k)^2)\delta((q+k)^2)}{(k^2)^2} \frac{1}{2} \mathrm{Tr}[\gamma^\mu(\not{q}+\not{k})\gamma^\nu \not{k}\gamma^\lambda \not{p}\gamma^\delta \not{k}] d_{\lambda\delta}(p-k) \tag{1.61}$$

Where g is the strong coupling and C_F is the colour factor, which in this case is equal to 4/3. We shall use now the Sudakov decomposition, that is we rewrite ,

$$k_\mu = \alpha p_\mu + \beta q'_\mu + k_{\perp\mu} \tag{1.62}$$

where α and β are the parameters and p_μ and q'_μ are two lightlike vectors forming together with $k_{\perp\mu}$ the basis for the Sudakov decomposition. These vectors have following properties,

$$q' = q + xp$$
$$p^2 \sim q'^2 \sim 0 \tag{1.63}$$
and (1.64)
$$q' \cdot p \simeq q \cdot p$$

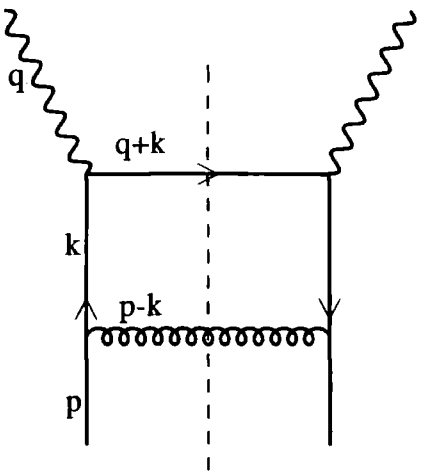

Figure 1.7: Elastic forward Compton scattering amplitude.

Using this decomposition (1.62) we can write the delta functions in (1.61) in the following way,

$$\int d^4k\ \delta((p-k)^2)\delta((q+k)^2) =$$
$$= \frac{\pi}{2p\cdot q} \int d\alpha d\beta dk^2\ \delta(\beta - \frac{k^2}{2p\cdot q})\ \delta(\alpha - x + \frac{(1-x)k^2}{2p\cdot q}) \tag{1.65}$$

where we have used the fact that

$$(p-k)^2 = 2p\cdot q\ \beta(\alpha - 1)$$

$$(q+k)^2 \;=\; 2p\cdot q\,[\alpha - x \;+\; \beta(\alpha - x) \;+\; \frac{k_\perp^2}{2p\cdot q}]$$

and (1.66)

$$k^2 \;=\; \frac{k_\perp^2}{1-\alpha} \tag{1.67}$$

We shall choose for the vector η the four-vector q'. In that case the gluon polarisation tensor reads,

$$d_{\lambda\delta}(p-k) \;=\; g_{\lambda\delta} \;-\; \frac{(p-k)_\lambda q'_\delta \;+\; (p-k)_\delta q'_\lambda}{(1-\alpha)p\cdot q'} \tag{1.68}$$

Performing explicit calculation, i.e. contracting tensor $d_{\lambda\delta}$ of the form (1.68) with the trace term in eq. (1.61) and using delta functions we get,

$$W_{\mu\nu}(p,q) \;=\; \frac{g^2}{6\pi^2}\int\frac{dk^2}{k^2}\left(\frac{1+x^2}{1-x}\right)\left[\frac{x}{\nu}\frac{p_\mu p_\nu}{p^2} \;+\; \ldots\right] \tag{1.69}$$

We now see that by the fact that we have allowed for the gluon radiation the virtuality of the parton's momentum k^2 is not restricted to very low values. Additionally we note that the integral over k^2 in eq. (1.69) is logarithmically divergent. One can find that the proper integration limits should be

$$\int_{p^2}^{Q^2}\frac{dk^2}{k^2} \;=\; \log(Q^2/m^2) \tag{1.70}$$

where $m^2 \sim p^2$. In order to derive the full DGLAP evolution equation [3] we need to consider higher order diagrams. The clue observation by Gribov and Lipatov was that the dominant contributions come from the ladder diagrams (in axial gauge) with the restriction that the momenta of the exchanged partons should be strongly ordered, see Figure 1.8.

$$p^2 \ll k_1^2 \ll k_2^2 \ll k_3^2 \ll \ldots \ll k_N^2 \ll Q^2 \tag{1.71}$$

so that the momenta of the partons which are closer to the photon vertex are dominated by the hard momentum scale Q^2. Now we will have the set of coupled integrations over the transverse and longitudinal parts of the momenta. We can define the transverse integral as,

$$\begin{aligned} I_T^{(N)}(\frac{Q^2}{m^2}) \;&=\; \int_{m^2}^{Q^2}\frac{dk_N^2}{2k_N^2}g^2(k_N^2)\int_{m^2}^{k_N^2}\frac{dk_{N-1}^2}{2k_{N-1}^2}g^2(k_{N-1}^2)\;\ldots\;\int_{m^2}^{k_2^2}\frac{dk_1^2}{2k_1^2}g^2(k_1^2) \;\simeq \\ &\simeq\; \frac{1}{N!}\left[\int_{m^2}^{Q^2}\frac{dk^2}{2k^2}g^2(k^2)\right]^N \equiv \frac{1}{N!}[\frac{1}{2\beta_0}(\ln\ln\frac{Q^2}{\mu^2} - \ln\ln\frac{m^2}{\mu^2})]^N \;\equiv\; \frac{1}{N!}\rho^N \end{aligned} \tag{1.72}$$

where $\rho = \frac{1}{2\beta_0}[\ln\ln Q^2/\mu^2 - \ln\ln m^2/\mu^2]$. Here the couplings have been taken at the value of the momentum k_i^2. The second integral is over longitudinal components,

$$\begin{aligned} I_L^{(N)} \;=\; &\int_0^1\frac{d\xi_N}{\xi_N}\delta(1-x/\xi_N)\ldots\int_{\xi_3}^1\frac{d\xi_2}{\xi_2}\int_{\xi_2}^1\frac{d\xi_1}{\xi_1}\times \\ &\times P(\xi_1)\,P(\xi_2/\xi_1)\;\ldots\;P(\xi_N/\xi_{N-1}) \end{aligned} \tag{1.73}$$

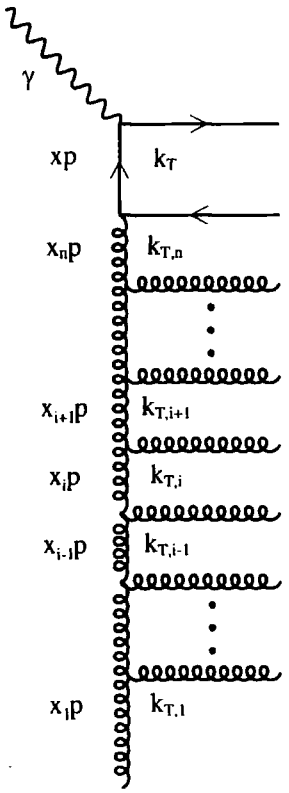

Figure 1.8: Ladder diagram contributing to the Altarelli-Parisi equations

Using Mellin transform we can write equation (1.73) as,

$$\int_0^1 dx\ x^{N-1}\ I_L^{(n)}(x)\ =\ [d^{(n)}]^N \tag{1.74}$$

Now we can take the moment of the structure function and sum the contributions from all diagrams at all N,

$$\sum_N \frac{1}{N!}\ [\ \rho\ d^{(n)}]^N\ =\ \exp[\ \rho\ d^{(n)}]\ =\ \left[\log\frac{Q^2}{\mu^2}\right]^{\frac{d^{(n)}}{2\beta_0}} \left[\log\frac{m^2}{\mu^2}\right]^{\frac{-d^{(n)}}{2\beta_0}} \tag{1.75}$$

We see now that the scale μ introduced previously plays a role of the factorisation scale. The contribution $\log(m^2/\mu^2)$ which contains singularity, cannot be explicitly calculated in the perturbative QCD but since it factorises it can be absorbed into the initial parton distributions.
We have finally obtained the DGLAP evolution equations which describe the scaling violations. We have showed that they result by factorising the mass singularities and by the summation of the leading logarithms. The DGLAP equations themselves do not predict the exact shape and magnitude of the measured structure functions.

They can only predict the evolution with the scale Q^2. In practice one has to parametrise the initial parton distributions at some low scale Q_0^2. For example one assumes the form:

$$q(x,Q_0^2) \;=\; Ax^a(1+c\sqrt{x}+dx)(1-x)^b \tag{1.76}$$

Then, these parton distributions are evolved to the values of (x,Q^2) which are probed by the deep inelastic measurements and can be used to calculate the structure functions $F_{L,T}(x,Q^2)$. The free parameters (a,A,c,d,b) are adjusted so that the best description of the data is obtained. This procedure, called global parton analysis gives as a result a certain set of parton distribution functions within a given renormalisation scheme. This kind of analysis has been performed and is being always updated by various groups MRS [11] , CTEQ [12] and GRV [13].

1.6 BFKL equation and the high energy limit

In the previous paragraphs we have discussed DGLAP evolution equations for the parton distributions. It has been shown that these equations effectively resum all powers of $(\alpha_s \log(Q^2))^n$. This has been achieved by making the approximation of the strong ordering of transverse momenta in the exchanged parton ladder. Consequently DGLAP equation is valid in the region where $\log(Q^2)$ terms are large. However in the kinematic regime accessible to HERA accelerator at DESY one can probe very small values of Bjorken x, $(x \sim 10^{-5})$. This is because the center of mass energy at HERA is about $\sqrt{s} = 300$ GeV. Since the energy W^2 of the virtual photon - nucleon system cannot exceed s, this implies that x can be as small as $\frac{Q^2}{s} \sim 10^{-5}$ when $Q^2 \sim 1\text{GeV}^2$.

One should thus worry that there are large logarithms $\log(1/x)$ which are not included in the standard renormalisation group calculation, see Fig. 1.1. The resummation of the leading powers of $\log(1/x)$ is accomplished by the Balitskii-Fadin-Kuraev-Lipatov evolution equation [4]. It corresponds to the summation of the ladder diagrams for the emitted gluons as well as virtual corrections. As a solution it gives so called *hard Pomeron*, an object which is characterized by a very large magnitude of its intercept $\lambda \equiv \alpha(0) - 1 = 4\ln 2\frac{N_c\alpha_s}{\pi} \sim 0.5$. This should lead to a characteristic rise of the structure functions with decreasing x, $(x^{-\lambda})$. Hard pomeron is a perturbative object which comes from QCD calculation. It has to be contrasted with the so called *soft Pomeron* introduced by Donnachie and Landshoff [14] which describes the high energy behaviour of the total cross section at soft processes of limited p_T. It has been determined phenomenologically from the fits to the hadronic cross sections and the value of its intercept is around $\alpha_{DL}(0) - 1.0 \simeq 0.08$. It originates from the old Regge theory which was developed before QCD and which tried to exploit all information from some universal properties of the scattering amplitudes.

The BFKL equation has been also recently calculated up to NLO [15]. The solution in this order is however unstable and gives rather unphysical result, that is, the Pomeron intercept becomes negative at quite small values of $\alpha_s \sim 1/6$. This

suggests that some resummation procedure is needed in order to get stable and phenomenologically acceptable result. First attempts establishing the resummation have already been done and they yield quite successful results [16, 17]. We shall come back and disscuss this problem later in the next chapter when we introduce consistency constraint in the presentation of the unified evolution equations.
The main features of the BFKL equation can be summarized in couple of points:

- It applies to the processes which are hard processes and high energy processes at the same time. *Hard* means that there is a hard scale which guarantees that the perturbative calculation is justified. *High energy*, defines the limit in which this equation is to be valid.

- It performs resummation of the powers of $\log(1/x)$ which could be important when considering deep inelastic processes at small values of x.

- The basic quantity used in this equation is the *unintegrated* gluon density $f(x, k^2)$ which is connected to the traditional integrated gluon density (see previous section 1.5) via following formula,

$$xg(x, Q^2) \equiv \int^{Q^2} \frac{dk^2}{k^2} f(x, k^2) \tag{1.77}$$

  Here k^2 is the value of the gluon momentum at the end of the ladder.

- There is no strong ordering of momenta in the ladder (in contrast to DGLAP evolution; see condition (1.71)). Instead the full phase space is allowed. This has the direct consequence in the diffusion of the transverse momenta along the gluon ladder.

- We are generally working in the *multi-regge* kinematics, see Figure 1.9, where:

$$s \gg s_{ij} \gg t_i \simeq -q_{iT}^2 \tag{1.78}$$

  where $s_{ij} = 2\ k_i \cdot k_j$ is the Mandelstam invariant for the subamplitude with partons i and j. Additionally we have strong ordering of rapidities of the produced outgoing partons,

$$y_0 \gg y_1 \gg \ldots \gg y_{n+1} \tag{1.79}$$

The general form of the BFKL equation in the leading order is the following,

$$f(x, k^2) = f^{(0)}(x, k^2) + \frac{N_c \alpha_s}{\pi} k^2 \int_x^1 \frac{dz}{z} \int \frac{dk'^2}{k'^2} \left[\frac{f(x/z, k'^2) - f(x/z, k^2)}{|k'^2 - k^2|} + \right.$$
$$\left. + \frac{f(x/z, k^2)}{\sqrt{4k'^4 + k^4}} \right] \tag{1.80}$$

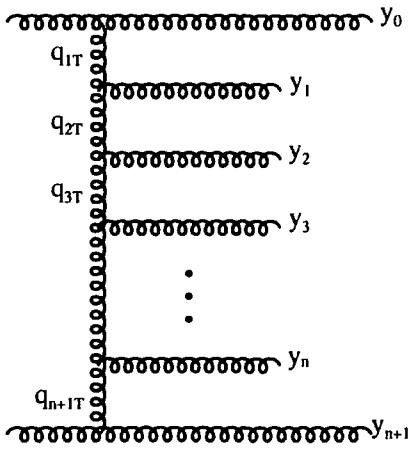

Figure 1.9: Multi-regge kinematics

where the inhomogenous term $f^{(0)}(x,k^2)$ will be discussed later. The solution to this equation for the case of fixed strong coupling constant α_s has the form ,

$$f(x,k^2) \sim (k^2)^{1/2} x^{-\lambda} \exp\left(-A \frac{\log^2 \frac{k^2}{k_0^2}}{\log(1/x)}\right) \tag{1.81}$$

where $\lambda = 4 \log 2 \frac{N_c \alpha_s}{\pi} \simeq 0.5$ is the hard Pomeron intercept. The term $(k^2)^{1/2}$ comes from the solution to the anomalous dimension which in case of BFKL is equal to $1/2$. The exponential term describes the diffusion in the transverse momenta in the gluon ladder. One can see that the lower the value of x the stronger the diffusion is going to be. This diffusion effect can have large impact on the final state configurations in different processes. In particular it can be the source of the decorellation of the produced dijets in deep inelastic scattering. Normally the dijets would be strongly corellated in the back to back configuration. However the BFKL dynamics together with the diffusion term can cause the decorellation of the two jets. This increases the value of the cross section (as compared to standard calculation without BFKL) for the configurations with smaller angles between the two produced jets. This can be treated as a signature of the underlying BFKL dynamics. We will come back to this point when considering the dijet production in chapter 4.

The traditional way to compute the BFKL equation is to consider the discontinuity of the forward elastic scattering amplitude. The many particle production amplitudes are then evaluated in the multi-regge kinematics. The terms with real emissions of gluons gather to give an effective gauge invariant Lipatov vertex and the virtual terms correspond to the reggeisation of the exchanged gluon. The resulting integral equation is of the form (1.80) in which the infrared divergencies cancel between real and virtual emission terms.
Following [18, 19] we shall present here an alternative way to derive this equation, namely the simpler heavy onium-onium scattering in the light-cone perturbation theory. We consider the simple model of the hadron as a heavy quark-antiquark

system (**onium**) . The single transverse momentum scale here is given by the inverse radius of the onium state. In the large N_c limit the heavy onium wavefunction can be viewed as a collection of simple dipoles. Then the total cross-section for the scattering of two onia can be expressed as the product of the dipole number densities which constitute the two onia times the elementary dipole-dipole cross section which is independent of the initial energies of the two onia.
We shall start at first with the onium wavefunction, which only contains two heavy quarks but no soft gluons. Consider the dipole on Figure 1.10, where $\bar{x}_0, \bar{x}_1$ are the transverse coordinates (*impact parameters*) and $(1-z_1), z_1$ are the longitudinal momentum fractions of the quark and anti-quark. The coordinate and momentum wavefunctions are related by the Fourier transform,

$$\tilde{\Psi}^{(0)}(\bar{x}_{01}, z_1) \;=\; \int \frac{d^2k_1}{(2\pi)^2}\, e^{i\bar{k}_1\cdot\bar{x}_{01}}\, \Psi^{(0)}(k_1, z_1) \tag{1.82}$$

where $\bar{x}_{01} \;=\; \bar{x}_1 - \bar{x}_0$. The advantage of using the impact parameter space is that

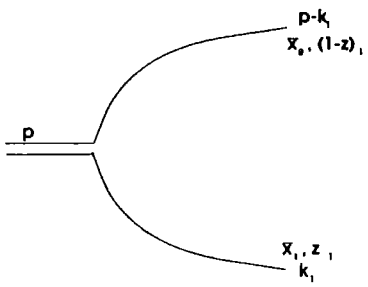

Figure 1.10: Diagrammatic representation of the $q\bar{q}$ dipole.

the soft gluons factorize more easily in that picture. This wavefunction is normalised so that:

$$\int d^2\bar{x} \int dz\; \Phi^{(0)}(\bar{x}, z) \;=\; 1 \tag{1.83}$$

where we have defined the square of the wavefunction:

$$\Phi^{(0)}(\bar{x}, z) \;=\; \sum_{\alpha\beta} |\tilde{\Psi}^{(0)}_{\alpha\beta}(\bar{x}, z)|^2 \tag{1.84}$$

We define α and β as the spin indices of the quark and antiquark spinors respectively. The lowest order cross section for the scattering between two onia is the following,

$$\sigma^{(0)} \;=\; \int d^2\bar{x}_{01} \int_0^1 dz_1\; \Phi^{(0)}(\bar{x}_{01}, z_1) \int d^2\bar{x}'_{01} \int_0^1 dz'_1\; \Phi^{(0)}(\bar{x}'_{01}, z'_1)\; \sigma_{dd}(\bar{x}_{01}, \bar{x}'_{01}) \tag{1.85}$$

Here σ_{dd} is the elementary dipole-dipole scattering cross-section. This cross-section can be easily evaluated because the time of the interaction between the two systems is very short compared to the time scales in the onium wavefunctions. From (1.85)

we see that the rise of the total cross-section will be connected with the increasing density of dipoles in the two onia.
When the onium consisting of two heavy quarks emits the gluon, it becomes the two-dipole state. There will be one dipole consisting of the quark and the antiquark part of the gluon and the second will be consisting of the quark part of the gluon and the remaining original antiquark of the parent dipole. This is shown on Figure 1.11. We assume that $z_2 \ll z_1, (1-z_1)$ which defines the gluon as a soft. We choose the light cone gauge where the polarisation of the gluon is,

$$\epsilon^\lambda_\mu(k) \;=\; (\epsilon^\lambda_+, \epsilon^\lambda_-, \bar{\epsilon}^\lambda) \;=\; (0, \frac{\bar{\epsilon}^\lambda \cdot \bar{k}}{k_+}, \bar{\epsilon}^\lambda) \tag{1.86}$$

In the soft gluon approximation k_+ is large and therefore we only have to consider $\epsilon^\lambda_- \;=\; \frac{\bar{\epsilon}^\lambda \cdot \bar{k}}{k_+}$ We can now calculate the wavefunction which corresponds to the onium with one additional soft gluon,

$$\Psi^{(1)}(k_1, k_2; z_1, z_2) \;=\; 2\,g\,T_a \frac{\bar{\epsilon}^\lambda \cdot \bar{k}}{k_+} \left[\Psi^{(0)}(k_1 + k_2, z_1) - \Psi^{(0)}(k_1, z_1)\right] \tag{1.87}$$

where T_a is the $SU(3)$ colour matrix. In derivation of (1.87) we have used the

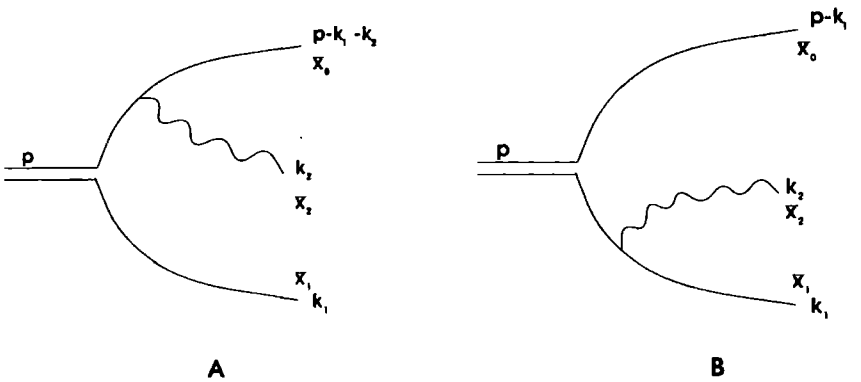

Figure 1.11: Diagrammatic representation of dipoles with additional soft gluon emission.

eikonal prescription for the coupling of the soft gluon.
The corresponding wavefunction in the transverse coordinate space will be:

$$\tilde{\Psi}^{(1)}(\bar{x}_{02}, \bar{x}_{21}; z_1, z_2) \;=\; \int \frac{d^2\bar{k}_1 d^2\bar{k}_2}{(2\pi)^4}\, e^{i\bar{k}_1\cdot\bar{x}_{01}}\, e^{i\bar{k}_2\cdot\bar{x}_{02}}\, \Psi^{(1)}(\bar{k}_1, \bar{k}_2; z_1, z_2) \tag{1.88}$$

We find that using (1.87) and (1.88) we get,

$$\tilde{\Psi}^{(1)}(\bar{x}_{02}, \bar{x}_{21}; z_1, z_2) \;=\; \frac{i\,g\,T_a}{\pi} \tilde{\Psi}^{(0)}(\bar{x}_1, z_1) \sum_\lambda \bar{\epsilon}^\lambda \cdot \left(\frac{\bar{x}_{21}}{x^2_{21}} - \frac{\bar{x}_{20}}{x^2_{20}}\right) \tag{1.89}$$

We can calculate the square of the onium wavefunction $\Phi^{(1)}$ in the transverse coordinate space using (1.89),

$$\Phi^{(1)}(\bar{x}_1, z_1) \;=\; \int d^2\bar{x}_2 \int_{z_0}^{z_1} \frac{dz_2}{z_2} \frac{\alpha_s C_F}{\pi^2} \frac{x^2_{10}}{x^2_{20} x^2_{21}} \Phi^{(0)}(x_1, z_1) \tag{1.90}$$

Next, we shall generalise our equation to include n soft gluons $k_2, k_3, \ldots, k_{n+1}$ which are ordered according to $z_2 \gg z_3 \gg z_4 \ldots \gg z_{n+1}$. The hardest of the soft gluons is emitted first then the next of the hardest, and in the end the softest gluon is emitted. We shall adopt here a *planar approximation* which greatly simplifies the calculation because it reduces the number of diagrams. One neglects the non-planar diargams since they will be supressed by powers $1/N_c$ relatively to the planar graphs. The planar limit corresponds to taking $g \to 0$, $N_c \to \infty$ while keeping $g^2 N_c$ fixed. The non-planar diagrams will behave like $1/N_c^2$ so the planar approximation is expected to be valid at roughly 10% level in the real $N_c = 3$ case. It is useful to introduce a generating functional $Z(\bar{x}_1, \bar{x}_0, z_1, u)$ of the light-cone wavefunction of the onium. We define Z by the following relation:

$$\frac{\delta}{\delta u(\bar{x}_2, z_2)} \frac{\delta}{\delta u(\bar{x}_3, z_3)} \cdots \frac{\delta}{\delta u(\bar{x}_{n+1}, z_{n+1})} Z(\bar{x}_1, \bar{x}_0, z_1, u)|_{u=0}\, \Phi^{(0)}(\bar{x}_1, z_1) =$$
$$= \Phi^{(n)}(\bar{x}_1, \bar{x}_2, \ldots, \bar{x}_{n+1}; z_1, z_2, \ldots, z_{n+1}) \qquad (1.91)$$

$\Phi^{(n)}$ here is the square of the wavefunction for the heavy quark-antiquark pair along with n soft gluons which have transverse coordinates $\bar{x}_2, \bar{x}_3, \ldots, \bar{x}_{n+1}$ and longitudinal momentum fractions $z_2, z_3, \ldots, z_{n+1}$. Then the functional Z obeys the following integral equation:

$$Z(\bar{x}_1, \bar{x}_0; z_1, u) = 1 + \frac{\alpha_s C_F}{\pi^2} \int d^2\bar{x}_2 \frac{x_{01}^2}{x_{20}^2 x_{21}^2} \int_{z_0}^{z_1} \frac{dz_2}{z_2}$$
$$u(\bar{x}_2, z_2)\, Z(\bar{x}_2, \bar{x}_1; z_2, u) Z(\bar{x}_2, \bar{x}_0; z_2, u) \qquad (1.92)$$

However the above equation for the generating functional Z is not complete because it doesn't give the probability conservation constraint,

$$\int d^2\bar{x}_1 \int dz_1 Z(\bar{x}_1, \bar{x}_0, z_1, u)|_{u=1}\, \Phi^{(0)}(\bar{x}_1, z_1) = 1 \qquad (1.93)$$

The above requirement can be achieved by including additionally the virtual emissions of the soft gluons. Normally constraint (1.93) is enforced order by order in perturbation theory. Here we adopt simpler approach where we introduce a cutoff ρ and define the region $R(x_{02}, x_{01})$ by requiring that $x_{02} \geq \rho$ and $x_{01} \geq \rho$. We take the ultraviolet cutoff ρ to be a small quantity when compared with the average onium radius. Virtual emissions can be calculated by integrating the single gluon emission over the phase space with the cutoff R:

$$\frac{\alpha_s C_F}{\pi^2} \int_0^Y dy \int_R \frac{d^2\bar{x}_2 x_{01}^2}{x_{02}^2 x_{12}^2} = \frac{4\alpha_s C_F}{\pi} Y \ln \frac{x_{01}}{\rho} \qquad (1.94)$$

providing that we can assume $x_{01} \gg \rho$. When we induce the virtual emissions then the formula for the Z generating functional is the following;

$$Z(\bar{x}, \bar{x}_0; z_1, u) = \exp[-\frac{4\alpha_s C_F}{\pi} \ln \frac{x_{01}}{\rho} \ln \frac{z_1}{z_0}]\, u(x_{01}) +$$
$$+ \frac{\alpha_s C_F}{\pi^2} \int_{z_0}^{z_1} \frac{dz_2}{z_2} \int_R d^2\bar{x}_2 \frac{x_{01}^2}{x_{02}^2 x_{12}^2} \exp[-\frac{4\alpha_s C_F}{\pi} \ln \frac{x_{01}}{\rho} \ln \frac{z_1}{z_2}]$$
$$Z(\bar{x}_2, \bar{x}_1; z_2, u)\, Z(\bar{x}_2, \bar{x}_0; z_2, u) \qquad (1.95)$$

Now, if we take $u = 1$ we see that it must be $Z = 1$. We can easily check this, if we take $Z = 1$ on the right hand side of (1.95) and using (1.94) we will get then:

$$\begin{aligned} Z(\bar{x}_1, \bar{x}_0; z_1, u)|_{u=1} &= \exp[-\frac{4\alpha_x C_F}{\pi}\frac{\ln x_{10}}{\rho}Y] + \\ &+ \frac{\alpha_s C_F}{\pi^2}\int_0^Y dy \int_R \frac{d^2\bar{x}_2 x_{01}^2}{x_{02}^2 x_{12}^2} \exp[-\frac{4\alpha_s C_F}{\pi}\ln\frac{x_{01}}{\rho}(Y-y)] = \\ = \quad & \exp[-\frac{4\alpha_x C_F}{\pi}\frac{\ln x_{01}}{\rho}Y] \cdot \\ & \cdot[1 + \frac{\alpha_s C_F}{\pi^2}\int_R \frac{d^2\bar{x}_2^2 x_{01}^2}{x_{02}^2 x_{12}^2} \frac{\exp[\frac{4\alpha_s C_F}{\pi}\ln\frac{x_{01}}{\rho}Y] - 1}{\frac{4\alpha_s C_F}{\pi}\ln\frac{x_{01}}{\rho}Y}] \\ = \quad & 1 \end{aligned} \tag{1.96}$$

This is fortunate because the virtual emissions cannot change the inclusive probability of having a dipole which consists of two heavy quarks. We shall now calculate the dipole density in the onium wavefunction and we will show that this leads to the BFKL kernel like in [4].
We define density $n(x_{10}, x, Y)$ such that :

$$N(x, Y) = \int d^2 x_{01} \int_0^1 dz_1 \Phi^{(0)}(x_{01}, z_1) n(x_{01}, x, Y) \tag{1.97}$$

The quantity $N(x, Y)$ is the number density of the dipoles at the transverse size x and the rapidity interval Y. The function $n(x_{01}, x, Y)$ obeys the dipole version of the BFKL equation and it describes the density of dipoles with separation x in the onium with transverse size x_{01}. The equation for the dipole density is as follows,

$$\begin{aligned} n(x_{01}, x, Y) &= x\,\delta(x - x_{01})\exp[-\frac{4\alpha_s C_F}{\pi}\log\frac{x_{01}}{\rho}Y] + \\ &+ \frac{\alpha_s C_F}{\pi^2}\int_R \frac{x_{01}^2 d^2\bar{x}_2}{x_{12}^2 x_{02}^2}\int_0^Y \exp[-\frac{4\alpha_s C_F}{\pi}(Y-y)\log\frac{x_{01}}{\rho}] n(x_{12}, x, Y) \end{aligned} \tag{1.98}$$

and it has been derived from the generating functional Z (1.95) :

$$n(x_{01}, x, Y) = x^2 \int d\phi(\bar{x}) \frac{\delta Z(x_{01}, Y, u)}{\delta u(x)}|_{u=1} \tag{1.99}$$

and $d\phi(\bar{x})$ means that we integrate over possible orientations of the dipole direction $\bar{x}$. Equation (1.98) can be illustrated on the Figure 1.12. One can solve this equation by going to the Mellin space. Define:

$$\tilde{n}(x_{12}, x, \omega) = \int dy e^{-\omega y} n(x_{12}, x, y) \tag{1.100}$$

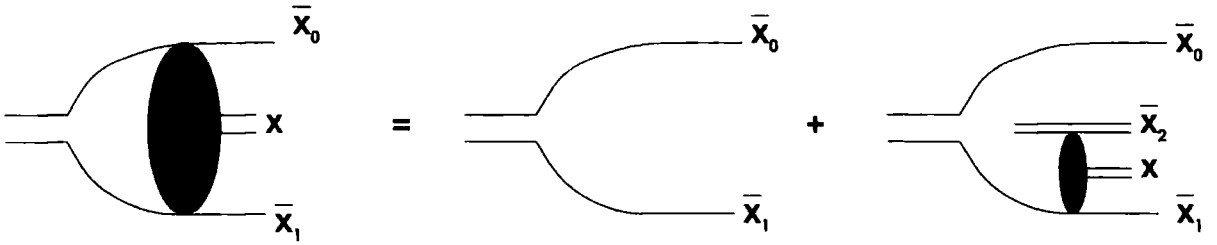

Figure 1.12: Diagrammatic representation of the dipole version of the BFKL equation

Then the equation (1.98) reads,

$$\begin{aligned}\tilde{n}(x_{01},x,\omega) &= \frac{\tilde{n}^{(0)}(x_{01},x,\omega)}{\omega+\frac{4\alpha_s C_F}{\pi}\ln\frac{x_{01}}{\rho}} + \frac{\alpha_s C_F}{\pi^2}\int\frac{d^2\bar{x}_2 x_{01}^2}{x_{12}^2 x_{02}^2}\int_0^\infty dY e^{-\omega Y} \\ &\int_0^Y dy\exp[-\frac{4\alpha_s C_F}{\pi}\log\frac{x_{01}}{\rho}(Y-y)]\,\tilde{n}(x_{12},x,y) \\ &= \frac{\tilde{n}^{(0)}(x_{01},x,\omega)}{\omega+\frac{4\alpha_s C_F}{\pi}\ln\frac{x_{01}}{\rho}} + \frac{\alpha_s C_F}{\pi^2}\frac{1}{\omega+\frac{4\alpha_s C_F}{\pi}\log\frac{x_{01}}{\rho}}\int\frac{d^2\bar{x}_2 x_{01}^2}{x_{12}^2 x_{02}^2}\tilde{n}(x_{12},x,\omega)\end{aligned} \tag{1.101}$$

One can introduce notation for the kernel in this equation,

$$\tilde{K}(x_{12},x_{01}) = \frac{1}{2\pi}\int_\rho dx_{02}\,\mathrm{Jac}\,\frac{x_{01}^2}{x_{12}^2 x_{02}^2} \tag{1.102}$$

where we have made a change of the integration variables, $dx_{02}dx_{12}\,\mathrm{Jac} = d^2\bar{x}_2$. Using this notation (1.102) we get from (1.101),

$$\begin{aligned}\tilde{n}(x_{01},x,\omega)[\omega+\frac{4\alpha_s C_F}{\pi}\ln\frac{x_{01}}{\rho}] &= \tilde{n}^{(0)}(x_{01},x,\omega) \\ &+ \frac{4\alpha_s C_F}{\pi}\int dx_{12}\hat{K}(x_{12},x_{01})\tilde{n}(x_{12},x,\omega)\end{aligned} \tag{1.103}$$

and finally ,

$$\begin{aligned}\tilde{n}(x_{01},x,\omega) &= \frac{\tilde{n}^{(0)}(x_{10},x_1,\omega)}{\omega} + \\ &+ \frac{4\alpha_s C_F}{\pi\omega}\int dx_{12}[\tilde{K}(x_{12},x_{01}) - \ln\frac{x_{01}}{\rho}\delta(x_{01}-x_{12})]\tilde{n}(x_{12},x,\omega)\end{aligned} \tag{1.104}$$

The kernel

$$K(x_{12},x_{01}) = \tilde{K}(x_{12},x_{01}) - \ln\frac{x_{01}}{\rho}\,\delta(x_{01}-x_{12}) \tag{1.105}$$

is equivalent to the BFKL kernel when the ultraviolet cutoff $\rho \to 0$. It has exactly the same eigenvalues,

$$\int dx_{12}\, K(x_{12}, x_{01})\, x_{12}^{\lambda} \;=\; \chi(\lambda)\, x_{10}^{\lambda} \tag{1.106}$$

where the eigenvalue of the kernel is,

$$\chi(\lambda) \;=\; \Psi(1) - \frac{1}{2}\Psi(1-\lambda/2) - \frac{1}{2}\Psi(1+\lambda/2) \tag{1.107}$$

Where Ψ is the Euler Digamma function. Using this result for the kernel eigenvalue (1.107) we can solve the dipole equation (1.104) by making one more Mellin transform, this time in variables x_{01}/x. This enables us to unfold the convolution in the impact parameter variables. We take,

$$\tilde{n}_{\omega}(x_{01}, x) \;=\; \int_C \frac{d\lambda}{2\pi i}\, n_{\omega}^{\lambda} \left(\frac{x_{01}}{x}\right)^{\lambda} \tag{1.108}$$

Now we use this in (1.104) and our dipole equation is,

$$n_{\omega}^{\lambda} \;=\; n_{\omega}^{\lambda(0)} \;+\; \frac{4\alpha_s C_F}{\pi}\chi(\lambda)\, n_{\omega}^{\lambda} \tag{1.109}$$

So the solution to the Mellin transform of the dipole density is,

$$n_{\omega}^{\lambda} \;=\; \frac{n_{\omega}^{\lambda(0)}}{\omega \;-\; \frac{4\alpha_s C_F}{\pi}\chi(\lambda)} \tag{1.110}$$

One can immediately see that the behaviour of the solution n_{ω}^{λ} will be controlled by the pole $\omega_0 \;=\; \frac{4\alpha_s C_F}{\pi}\chi(\lambda)$. We can thus easily perform the integration over ω and our result for the density of dipoles $n(x_{01}, x, Y)$ is as follows,

$$n(x_{01}, x, Y) \;=\; \int_C \frac{d\lambda}{2\pi i}\, n^{(0)}\, \exp\!\left[\frac{4\alpha_s C_F}{\pi}\chi(\lambda)\, Y\right] \left(\frac{x_{01}}{x}\right)^{\lambda} \tag{1.111}$$

We can evaluate this integral because the function $\chi(\lambda)$ has a saddle point at $\lambda = 0$. It has minimum as $-1/2 < \lambda < 1/2$ and a maximum as we move along the imaginary axis.

Let us take $\lambda = i\nu$ and evaluate the integral (1.111),

$$\begin{aligned} n(x_{01}, x, Y) \;&=\; C \int_{-\infty}^{\infty} \frac{d\nu}{2\pi} \left(\frac{x_{01}}{x}\right)^{1+2i\nu} \exp\!\left[\frac{4\alpha_s C_F}{\pi}\chi(i\nu)\, Y\right] \\ &=\; C\frac{x_{01}}{x} \int_{-\infty}^{\infty} \frac{d\nu}{2\pi} \exp\!\left[\frac{4\alpha_s C_F}{\pi}\chi(0) Y + 2i\nu \ln\frac{x_{01}}{x} - \frac{2\alpha_s C_F}{\pi}\nu^2 \chi''(0) Y\right] = \\ &=\; C\frac{x_{01}}{2x} \frac{1}{\sqrt{2\alpha_s C_F \chi''(0) Y}} \exp\!\left[\frac{4\alpha_s C_F}{\pi}\chi(0) Y\right] \exp\!\left[-\frac{\pi \ln^2 \frac{x_{01}}{x}}{2\alpha_s C_F \chi''(0) Y}\right] \end{aligned} \tag{1.112}$$

where C is some constant determined from $n^{(0)}$. The last line of (1.112) is the solution to the density of dipoles in the onium which is controlled by the zero momentum transfer BFKL hard pomeron Δ_P. The first term with exponent describes the rapid growth of dipole desity as rapidity Y becomes large. This growth is controlled by the intercept $\Delta_P = \frac{4\alpha_s C_F}{\pi}\chi(0) = \frac{\alpha_s N_c}{\pi} 4 \ln 2 \simeq 0.5$. Second term with exponent describes the diffusion in transverse variable x. Even when we start with very small perturbative dipoles , we will eventually hit, at large Y, a non-perturbative region where dipoles can get quite large size x. This type of behaviour is typical for the BFKL equation (1.80) and its solution (1.81) . In the tradtional momentum space this means that the difffusion is likely to bring us to the region where the transverse momenta are quite small. Therefore the infrared behaviour of the unintegrated gluon density will play very important role.
The picture of colour dipoles has been already used to describe different processes like: virtual photon collisions with exchange of the BFKL pomeron [21] and diffractive processes [22]. Finally fits to deep inelastic data have been made [23].

1.7 Unitarization and saturation at large rapidities

When $\alpha_s Y$ is much less than 1, then the cross section for scattering between two onia is small. But when $\alpha_s Y$ becomes large then the cross section grows rapidly and the unitarity bound can be violated, see eq. (1.112). In the dipole picture it is quite easy to understand this fact because the onium-onium scattering cross section is proportional to the product of the dipole densities in both onia. It is then obvious that the unitarity is violated when the dipole densities are large. The two onia become essentially black on scattering. However, when there are many dipoles the multiple interactions can occur and they will actually have to be taken into account in order to get the correct result which will not violate the unitarity. The multiple scatterings are dependent on the distribution of the dipoles in two onia. In the normal transverse momentum picture the multiple scaterings of dipoles correspond to the multiple t-channel pomeron exchange diagrams. The detailed numerical calculations including multiple scattering have been performed in [20] and yield unitarized cross section. The idea was to simulate the small x dipole branching producing random dipole configurations. Then the interaction between the pairs of these random configurations were determined. Finally an average over all possible configurations has been taken. The results in [20] indicate an interesting fact that the shadowing corrections have more profound impact on elastic cross section than on the total cross section. This is probably due to the fact that the leading dependence of the amplitude is $1/r^2$ (where r is the impact parameter). Then because the elastic cross section is proportional to the integral of the amplitude squared then it will be more sensitive to the small values of impact parameters that is the space where unitarity corrections are quite large. The total cross section is proportional to the amplitude therefore due to diffusion in the BFKL will probe much larger space of impact parameters and the shadowing corrections will switch on much later.

Chapter 2

Towards the unified BFKL and DGLAP description

So in addition to what is asked about, an inquiry has that which is interrogated. In investigative questions - that is in questions which are specifically theoretical - what is asked about is determined and conceptualized. Furthermore, in what is asked about there lies also that which is to be found out by the asking; this is what is really intended: with this the inquiry reaches its goal.

- M. Heidegger

2.1 Introduction

In the sections 1.5 and 1.6 we have introduced and discussed two types of evolution equations which can be used to evaluate the parton distributions at different scales. In principle both approaches are designed to work well in two different kinematic regimes, see Figure 1.1. The renormalisation group approach is basically summing up the logarithms of the hard scale Q^2 and does not care about possible novel low x effects. On the other hand the BFKL equation does indeed sum the powers $\ln(1/x)$ in LO and NLO approximation, however it is valid in the region where Q^2 scales are moderate. The strong rise of F_2 at HERA with decreasing x would suggest the presence of the BFKL pomeron. However, it could be equally well described with DGLAP equations by choosing the appropriate input for the distribution functions and the sufficiently low value for the initial scale Q_0^2 (see eq. (1.76) and the disscusion there). Several descriptions based on global data analysis and renormalisation group equations are available at present: MRS [11], CTEQ [12], GRV [13]. Further studies [24] based on LO BFKL have shown that it generates too steep rise and therefore is likely to be excluded by the data. This approach however involved parametrisation of the unintegrated gluon distribution function in the strictly non-perturbative region and it is well known that BFKL predictions can be very sensitive on the form of this parametrisation. We will not try to judge

which one of these two approaches is correct but rather concentrate ourselves on the unification of these two. Since BFKL and DGLAP resum different contributions at certain approximation they are both incomplete and their unification would exhaust most of our knowledge about the perturbative phenomena whilst minimising the parametrisation for the non-perturbative part. We shall first start with the demonstration that at the leading twist level the BFKL k_T factorization approach can be reduced to the conventional collinear factorization of the renormalisation group in which the anomalous dimensions and coefficient functions are extended to include the full resummation of leading $\ln(1/x)$ terms [25, 26, 27]. This will enable us to gain more detailed insight which contributions are included in the evolution equations and what are the common parts of both DGLAP and BFKL approaches. It will prevent us from possible double counting when building up the framework of unified evolution equations.

2.1.1 k_T versus collinear factorisation and the anomalous dimension of the gluon

In the section 1.6 of the previous chapter we have disscussed the BFKL equation for the unintegrated gluon distribution function $f(x,k^2)$ (1.80). But we didn't specify how to calculate the observable structure functions from this type of parton distribution. The connection between the unintegrated gluon distribution and the observable structure functions F_i is given in terms of the so called k_T *factorisation* or *high energy factorisation* formula [25], see Figure 2.1,

$$F_i(x,Q^2) = \int_x^1 \frac{dz}{z} \int \frac{dk^2}{k^2} F_i^{\rm box}(z,k^2,Q^2)\, f\left(\frac{x}{z},k^2\right) \tag{2.1}$$

Here, $f(x,k^2)$ is the solution of the BFKL equation (1.80) and $F_i^{\rm box}$ are the partonic cross sections for the process $gV \to q\bar{q}$, where the gluon g is off-shell. At lowest order they are determined by the quark box (a) (and crossed box (b)) contributions, Figure 2.2. In order to see the connection between the k_T factorisation and the collinear approach (1.57), we will use the Mellin transform technique well known already from previous sections. For simplicity we assume that the coupling α_S is fixed and that the quarks are massless. This of course is only an approximation, however it will give us reasonable qualitative results. After making these assumptions the functions $F_i^{\rm box}$ are only functions of the ratio Q^2/k^2. In terms of moments in z the k_T factorisation formula (2.1) will give,

$$\overline{F}_i(\omega,Q^2) = \int \frac{dk^2}{k^2} \overline{F}_i^{\rm box}(\omega,Q^2/k^2)\, \overline{f}(\omega,k^2). \tag{2.2}$$

We may again factorise this equation by taking Mellin moments in k^2 variable. We find,

$$\overline{F}_i(\omega,Q^2) = \frac{1}{2\pi i} \int_{c-i\infty}^{c+i\infty} d\gamma \tilde{F}_i^{\rm box}(\omega,\gamma)\tilde{f}(\omega,\gamma)(Q^2)^\gamma \tag{2.3}$$

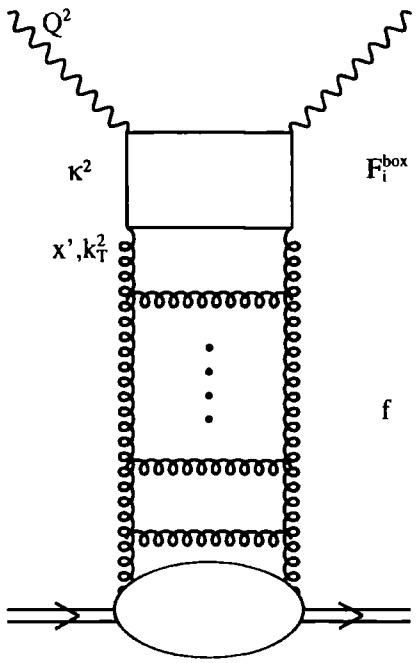

Figure 2.1: Diagrammatic representation of the high energy factorisation.

with $c = 1/2$. We remind that the double moments $\tilde{F}$ and $\tilde{f}$ are defined here as,

$$\begin{aligned} \tilde{F}_i^{\rm box}(\omega,\gamma) &= \int d\left(\frac{Q^2}{k^2}\right)\left(\frac{Q^2}{k^2}\right)^{-\gamma-1} \overline{F}_i^{\rm box}(\omega, Q^2/k^2) \\ \tilde{f}(\omega,\gamma) &= \int dk^2\,(k^2)^{-\gamma-1}\,\overline{f}(\omega,k^2) \end{aligned} \tag{2.4}$$

The representation defined by formulae (2.2), (2.3), (2.4) indicates that if we know the analytic properties of the solution $\tilde{f}$ and the cross section $\tilde{F}_i^{\rm box}$ in the complex plane of Mellin variable γ then we will be able to determine the behaviour with Q^2 of the structure function $\overline{F}_i(\omega, Q^2)$.

The function $\tilde{f}(\omega,\gamma)$ satisfies the BFKL equation and hence it is given by the solution of the similar form as that one found previously for the dipole density (1.110)

$$\tilde{f}(\omega,\gamma) = \frac{\tilde{f}^{(0)}(\omega,\gamma)}{1-\frac{\bar{\alpha}_s}{\omega}\chi(\gamma)} \tag{2.5}$$

where we have defined $\bar{\alpha}_s = \frac{N_C\alpha_s}{\pi}$. Here $\tilde{f}^{(0)}(\omega,\gamma)$ is the double Mellin transform of the inhomogenious term of the BFKL equation. It can be shown that the kernel can have an expansion in terms of series in γ of the following form, (for example using

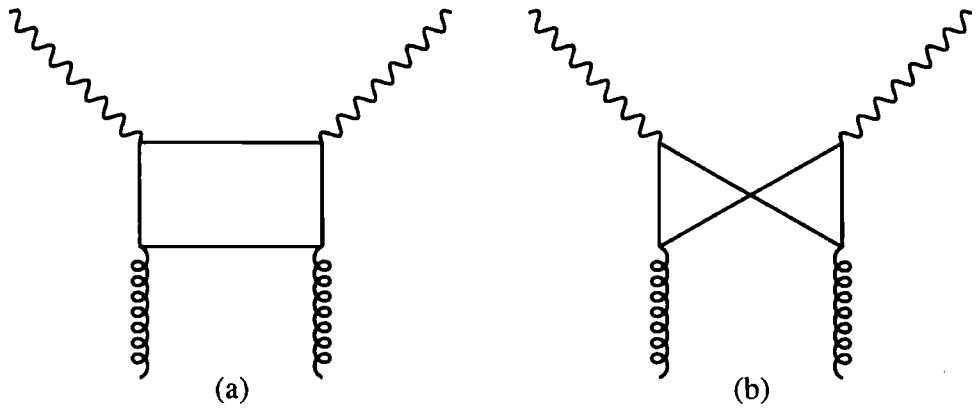

Figure 2.2: Diagrams contributing to the partonic cross section $Vg \to q\bar{q}$.

expansions for digamma functions from [28])

$$\chi(\gamma) = 2\Psi(1) - \Psi(\gamma) - \Psi(1-\gamma) = \frac{1}{\gamma}[1 + \sum_{n}^{\infty} 2\zeta(2n+1)\gamma^{2n+1}] \tag{2.6}$$

where ζ is the Riemann zeta function. The dominant pole of equation (2.5) arises from the zero in the denominator,

$$\frac{1}{1 - \frac{\bar{\alpha}_s}{\omega}\chi(\gamma)} = \frac{\gamma R}{\gamma - \bar{\gamma}} \tag{2.7}$$

As solution for $\bar{\gamma}$ and R we get, using (2.6)

$$\begin{aligned} \bar{\gamma} &= \frac{\bar{\alpha}_s}{\omega} + 2\zeta(3)(\frac{\bar{\alpha}_s}{\omega})^4 + 2\zeta(5)(\frac{\bar{\alpha}_s}{\omega})^6 + \ldots \\ R &= \left(1 - \frac{\bar{\alpha}_s}{\omega}\frac{d(\gamma\chi)}{d\gamma}|_{\gamma=\bar{\gamma}}\right)^{-1} \end{aligned} \tag{2.8}$$

We interpret $\bar{\gamma}$ as a leading twist anomalous dimension of the gluon density. We can insert now (2.8) into the formula for the structure function (2.3) and close the contour in the left half plane. In that way we obtain the leading behaviour at high values of Q^2,

$$\bar{F}_i(\omega, Q^2) = \tilde{F}_i^{\text{box}}(\omega, \bar{\gamma})\bar{\gamma}R(\frac{\bar{\alpha}_s}{\omega})\tilde{f}^{(0)}(\omega, \gamma)(Q^2)^{\bar{\gamma}} \tag{2.9}$$

If we define:

$$\begin{aligned} C_i^{\text{box}}(\omega, \bar{\gamma}) &\equiv \bar{\gamma}\,\tilde{F}_i^{\text{box}}(\omega, \bar{\gamma})\,R(\bar{\alpha}_s/\omega) \\ g(\omega, Q^2) &\equiv (Q_0^2)^{\bar{\gamma}}\,\tilde{f}^{(0)}(\omega, \bar{\gamma})\left(\frac{Q^2}{Q_0^2}\right)^{\bar{\gamma}} \end{aligned} \tag{2.10}$$

then we have apparently reduced the k_T factorisation into the collinear form, see (1.57):

$$\bar{F}_i(\omega, Q^2) \;=\; C_i(\omega, \bar{\gamma})\, g(\omega, Q^2) \tag{2.11}$$

Where $C_i(\omega, \bar{\gamma})$ are the perturbative coefficient functions which happen to be connected to the Mellin moments of the partonic cross-section for $gV \to q\bar{q}$ and function $g(\omega, Q^2)$ is the integrated gluon density which evolves with Q^2 according to the leading anomalous dimension $\bar{\gamma}$. This factorisation formula is correct when we are considering longitudinal structure function F_L. $\bar{F}_L^{\rm box}$ is constant at large values of Q^2/k^2 and therefore $\tilde{F}_L^{\rm box}(\omega, \gamma) \sim 1/\gamma$. This singularity is cancelled by γ in the numerator of formula (2.7). But on the other hand the $\bar{F}_2^{\rm box} \to \log(Q^2/k^2)$ and thus we get $\tilde{F}_2^{\rm box} \sim 1/\gamma^2$ and together with (2.7) this gives the pole $1/\gamma$ for the structure function $\tilde{F}_2$. This additional pole at $\gamma = 0$ gives the contribution to structure function F_2 which is independent of Q^2 and therefore it is a scaling part. In order to be able to study the behaviour of the perturbative part arising from the pole at $\gamma = \bar{\gamma}$ we have to consider the derivative of $\bar{F}_2$,

$$Q^2 \frac{\partial \bar{F}_2(\omega, Q^2)}{\partial Q^2} \;=\; \alpha_s \sum_q e_q^2 \bar{P}_{qg}(\omega, \bar{\gamma})\, g(\omega, Q^2) \tag{2.12}$$

where we can identify the moment of the P_{qg} splitting function to be

$$\frac{\alpha_S}{2\pi} \bar{P}_{qg}(\omega, \alpha_S) = \bar{\gamma}^2(\bar{\alpha}_S, \omega) \tilde{F}_2^{\rm box}\left(\omega, \bar{\gamma}(\bar{\alpha}_S, \omega)\right) \tag{2.13}$$

in the so-called Q_0^2 regularization and DIS scheme [25] which we implicitly adopt here.

In the leading $\ln(1/x)$ approximation we have

$$\frac{\alpha_S}{2\pi} \bar{P}_{qg}(\omega, \alpha_S) = (\bar{\gamma})^2 \tilde{F}_2^{\rm box}\left(\omega = 0, \bar{\gamma}\right). \tag{2.14}$$

The leading logarithmic expansion for the anomalous dimension $\bar{\gamma}$ has the form calculated previously (2.8),

$$\bar{\gamma}\left(\frac{\bar{\alpha}_S}{\omega}\right) \;=\; \sum_{n=1}^{\infty} c_n \left(\frac{\bar{\alpha}_S}{\omega}\right)^n \tag{2.15}$$

which in turn gives for the splitting function P_{gg}

$$z P_{gg}(z, \alpha_S) = \sum_{n=1}^{\infty} c_n \frac{[\bar{\alpha}_S \ln(1/z)]^{n-1}}{(n-1)!}, \tag{2.16}$$

whereas representation (2.14) generates the following expansion of the splitting function $P_{qg}(z, \alpha_S)$ at small z

$$z P_{qg}(z, \alpha_S) \;=\; z P_{qg}^{(0)}(z) + \bar{\alpha}_s \sum_{n=1}^{\infty} b_n \frac{[\bar{\alpha}_S \ln(1/z)]^{n-1}}{(n-1)!}. \tag{2.17}$$

The first term on the right hand side vanishes at $z = 0$. It should be noted that the splitting function P_{qg} is formally non-leading at small z when compared with the splitting function P_{gg} because it has additional power of $\bar{\alpha}_s$. For moderately small values of z however, when the first few terms in the expansions (2.16) and (2.17) dominate, the BFKL effects can be much more important in P_{qg} than in P_{gg}. This comes from the fact that all coefficients b_n in (2.17) are different from zero, and relatively large, while in (2.16) we have $c_2 = c_3 = 0$ [29]. The small x resummation effects within the conventional QCD evolution formalism have been discussed in refs. [30, 31, 32, 33, 34]. These studies already emphasize this point, namely that at the moderately small values of x which are relevant for the HERA measurements, the $\ln(1/x)$ resummation effects in the splitting function P_{qg} have a much stronger impact on F_2 than do those in the splitting function P_{gg}. In particular we should also recall that the BFKL effects in the splitting function P_{qg} can significantly affect the extraction of the gluon distribution from the experimental data on the slope of the structure function F_2

$$Q^2 \frac{\partial F_2(x,Q^2)}{\partial Q^2} = \sum_q e_q^2 \frac{\alpha_S(Q^2)}{2\pi} \int_x^1 dz P_{qg}(z, \alpha_S(Q^2)) \frac{x}{z} g\left(\frac{x}{z}, Q^2\right). \qquad (2.18)$$

Different P_{qg} calculated within various perturbative frameworks will result in a different gluon distribution functions. This is a direct consequence of the factorisation prescription and shows again that the parton densities are not directly observable quantities. We shall come back to the point of the resummation in P_{gg} and P_{qg} in the section with numerical results.

Here we also include the subleading $\ln(1/x)$ terms which would come from the subleading terms in γ_{gg} etc. Keeping the exact k_T factorisation (and not just its large Q^2 limit) we also include the non-leading twist contributions to F_2. They would formally be generated by the contributions given by the anomalous dimensions at non-leading twist .

We should also note that the expansion of the type (2.16) is well behavied in the sense that the potential big terms $(\ln 1/z)^n$ which would occur at small z are regularised by the factorial term in the denominator of the expansion (2.16).

In this paragraph we have therefore shown that the k_T factorisation formula can be recast into the collinear form familiar from the renormalisation group equations. In this case the leading logarithmic effects $\ln(1/x)$ have been resummed in the perturbative coefficient functions C_i and the anomalous dimensions γ_{ij} which are just Mellin transforms of the splitting functions P_{ij}. In order to build the unified picture of BFKL and DGLAP equations we need to resum also the remaining DGLAP terms in the P_{gg} splitting function.

2.2 Unified BFKL and DGLAP equation for the gluon

We recall here for the convenience the standard form of the LO BFKL (1.80) equation for the unintegrated gluon distribution,

$$f(x,k^2) = f^{(0)}(x,k^2) + \overline{\alpha}_S k^2 \int_x^1 \frac{dz}{z} \int \frac{dk'^2}{k'^2} \left\{ \frac{f(x/z,k'^2) - f(x/z,k^2)}{|k'^2 - k^2|} + \frac{f(x/z,k^2)}{[4k'^4 + k^4]^{\frac{1}{2}}} \right\} \tag{2.19}$$

where $\overline{\alpha}_S = N_c \alpha_S/\pi$ and $k \equiv k_T, k' \equiv k'_T$ denote the transverse momenta of the exchanged gluons.

In order to make the BFKL equation for the gluon more realistic and to extend its validity to cover the full range of x we make the following modifications:

- **First**: we allow for the running coupling which is already a pure NLO correction to LO BFKL equation. The way to make the α_s run in the LO BFKL is of course arbitrary, we choose here to leave α_s outside the integration over momentum k^2.

- **Second**: to incorporate leading order DGLAP evolution, we add on to the right-hand side of (2.19) the following term,

$$\overline{\alpha}_S(k^2) \int_x^1 \frac{dz}{z} \left(\frac{z}{6} P_{gg}(z) - 1 \right) \frac{x}{z} g\left(\frac{x}{z}, k^2\right) \equiv \overline{\alpha}_S(k^2) \int_x^1 \frac{dz}{z} \left(\frac{z}{6} P_{gg}(z) - 1 \right) \left\{ \frac{x}{z} g\left(\frac{x}{z}, k_0^2\right) + \int_{k_0^2}^{k^2} \frac{dk'^2}{k'^2} f\left(\frac{x}{z}, k'^2\right) \right\}, \tag{2.20}$$

  where we have used the formula connecting the integrated with the unintegrated gluon distribution function (1.77). We have to subtract –1 in (2.20), because this leading term α_s/z is already included in the BFKL part. The inclusion of the additional term (2.20) gives contributions to the gluon anomalous dimension γ_{gg} which are subleading in $\alpha_s \ln(1/x)$ but leading in α_s. These standard leading order DGLAP contributions have an impact on the overall normalisation of the unintegrated gluon distribution. They do also lower the value of the hard pomeron intercept (see subsection 2.2.1). Note, that we have introduced here a non-perturbative input $xg(x,k_0^2)$. We shall choose some simple parametrisation for this term and tune the free parameters in order to be able to fit the data.

- **Third**: we impose the *consistency constraint* on the BFKL equation which mimics the resummation of the subleading corrections in $\ln(1/x)$. The above

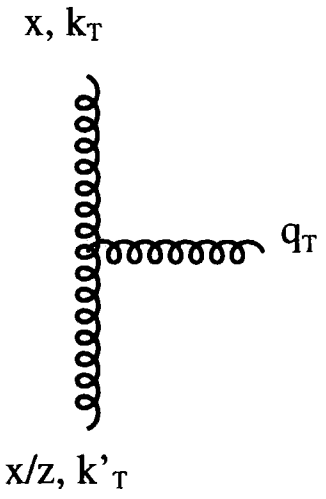

Figure 2.3: Kinematic variables used to derive the consistency constraint.

BFKL equation is given in the leading logarithmic approximation which as we have seen already earlier, yields quite a significant rise of the structure function at small x. The $\ln(1/x)$ resummation has recently been carried out [15] at next-to-leading order (NLO). It is found to give a very large $O(\alpha_S^2)$ correction to the hard pomeron intercept λ,

$$\lambda \simeq \overline{\alpha}_S 4 \ln 2(1 - 6\overline{\alpha}_S), \tag{2.21}$$

which implies that the NLO approximation only, is unreliable for realistic values of α_S. Rather we must use a formalism which contains an estimate of an all-order resummation. Clearly it would be desirable to identify physical effects which could be resummed to all orders and which at the same time yield a NLO value of λ that is comparable to (2.21). As it happens the imposition of the consistency constraint [35, 36]

$$k'^2 < k^2/z \tag{2.22}$$

on the real gluon emission term gives just such an effect. The variables are shown on Fig. 2.3. The origin of this constraint is the requirement that the virtuality of the exchanged gluon is dominated by its transverse momentum $|k'^2| \simeq k_T'^2$. In the derivation of the BFKL equation one assumes the multi-Regge kinematics. This configuration forces the longitudinal components of the exchanged particles in the t-channel to be small and therefore only transverse components can dominate the overall particle's momentum. We sketch the derivation of the consistency constraint following [35].

We use here the light cone decomposition of the momenta,

$$\begin{aligned} k^\mu &= (k^+, k^-, k_T) \\ k^2 &= k^+ k^- - k_T^2 \end{aligned} \tag{2.23}$$

Because $k^2 \simeq k_T^2$, we immediately have $|k_T^2| > |k^+k^-|$. From figure 2.3 we see that,

$$k^- = k'^- - q^- \simeq -q^- \tag{2.24}$$

Because the emitted gluon is on-shell we have the following relation,

$$q^+q^- = q_T^2 \Rightarrow q^- = \frac{q_T^2}{q^+} = \frac{q_T^2}{k'^+ - k^+} \tag{2.25}$$

Using (2.24) and (2.25) we get,

$$k^+k^- \simeq -\frac{k^+q_T^2}{k'^+ - k^+} = -\frac{z}{1-z}q_T^2 \tag{2.26}$$

where we have used the fact that $k^+ = xp$ and $k'^+ = x/zp$.

So we immediately get the constraint,

$$k_T^2 > \frac{zq_T^2}{1-z} \tag{2.27}$$

In our calculation we have however used different form of the constraint $k_T^2 > zk_T'^2$ which follows from (2.27) when z is small and because high values of momentum q_T^2 imply also high values of $k_T'^2$ at the same time. Thus we have that $k_T'^2 \simeq q_T^2$.

If condition (2.22) is imposed on the BFKL equation (2.19) it can be still solved analytically. The result is an all-order effect, which at NLO gives the large modification

$$\lambda \simeq \overline{\alpha}_S 4 \ln 2(1 - 4.2\overline{\alpha}_S) \tag{2.28}$$

of the LO value. However it is found that the all-order correction is a much milder modification, although still significant. A related result can be found in ref. [16]. We can therefore make the BFKL equation (2.19) for the gluon much more realistic by imposing the consistency condition (2.22). We will show this effect in the next subsection when we study the solution of the unifed equation for the gluon in the anomalous dimension space.

- **Fourth**: we notice that the integration region over k'^2 in (2.19) extends down to $k'^2 = 0$ where we expect that non-perturbative effects will affect the behaviour of $f(x, k'^2)$. We are only going to solve equation (2.19) in the perturbative region, defined by $k^2 > k_0^2$, so we only have to worry about the infrared contribution due to the real emission term from the interval $0 < k'^2 < k_0^2$. We may rewrite this infrared contribution in the form

$$k^2 \int_0^{k_0^2} \frac{dk'^2}{k'^2|k'^2 - k^2|} f\left(\frac{x}{z}, k'^2\right) \simeq \int_0^{k_0^2} \frac{dk'^2}{k'^2} f\left(\frac{x}{z}, k'^2\right) \equiv \frac{x}{z} g\left(\frac{x}{z}, k_0^2\right). \tag{2.29}$$

The parameter $k_0^2 \sim 1$ GeV^2 denotes the border between the perturbative and non-perturbative regions. Its magnitude will be taken to be around 1GeV^2.

This procedure seems to work better than the one proposed in [24] since we avoid the parametrisation of $f(x,k^2)$ below the scale $k^2 < k_0^2$. BFKL equation (as noted before in the introduction) can get quite a lot of contribution from the infrared region and the evolution can be affected very dramatically as we change this input.

- **Fifth**: finally we must of course add to the right-hand side of (2.19) the term which allows the quarks to contribute to the evolution of the gluon, that is

$$\frac{\alpha_S(k^2)}{2\pi}\int_x^1 dz P_{gq}(z)\Sigma\left(\frac{x}{z},k^2\right) \tag{2.30}$$

where Σ is the singlet quark momentum distribution. This term is numerically small as compared to the rest but has to be included in order that our constructed unifed equations will be compatible with DGLAP in the strong ordering configuration of k_T. To be explicit, we define as singlet:

$$\begin{aligned}\Sigma(x,k^2) &= \sum_{q=u,d,s} x(q+\bar{q}) + x(c+\bar{c}) \\ &\equiv V(x,k^2) + S_{uds}(x,k^2) + S_c(x,k^2)\end{aligned} \tag{2.31}$$

where V, S_{uds} and S_c denote the valence, the light sea quark and the charm quark sea contributions respectively. We discuss the evolution equation for $\Sigma(x,k^2)$ in section 2.3 .

Gathering together all the above modifications, equation (2.19) for the gluon becomes

$$\begin{aligned}f(x,k^2) &= \tilde{f}^{(0)}(x,k^2) + \\ &+\bar{\alpha}_S(k^2)k^2\int_x^1\frac{dz}{z}\int_{k_0^2}\frac{dk'^2}{k'^2}\left\{\frac{f\left(\frac{x}{z},k'^2\right)\Theta\left(\frac{k^2}{z}-k'^2\right)-f\left(\frac{x}{z},k^2\right)}{|k'^2-k^2|}+\frac{f\left(\frac{x}{z},k^2\right)}{[4k'^4+k^4]^{\frac{1}{2}}}\right\} \\ &+\bar{\alpha}_S(k^2)\int_x^1\frac{dz}{z}\left(\frac{z}{6}P_{gg}(z)-1\right)\int_{k_0^2}^{k^2}\frac{dk'^2}{k'^2}f\left(\frac{x}{z},k'^2\right)+\frac{\alpha_S(k^2)}{2\pi}\int_x^1 dz P_{gq}(z)\Sigma\left(\frac{x}{z},k^2\right),\end{aligned} \tag{2.32}$$

where now the driving term has the form

$$\tilde{f}^{(0)}(x,k^2) = f^{(0)}(x,k^2) + \frac{\alpha_S(k^2)}{2\pi}\int_x^1 dz P_{gg}(z)\frac{x}{z}g\left(\frac{x}{z},k_0^2\right). \tag{2.33}$$

In (2.32) we include the cutoff $k'^2 > k_0^2$ on the virtual, as well as the real, contributions in order to avoid spurious singularities at $k^2 = k_0^2$. In the perturbative region, $k^2 > k_0^2$, we may safely neglect the genuinely non-perturbative contribution

$f^{(0)}(x,k^2)$ which is expected to decrease strongly with increasing k^2. It is important to note once more that we have avoided the necessity to parametrize $f(x,k^2)$ in the non-perturbative region. Equation (2.32) only involves $f(x,k^2)$ in the perturbative domain, $k^2 > k_0^2$. The input (2.33) is provided by the conventional integrated gluon $xg(x,k^2)$ at the scale k_0^2. That is the input to our 'unified BFKL + DGLAP' equation is determined by the same distribution as in conventional DGLAP evolution. Surprisingly, we find that we can achieve an excellent description of all deep inelastic data using the most economical parametrization of the input gluon

$$xg(x,k_0^2) \;=\; N(1-x)^{\beta}.$$

In particular the observed growth in $F_2(x,Q^2)$ with decreasing x is generated entirely by *perturbative* ($\ln(1/x)$ and $\ln Q^2$) dynamics.

It is easy to see how eq. (2.32) reduces to the conventional DGLAP evolution equation for the gluon in the leading $\ln Q^2$ (or rather $\ln k^2$) approximation. The leading $\ln k^2$ terms arise from the strongly ordered configuration, $k_0^2 \ll k'^2 \ll k^2$, for the real emission contributions. In the leading $\ln k^2$ approximation we also neglect the virtual contributions. Then (2.32) becomes

$$f(x,k^2) \;=\; \frac{\alpha_S(k^2)}{2\pi}\int_x^1 dz\, P_{gg}(z)\left[\frac{x}{z}\,g\left(\frac{x}{z},k_0^2\right) + \int_{k_0^2}^{k^2}\frac{dk'^2}{k'^2}\,f\left(\frac{x}{z},k'^2\right)\right] \tag{2.34}$$

$$+\,\frac{\alpha_S(k^2)}{2\pi}\int_x^1 dz P_{gq}(z)\Sigma\left(\frac{x}{z},k^2\right),$$

where we have taken into account (2.33) and the remarks concerning the omission of $f^{(0)}$. Using the integrated gluon distribution we see that (2.34) becomes

$$k^2\frac{\partial(xg(x,k^2))}{\partial k^2} \;=\; \frac{\alpha_S(k^2)}{2\pi}\int_x^1 dz\left[P_{gg}(z)\frac{x}{z}\,g\left(\frac{x}{z},k^2\right) + P_{gq}(z)\Sigma\left(\frac{x}{z},k^2\right)\right], \tag{2.35}$$

which is simply the conventional DGLAP evolution equation for the gluon.

2.2.1 Solution of the generalised BFKL-DGLAP equation for the gluon

We will study now the properties of the equation (2.32) in ω and γ space using techniques presented in subsection 2.1.1. In the case of fixed α_s and without the contribution from the quarks (which is numerically small anyway) we rewrite the equation (2.32) in the moment space ω,

$$\overline{f}(\omega,k^2) \;=\; \overline{f}^{(0)}(\omega,k^2) + \frac{\overline{\alpha}_S(k^2)}{\omega}\,k^2\int_{k_0^2}^{\infty}\frac{dk'^2}{k'^2}$$

$$\left\{ \frac{\overline{f}(\omega,k'^2)\left[\Theta(k^2-k'^2) + (k^2/k'^2)^{\omega}\,\Theta(k'^2-k^2)\right] - \overline{f}(\omega,k^2)}{|k'^2-k^2|} + \frac{\overline{f}(\omega,k^2)}{(4k'^4+k^4)^{\frac{1}{2}}} \right\}$$

$$+ \overline{\alpha}_S(k^2)\,P(\omega)\int_{k_0^2}^{k^2}\frac{dk'^2}{k'^2}\overline{f}(\omega,k'^2) \tag{2.36}$$

where $P(\omega)$ is the moment function of the gluon splitting function $(zP_{gg}(z)/6-1)$ with subtraction of the leading term in $1/z$. The term in square brackets in (2.36) is due to the kinematic constraint. Without this constraint we would have 1 instead of $(k^2/k'^2)^{\omega}$, and the two Θ functions would simply sum to unity. For large k^2 the moment function behaves as

$$\overline{f}(\omega,k^2) \sim \left(\frac{k^2}{k_0^2}\right)^{\gamma_{gg}(\omega,\overline{\alpha}_S)} \tag{2.37}$$

where, for illustration, we take fixed α_S. The quantity γ_{gg} is as before the anomalous dimension of the gluon but this time calculated from the generalised evolution equation 'corrected' with DGLAP term and the consistency constraint (2.22) . If we now go to γ space and perform yet another Mellin transform as before we get the following implicit equation for γ_{gg}

$$1 - \frac{\overline{\alpha}_S}{\omega}K(\gamma_{gg},\omega) - \frac{\overline{\alpha}_S}{\gamma_{gg}}P(\omega) = 0 \tag{2.38}$$

where K, the double moment of the kernel in (2.38), is given by

$$K(\gamma,\omega) = \int_0^{\infty}\frac{d\rho}{\rho}\left\{\frac{[\rho^{\gamma}\Theta(1-\rho)+\rho^{\gamma-\omega}\Theta(\rho-1)]-1}{|\rho-1|} + \frac{1}{[4\rho^2+1]^{\frac{1}{2}}}\right\}. \tag{2.39}$$

which happens to be equal to

$$K(\gamma,\omega) = 2\Psi(1) - \Psi(\gamma) - \Psi(1-\gamma+\omega) \tag{2.40}$$

Of course when we take $\omega = 0$ then the kernel $K(\gamma,\omega)$ will reduce to the ordinary LO BFKL kernel $\chi(\gamma)$, see (2.6). It is clear that γ_{gg}, which satisfies (2.38), is of the form

$$\gamma_{gg}(\omega,\overline{\alpha}_S) = \gamma^{\mathrm{BFKL}}\left(\frac{\overline{\alpha}_S}{\omega}\right) + \overline{\alpha}_S\,P(\omega) + \text{higher order terms}, \tag{2.41}$$

where γ^{BFKL} satisfies the usual LO equation

$$1 - \frac{\overline{\alpha}_S}{\omega}K\left(\gamma^{\mathrm{BFKL}},\omega=0\right) = 0. \tag{2.42}$$

and we have

$$K(\gamma^{BFKL},\omega=0) = \chi(\gamma). \tag{2.43}$$

where $\chi(\gamma)$ is as before eigenvalue of the LO kernel (2.6). The higher order terms include contributions which are subleading in $\overline{\alpha}_S/\omega$ as well as in $\overline{\alpha}_S$. This is illustrated

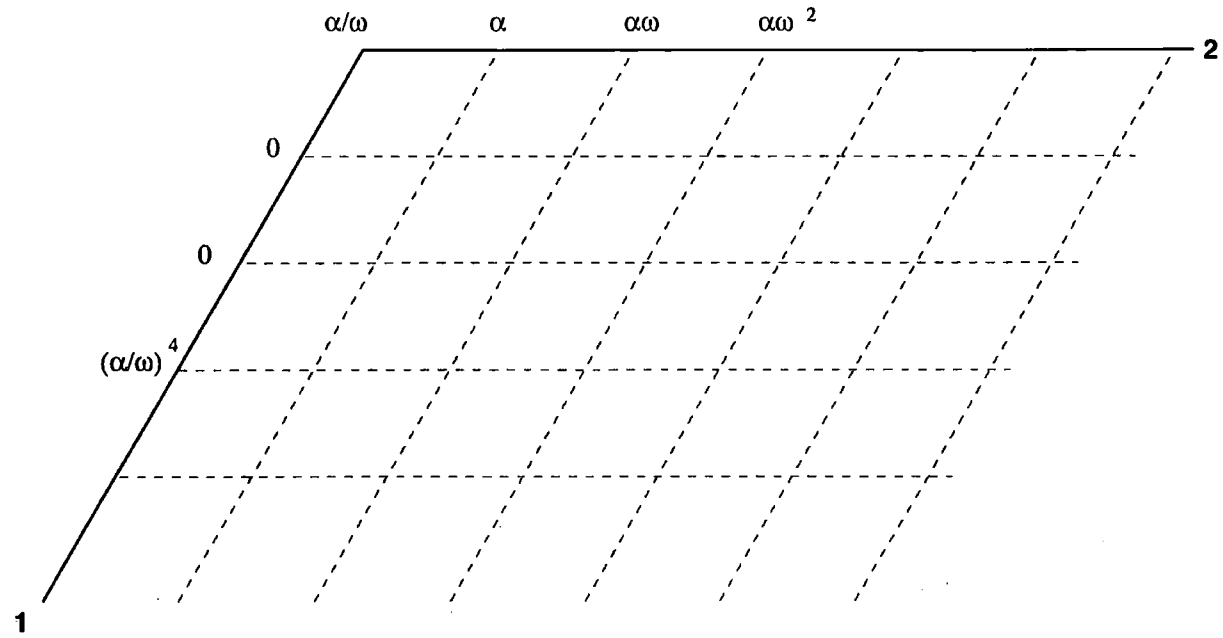

Figure 2.4: Schematic representation of the anomalous dimension plane. Resummation of leading $\ln(1/x)$ effects is performed along path 1 and the leading α effects along path 2. Points at the crossing of the dashed lines correspond to the unknown subleading effects.

in Figure 2.4 where the $\bar{\alpha}_s/\omega$ terms are being resummed along the path labeled 1 and the DGLAP ones are summed along path 2. One should note that there is a common point α_s/ω and therefore we had put -1 in the DGLAP parts in order to avoid double counting. The subleading corrections correspond to the points in the middle region of the plane shown in Figure 2.4. Let us first see what is the effect of DGLAP terms on the evolution. That is we consider the equation:

$$1 - \frac{\bar{\alpha}_s}{\omega}\chi(\gamma) - \frac{\bar{\alpha}_s}{\gamma}P(\omega) = 0 \tag{2.44}$$

where our modifed splitting function $P(\omega)$ has the following form of,

$$P(\omega) = -\frac{1}{\omega+1} + \frac{1}{\omega+2} - \frac{1}{\omega+3} - \Psi(\omega+2) - \gamma_E + \frac{11}{12} - \frac{N_f}{18} \tag{2.45}$$

Singularity defined by equation (2.44) is a pinch singularity therefore we require that also the derivative of this expression should be equal to zero,

$$-\frac{\bar{\alpha}_s}{\omega}\frac{d}{d\gamma}\chi(\gamma) + \frac{\bar{\alpha}_s}{\gamma^2}P(\omega) = 0. \tag{2.46}$$

We can rewrite these two equations, (2.44), (2.46), in the following form,

$$\begin{aligned} \omega P(\omega) &= \gamma^2 \frac{d}{d\gamma}\chi(\gamma) \\ \omega &= \bar{\alpha_s}[\chi(\gamma) + \gamma\frac{d}{d\gamma}\chi(\gamma)] \end{aligned} \tag{2.47}$$

This set of equations will give us the solutions for γ and ω as functions of the coupling constant $\bar{\alpha}_s$. In Figures 2.5 and 2.6 we illustrate the results (marked as dashed lines) for the intercept ω and the anomalous dimension γ. We see that the intercept is lowered as compared to the pure LO BFKL $\omega_0 = 4\log 2\bar{\alpha}_s$ which is marked as a dotted-dashed line. This confirms previous results found in [37]. It also has the effect on the anomalous dimension γ and makes it lower as compared to the leading value $\gamma_0 = 1/2$.

Next, we include the consistency constraint and study the full equation (2.38). We consider two coupled equations for ω and γ.

$$\begin{aligned} 1 &= \frac{\bar{\alpha}_s}{\omega}K(\gamma,\omega) + \frac{\bar{\alpha}_s}{\gamma}P(\omega) \\ \omega P(\omega) &= \gamma^2\frac{d}{d\gamma}K(\gamma,\omega) \end{aligned} \tag{2.48}$$

where $K(\gamma,\omega)$ is the kernel of the form (2.40) with the consistency constraint imposed.

The results for $\gamma(\bar{\alpha}_s)$ and $\omega(\bar{\alpha}_s)$ are shown on Figures 2.5 and 2.6 as solid lines. We see that the imposition of the consistency constraint has the effect of lowering the value of the intercept ω, even lower as compared to DGLAP terms, yet it is a stable solution. Namely, it does not give unphysical negative value of the intercept as it happens when one considers only the NLO corrections. This is the consequence of the fact that the consistency constraint together with additional DGLAP terms generate resummation of the major part of the subleading $\ln 1/x$ terms. The anomalous dimension in that case is bigger than $1/2$ which results in the faster (as compared to LO solution) evolution in transverse momentum k^2 of the unintegrated gluon distribution function. It generates in turn stronger scaling violations of the low x observables, like the F_2 etc.
We can identify the NLL terms which come from consistency constraint and the DGLAP part. Let us rewrite the equation (2.38) in the following way,

$$1 - \frac{\bar{\alpha}_s}{\omega}\tilde{K}(\gamma,\omega) = 0 \tag{2.49}$$

where the full kernel is now:

$$\tilde{K}(\gamma,\omega) = 2\Psi(1) - \Psi(\gamma) - \Psi(1-\gamma+\omega) + \frac{\omega}{\gamma}P(\omega) \tag{2.50}$$

We can now perform formal expansion of the kernel like in [16]:

$$\tilde{K}(\gamma,\omega) = \sum_n \bar{\alpha}_s^n \chi_n(\gamma) \tag{2.51}$$

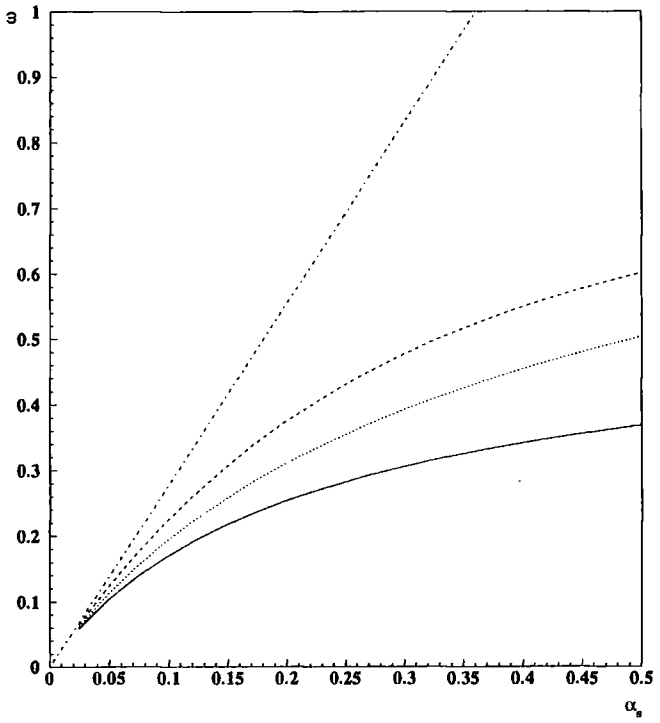

Figure 2.5: The solution for the intercept of the hard pomeron. Dashed-dotted line: LO solution; dashed line: LO + DGLAP terms; dotted: LO + consitency constraint; solid: full solution LO + consistency constraint + DGLAP terms added.

Differentiating the kernel (2.50) we find :

$$\chi_0(\gamma) = \chi(\gamma)$$

$$\chi_1(\gamma) = -\Psi'(1-\gamma)\chi_0(\gamma) + \frac{P(\omega=0)}{\gamma}\chi_0(\gamma) \tag{2.52}$$

(2.53)

This kernel reproduces the most divergent part of the full NLL BFKL kernel namely (compare [16]):

$$\gamma \to 0 \quad \chi_1 \to -\frac{P(\omega=0)}{\gamma^2} + \dots$$

$$\gamma \to 1 \quad \chi_1 \to -\frac{1}{(1-\gamma)^3} + \dots \tag{2.54}$$

(2.55)

Thus we see that the addition of the non-leading DGLAP terms $P(\omega)$ affects the behaviour near the $\gamma = 0$ pole of the kernel, whereas the consistency constraint modifies the $\gamma \to 1$ behaviour i.e. the reversed DGLAP configuration.

In this subsection we have analysed the general properties of our equation for the gluon density $f(x, k^2)$. Although we have simplifed our consideration by omitting

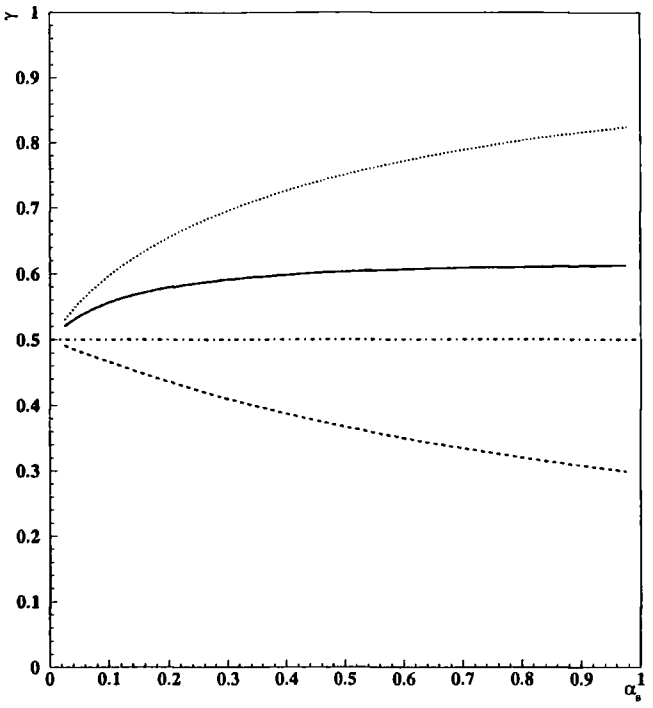

Figure 2.6: The solution for the anomalous dimension of the gluon distribution function. Dashed-dotted line: LO solution, $\gamma = 1/2$; dashed line: LO + DGLAP terms; dotted: LO + consitency constraint; solid: full solution LO + consistency constraint + DGLAP terms added.

the masses of quarks and fixing α_s the overall qualitative features of the solution are well reproduced by this formalism. However in addition to our gluon equation we still need an equation for the singlet quark distribution.

2.3 The equation for the quark distribution

At small x the gluon drives the sea quark (momentum) distribution S via the $g \to q\overline{q}$ transition, see Figure 2.1. We evaluate the effect using the k_T factorization theorem. To be precise we use the k_T factorization prescription to calculate observables (such as F_2) directly from the unintegrated gluon distribution $f(x, k_T^2)$. For F_2 we interpret the result in terms of the sea quark distributions, implicity assuming the DIS scheme. The total sea is the sum of the individual quark contributions

$$S(x,Q^2) = \sum_q S_q(x,Q^2). \tag{2.56}$$

At small x the k_T factorization theorem gives

$$S_q(x,Q^2) = \int_x^1 \frac{dz}{z} \int \frac{dk^2}{k^2} S^q_{\rm box}(z,k^2,Q^2)\, f\left(\frac{x}{z},k^2\right) \tag{2.57}$$

where $S_{\rm box}$ describes the quark box (and crossed box) contributions shown in Figure 2.2. $S_{\rm box}$ implicitly includes an integration over the transverse momentum, κ, of the exchanged quark. Indeed, evaluating the box contributions we find

$$S_q(x,Q^2) = \frac{Q^2}{4\pi^2}\int\frac{dk^2}{k^4}\int_0^1 d\beta\int d^2\kappa'\alpha_S\left\{[\beta^2+(1-\beta)^2]\left(\frac{\boldsymbol{\kappa}}{D_{1q}}-\frac{\boldsymbol{\kappa}-\boldsymbol{k}}{D_{2q}}\right)^2\right.$$
$$\left. + [m_q^2+4Q^2\beta^2(1-\beta)^2]\left(\frac{1}{D_{1q}}-\frac{1}{D_{2q}}\right)^2\right\} f\left(\frac{x}{z},k^2\right)\Theta\left(1-\frac{x}{z}\right) \tag{2.58}$$

where $\kappa' = \kappa-(1-\beta)k$ and

$$D_{1q} = \kappa^2+\beta(1-\beta)Q^2+m_q^2$$
$$D_{2q} = (\boldsymbol{\kappa}-\boldsymbol{k})^2+\beta(1-\beta)Q^2+m_q^2$$
$$z = \left[1+\frac{\kappa'^2+m_q^2}{\beta(1-\beta)Q^2}+\frac{k^2}{Q^2}\right]^{-1}. \tag{2.59}$$

where β is the Sudakov variable, k is the transverse momentum of the off-shell gluon and κ is the transverse momentum of the exchaned quark. In these definitions (2.58) and (2.59) we have omitted subscripts T for κ and k. The argument of α_S is taken as $(k^2+\kappa'^2)+m_q^2$. We set the quark masses to be $m_u = m_d = m_s = 0$ and $m_c = 1.4$ GeV.

2.3.1 The light quark component of the sea

We first discuss the calculation of the contribution of the "massless" u,d,s quarks to the total sea distribution S. It is necessary to consider three different regions of the k and κ' integrations of (2.57).

(a) The contribution from the purely non-perturbative region $k^2,\kappa'^2 < k_0^2$ is evaluated phenomenologically assuming that it is dominated by "soft" Pomeron exchange [14]. The contribution is parametrized in the form

$$S^{(a)} = S_u^{I\!P}+S_d^{I\!P}+S_s^{I\!P} \tag{2.60}$$

where

$$S_u^{I\!P} = S_d^{I\!P} = 2S_s^{I\!P} = C_{I\!P}\,x^{-0.08}(1-x)^8. \tag{2.61}$$

The coefficient $C_{I\!P}$ is independent of Q^2 (in the large Q^2 region) since the contribution arises from the region in which the struck quarks have limited transverse momentum, $\kappa^2 < k_0^2$.

(b) In the region $k^2 < k_0^2 < \kappa'^2$ we apply the strongly-ordered approximation at the quark-gluon vertex, that is we neglect k^2 as compared to Q^2 and κ^2 and take [38]

$$S_{\rm box} \to S_{\rm box}^{(b)}(z, k^2 = 0, Q^2). \tag{2.62}$$

We then only leave terms which are proportional to k^2 and neglect the higher order terms. Then the contribution to (2.57) from this domain becomes

$$\begin{aligned} S^{(b)} &= \int_x^1 \frac{dz}{z} S_{\rm box}^{(b)}(z, k^2 = 0, Q^2) \int_0^{k_0^2} \frac{dk^2}{k^2} f\left(\frac{x}{z}, k^2\right) \\ &= \int_x^1 \frac{dz}{z} S_{\rm box}^{(b)}(z, k^2 = 0, Q^2) \frac{x}{z} g\left(\frac{x}{z}, k_0^2\right) \end{aligned} \tag{2.63}$$

where the summation over u, d, s is implicitly assumed. The potential collinear singularities in the on-shell structure function $S_{\rm box}$ are regulated by the cut-off k_0^2. Recall that $\kappa^2 \simeq \kappa'^2 > k_0^2$.

(c) In the remaining region, $k^2 > k_0^2$, eq. (2.57) is left unchanged. To be precise we use the perturbative expression for $S_q(x, Q^2)$, see (2.58).

2.3.2 The charm component

We assume that the charm component of Σ is generated dynamically and entirely perturbatively, i.e. there is no $S^{(a)}$ contribution for the charm quark. To evaluate $S_{q=c}$ we divide the integration over k^2 into the regions $k^2 < k_0^2$ and $k^2 > k_0^2$. For $k^2 < k_0^2$, which we denote region (b), we use the on-shell approximation to evaluate $S_{\rm box}$. That is we calculate $S_{\rm box}(z, k^2 = 0, Q^2; m_c^2)$, which is finite due to $m_c \neq 0$. $S_{\rm box}(z, k^2 = 0, Q^2; m_c^2)$ is given in Appendix A. Then (2.57) gives

$$S_{q=c}^{(b)}(x, Q^2) = \int_x^a \frac{dz}{z} S_{\rm box}(z, k^2 = 0, Q^2; m_c^2) \int_0^{k_0^2} \frac{dk^2}{k^2} f\left(\frac{x}{z}, k^2\right) \tag{2.64}$$

where $a = (1 + 4m_c^2/Q^2)^{-1}$ and it comes from the threshold on the production of the massive charm quark. For $k^2 > k_0^2$, which we call region (c), we use the full perturbative formula. Thus adding the two contributions (b) and (c) we have

$$\begin{aligned} S_{q=c}(x, Q^2) &= \int_x^a \frac{dz}{z} S_{\rm box}(z, k^2 = 0, Q^2; m_c^2) \frac{x}{z} g\left(\frac{x}{z}, k_0^2\right) \\ &+ \int_x^a \frac{dz}{z} \int_{k_0^2} \frac{dk^2}{k^2} S_{\rm box}(z, k^2, Q^2; m_c^2) f\left(\frac{x}{z}, k^2\right), \end{aligned} \tag{2.65}$$

where we have used (2.29) which enables $S_{q=c}$ is to be specified in terms of the conventional gluon input distribution.

In this description we do not consider b quark contribution because in the region of Q^2 of about $10 - 100\,{\rm GeV}^2$ it is expected to have a very small value. Moreover, because it has a charge $-1/3$ its contribution to F_2 is further suppressed ($F_2 = \sum_q e_q^2 S_q$).

2.3.3 The equation for the quark singlet distribution

Besides S, the singlet momentum distribution Σ also contains a valence quark contribution V, which is taken from a known set of partons [13]. Thus in summary the singlet distribution is

$$\Sigma = (S^{(a)} + S^{(b)} + S^{(c)})_{uds} + (S^{(b)} + S^{(c)})_{q=c} + V, \tag{2.66}$$

where $S^{(a)}$ is phenomenologically parametrized in terms of "soft" Pomeron exchange and the $S^{(b)}$ terms are determined perturbatively except for the (non-perturbative) input gluon distribution at the scale k_0^2. The $S^{(c)}$ terms are defined entirely in terms of the unintegrated gluon distribution f in the perturbative region $k^2 > k_0^2$. Finally, $V = x(u_{\rm val} + d_{\rm val})$ is the valence quark contribution.

In order to see the connection with the DGLAP evolution of the (light) quark sea we first note that

$$S_q(x,Q^2) = S_q(x,k_0^2) + \int_{k_0^2}^{Q^2} \frac{\partial S_q(x,Q'^2)}{\partial Q'^2} dQ'^2, \tag{2.67}$$

where here S denotes the sum over just the u, d and s quarks. We next recall that the leading twist part of the k_T factorization formula (2.57), written in the form

$$Q^2 \frac{\partial S_q(x,Q^2)}{\partial Q^2} = \int_x^1 \frac{dz}{z} \int \frac{dk^2}{k^2} Q^2 \frac{\partial S^q_{\rm box}(z,k^2,Q^2)}{\partial Q^2} f\left(\frac{x}{z},k^2\right), \tag{2.68}$$

can be reduced to the collinear form [27]

$$Q^2 \frac{\partial S_q(x,Q^2)}{\partial Q^2} = \frac{\alpha_S(Q^2)}{2\pi} \int_x^1 dz\, P_{qg}(z,\alpha_S(Q^2)) \frac{x}{z} g\left(\frac{x}{z},Q^2\right) \tag{2.69}$$

which incorporates leading $\ln 1/x$ resummation effects in both the splitting function P_{qg} and in the integrated gluon distribution g see subsection 2.1.1. Thus (2.67) may be written in the form

$$S_q(x,Q^2) = S_q(x,k_0^2) + \int_{k_0^2}^{Q^2} \frac{dQ'^2}{Q'^2} \frac{\alpha_S(Q'^2)}{2\pi} \int_x^1 dz \left[P_{qg}(z,\alpha_S(Q'^2)) \frac{x}{z} g\left(\frac{x}{z},Q'^2\right) + P_{qq}(z,\alpha_S(Q'^2)) S_q\left(\frac{x}{z},Q'^2\right)\right], \tag{2.70}$$

where for consistency we have included the $S \to S$ contribution to the evolution. This additional term is needed to ensure the correct DGLAP structure. Of course, at small x we expect S to be dominantly driven by the gluon. Equation (2.70) is simply the integral form of the DGLAP evolution equation for the light sea quark distribution, S.

Guided by the DGLAP structure, it is clear that we should also add the $S \to S$ contribution to the complete equation (2.66) based on k_T factorization. Then (2.66)

becomes

$$\begin{aligned}\Sigma(x,k^2) &= S^{(a)}(x) + \sum_q \int_x^a \frac{dz}{z} S^q_{\rm box}(z,k'^2=0,k^2;m_q^2)\frac{x}{z}\, g\left(\frac{x}{z},k_0^2\right) + V(x,k^2) \\ &+ \sum_q \int_{k_0^2}^{\infty} \frac{dk'^2}{k'^2} \int_x^1 \frac{dz}{z} S^q_{\rm box}(z,k'^2,k^2;m_q^2) f\left(\frac{x}{z},k'^2\right) \\ &+ \int_{k_0^2}^{k^2} \frac{dk'^2}{k'^2} \frac{\alpha_S(k'^2)}{2\pi} \int_x^1 dz\, P_{qq}(z) S_{uds}\left(\frac{x}{z},k'^2\right)\end{aligned} \tag{2.71}$$

where $S^{(a)}$ is given by (2.60) and where the *uds* subscript indicates that the additional $S \to S$ term is only included for the light quarks.
This equation for the singlet quark distribution Σ, together with eq. (2.32) for the gluon, form the pair of coupled equations which we will solve. In this way we can specify the structure function F_2 in terms of the parameters of the input distributions, and hence determine the values of the parameters by fitting to the data for F_2 structure function. We are then going to determine the gluon distribution function and compare its integrated form with the other parametrisations which are available at present.

2.4 Numerical analysis and the description of F_2

We now have a closed system of two coupled integral equations for two unknowns. Namely equation (2.32) for the unintegrated gluon distribution $f(x,k^2)$ and equation (2.71) for the integrated quark singlet distribution $\Sigma(x,k^2)$. The effect of the gluon in the perturbative region, $k^2 > k_0^2$, is of special interest. It is the 'dynamo' which drives small x physics.

The advantage of this formulation of the unified BFKL/DGLAP equation is that the input is well-controlled. We emphasized already previously that the equation for $f(x,k^2)$ required only the specification of an input form for the integrated gluon,

$$xg(x,k_0^2) = N(1-x)^{\beta}. \tag{2.72}$$

Moreover, the equation for the singlet $\Sigma(x,k^2)$ requires as input only the non-perturbative sea contribution whose form we assume is given by the "soft" Pomeron

$$S^{(a)} = C_{I\!P} x^{-0.08}(1-x)^8 \tag{2.73}$$

and the contributions $S^{(b)}$ of (2.63) and (2.64) which depend on $xg(x,k_0^2)$ of (2.72). The choice of the exponent -0.08 is motivated by the Regge pomeron intercept found in the analysis of total cross section data [14]. We choose the exponent of $(1-x)$ to be 8, typical of the behaviour of the sea distribution. In our small x analysis any similar choice (for example 10) would be equally good and would not change the quality of the description.

The valence quark contribution $V(x,k^2)$ in (2.71), which is determined mainly by fixed target deep inelastic data at large values of Bjorken x, is taken from the leading order GRV set of partons [13]. We are therefore able to self-consistently determine $f(x,k^2)$ and $\Sigma(x,k^2)$ as functions of a small number of physically motivated parameters. In fact, we have only the two free parameters for our fit, namely N and β determining the input gluon distribution (2.72). The momentum sum rule fixes the value of $C_{I\!P}$, which determines the input sea, (2.73),

$$1 = \int_0^1 dx(xg(x,k_0^2) + C_{I\!P}x^{-0.08}(1-x)^8 + V(x,Q^2=1)) \qquad (2.74)$$

The presence of BFKL - like terms means that the momentum sum rule is not exactly conserved. It would be conserved if we were only using the DGLAP terms as it is done in global parton analysis, for example [11], [12], [13]. However the violation is quite small. For example, after evolution to $Q^2 = 50\,\mathrm{GeV}^2$ we find that the sum of the momentum fractions carried by the gluon and the light quarks is only increased from 1 to 1.007, so the effect is below 1%. We neglect this small violation of momentum conservation.

2.4.1 The optimum description of the F_2 data at small x

We determine the values of the input parameters by fitting to the HERA measurements of the proton structure function F_2 using

$$F_2 = \sum_q e_q^2(S_q + V_q), \qquad (2.75)$$

which holds in the DIS scheme. We thus have to calculate $S_q(x,Q^2)$ in terms of the input gluon parameters N and β. To do this we solve the pair of equations (2.32) and (2.71) for $f(x,k^2)$ and $\Sigma(x,k^2)$ using an extension of the method proposed in [39]. We performed an interpolation of $f(x,k^2)$ and $\Sigma(x,k^2)$ in the two variables x and k^2 using orthogonal polynomials. The details of the method of solving these equations is given in Appendix B. In this way we can express $F_2(x,Q^2)$ in terms of N and β. We then determine the optimum values of these parameters by fitting to the HERA [2] and fixed-target [40] data for $F_2(x,Q^2)$ that are available in the small x domain, $x < 0.1$. We also take a running coupling which satisfies $\alpha_S(M_Z^2) = 0.12$. We actually show the results of two fits. The first is the 'realistic' fit with the kinematic constraint imposed (which requires the virtuality of the exchanged gluons along the ladder to satisfy $|k'^2| \simeq k_T'^2$. Then for comparison we repeat the analysis without imposing the kinematic constraint, that is we omit Θ function in (2.32). The quality of the fits are shown in Figs. 2.7 and 2.8, and the parameters given in Table 2.1. To be precise, Figs. 2.7 and 2.8 respectively show the description of the H1 and ZEUS data [2] together with those fixed-target data that occur at the same values of Q^2.

The fit with the kinematic constraint included (continuous curves) is significantly better, see the χ^2 in Table 2.1, than that in which it is omitted (shown by the dashed

curves). Without the constraint the predicted rise of F_2 is a little too steep at the smallest values of x and Q^2. In the remaining part of x, Q^2 domain the fit (fit 2) gives a good description of F_2. It is far better, for example, than that shown in ref. [24].

The kinematic constraint, which corresponds to subleading $\ln(1/x)$ corrections, lowers the 'hard' pomeron intercept and improves the description of the data, particularly at the smaller values of x. In fact the resulting description of $F_2(x, Q^2)$ with just two free parameters (N and β) is excellent, and is comparable, even a little better than, to that achieved in the global parton analyses, see again the χ^2 listed in Table 2.1. Moreover, the overall behaviour of the gluon is much more realistic than that of the fit without the kinematic constraint. It gives an acceptable description of the WA70 prompt photon data [41], which directly sample the gluon at $x \simeq 0.4$. These data were not used to constrain the gluon. For fit 1 the prediction is some 30% above WA70 data, which is within the QCD scale uncertainties, whereas the gluon of fit 2 gives a prediction which is a factor of about 2.5 above the data. It is not surprising that the gluons are so different in the two fits since they are both contrived to give satisfatory description of the measurements of F_2 at small x, despite the fact that the kinematic constraint significantly reduces the gluon intercept ω_0. It is encouraging that it is the description with the kinematic constraint that gives the acceptable large x behaviour of the gluon. For completeness we use our determination of the unintegrated gluon to compute the conventional gluon distribution $xg(x, Q^2)$ and compare the result with the gluons of recent sets of partons obtained in DGLAP-based global analyses of deep inelastic and related data. To be specific the continuous curves in Fig. 2.9 compare the integrated gluon distribution obtained from $f(x, k_T^2)$ of the fit 1 with the gluon distributions of the MRS(R2) [11] and GRV [13] set of partons in DIS scheme (shown by the dashed and dotted curves respectively). We see that the behaviour of the integrated gluon is very similar to that of MRS(R2). This may be expected since the MRS analysis used to the same HERA data as those fitted in the present work, whereas these data were not available at the time of the GRV analysis. However, we emphasize the different underlying structure of the present analysis and the pure DGLAP-based descriptions. We shall see below that in the unified BFKL/DGLAP approach the rise of F_2 is generated essentially by $\ln(1/x)$ effects in the off-shell gluon structure, F_2^{box} of Fig. 2.1.

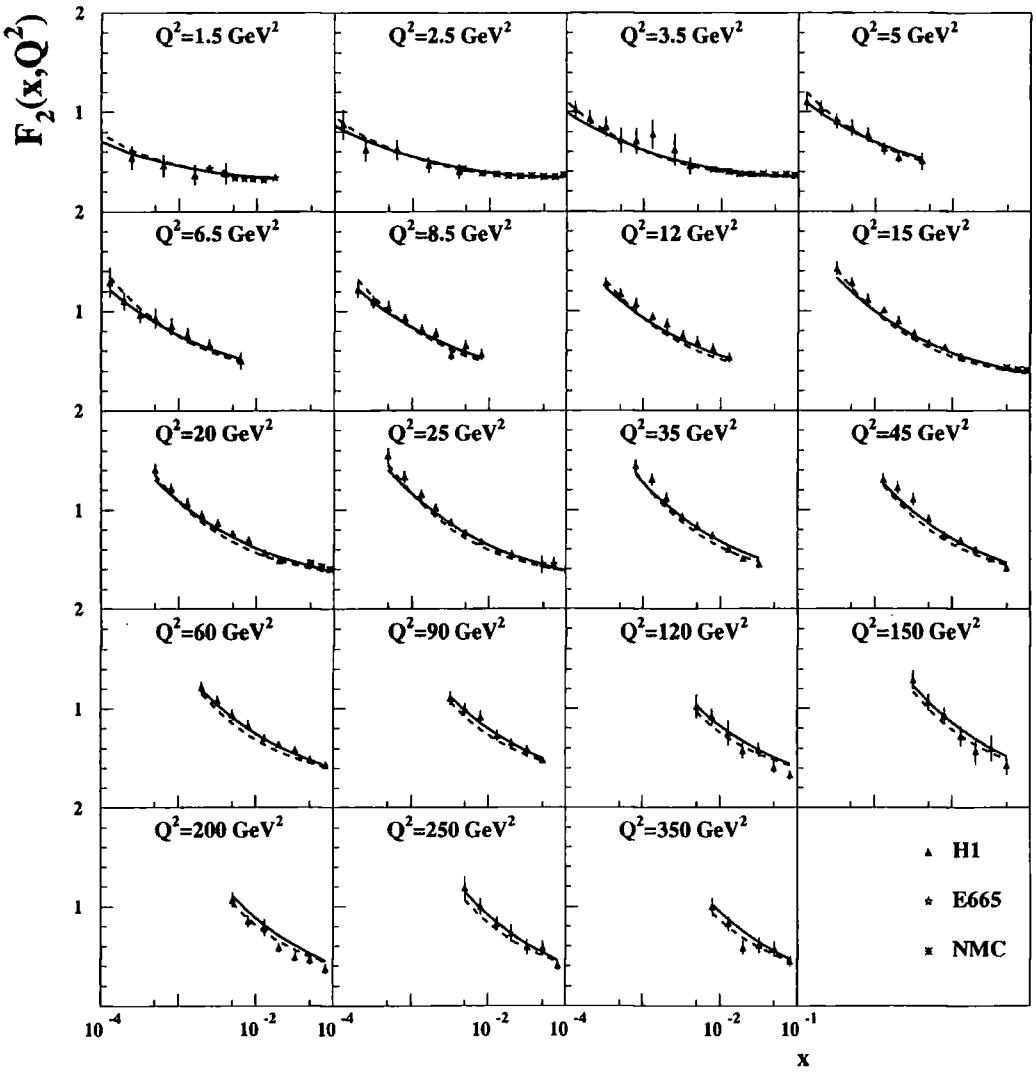

Figure 2.7: The two-parameter fit to the F_2 data at small x using eq. (2.32) for $f(x,k^2)$ with (continuous curves) and without (dashed curves) the kinematic constraint. The optimum values of the parameters N and β, which describe the input form of the gluon, are given in Table 2.1. The figure shows the H1 data [2] together with the E665 and NMC measurements [40] which occur at the same values of Q^2.

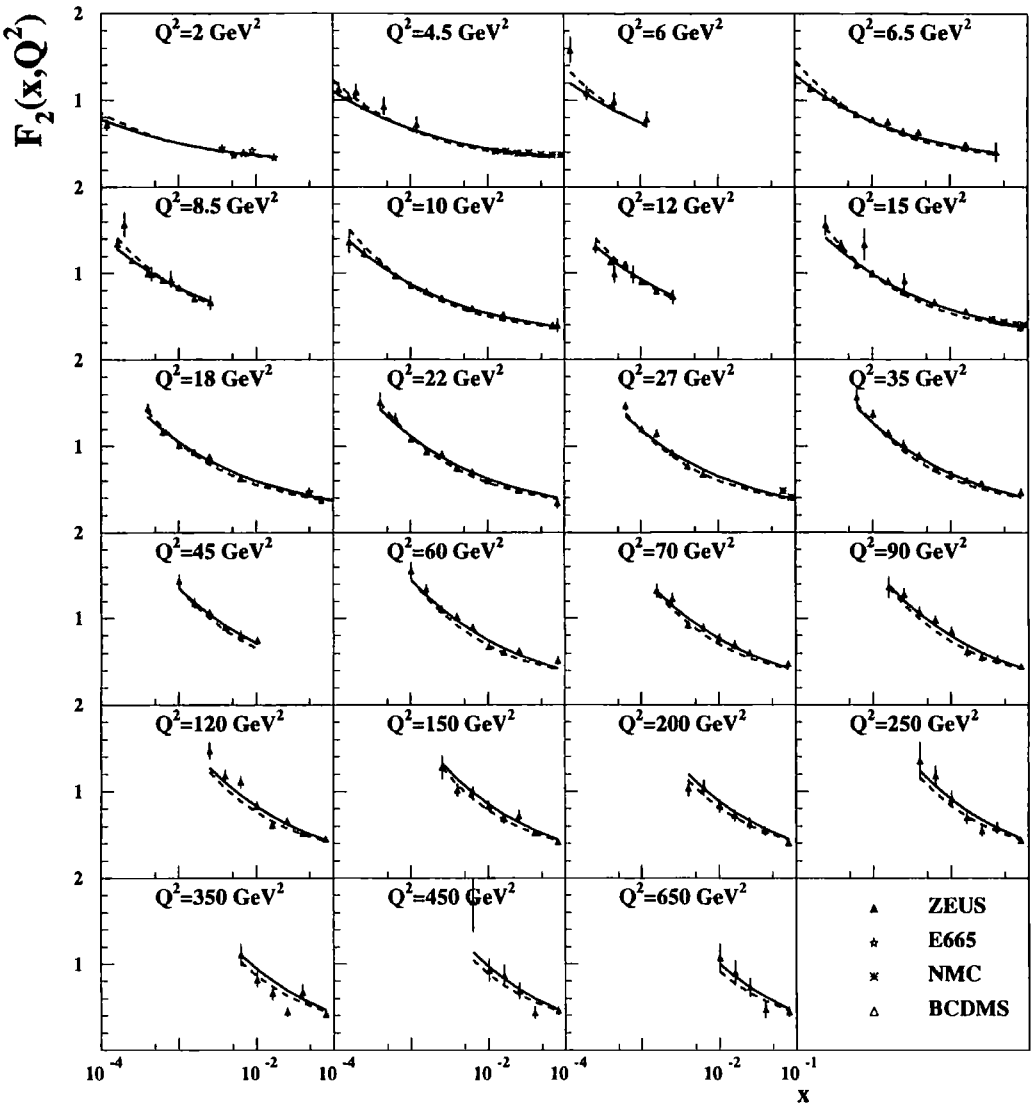

Figure 2.8: As for Fig. 2.7, but for the ZEUS measurements [2] of F_2, together with the E665, NMC and BCDMS data [40] which occur at the same values of Q^2.

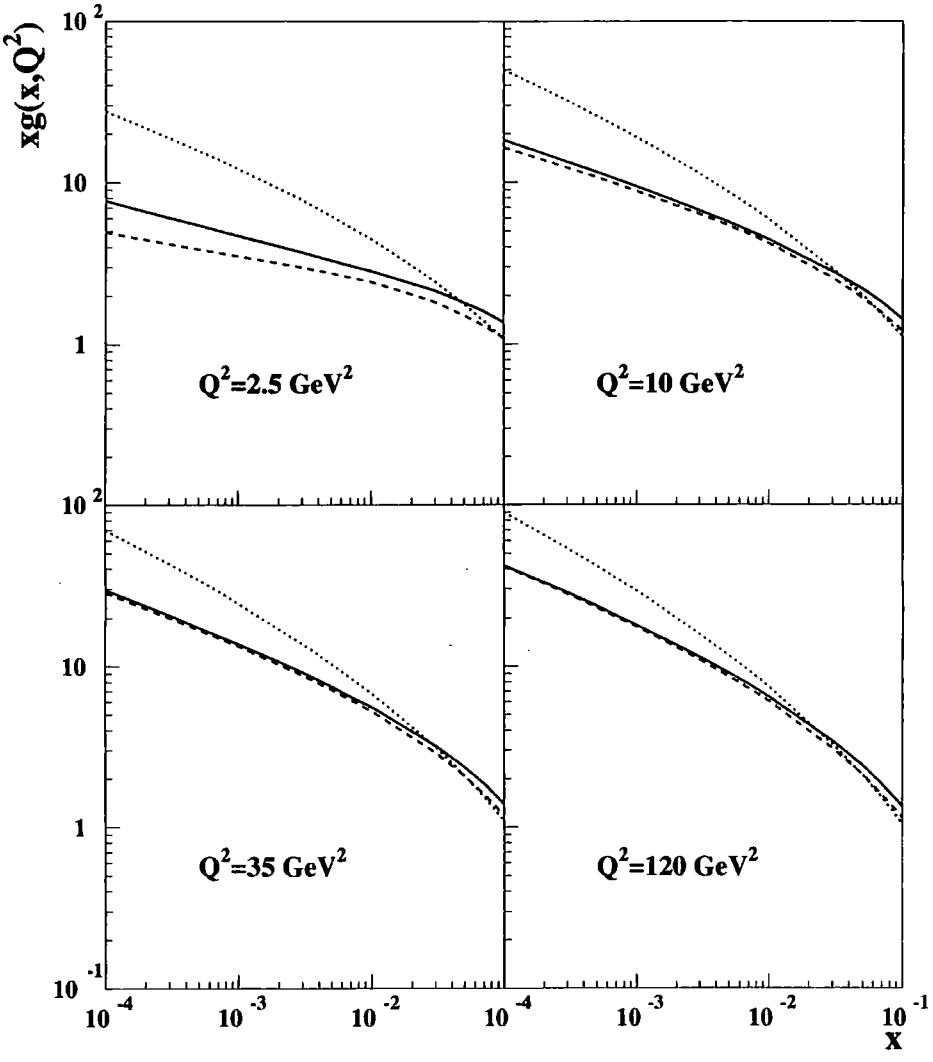

Figure 2.9: The continuous curves show the behaviour of the conventional gluon distribution $xg(x,Q^2)$ corresponding to fit 1, and calculated using eq. (2.32). For comparison we also show the gluon distributions of the MRS (R2) [11] (dashed curve) and GRV [13] (dotted curve) sets of partons.

	Kinematic constant	$xg = N(1-x)^\beta$ N	β	$C_{I\!P}$	χ^2/datapoint [393 points]
Fit 1	yes	1.57	2.5	0.269	1.07
Fit 2	no	0.85	0.9	0.269	1.8
MRS(R2)					1.12

Table 2.1 : The parameters N and β determined in the optimum fit to the available data [2, 40] for F_2 with $x < 0.05$ and $Q^2 > 1.5\text{GeV}^2$, without and with the inclusion of the kinematic constraint along the gluon ladder. The value of $C_{I\!P}$ of (2.73) is also shown, although this is fixed in terms of N and β by the momentum sum rule. For comparison we also show the χ^2 for the same set of HERA and fixed-target data obtained in a next-to-leading order DGLAP global parton analysis [11]. For both fit 1 and 2 the gluon carries 45% of the proton's momentum at the input scale $k_0^2 = 1\text{GeV}^2$.

2.4.2 The effect of the $\ln(1/x)$ resummation on the gluon

In subsection 2.2.1 we were analysing in Mellin space the solution to the gluon equation (2.32). We are now going to confront these results with the direct numerical solution in x space.

Fig. 2.10 shows the behaviour of the unintegrated gluon distribution $f(x,k^2)$ as a function of k^2 for $x = 10^{-3}$ and 10^{-4}. Three different determinations are shown, each of which start from the same input

$$xg(x,k_0^2) \;=\; 1.57(1-x)^{2.5}$$

of fit 1 of Table 2.1. This is because we want to show certain dynamical effects in different scenarios of BFKL and DGLAP evolution which are not dependent on the form of initial input. The continuous and dashed curves correspond, respectively, to the behaviour of $f(x,k^2)$ with and without the kinematic constraint. The dotted curve is obtained from a DGLAP determination in which the BFKL kernel in (2.32) is replaced by the leading order P_{gg} function. That is (2.32) is replaced by

$$f(x,k^2) \;=\; \frac{\alpha_S(k^2)}{2\pi}\left[\int_x^1 dz P_{gg}(z)\frac{x}{z}g\left(\frac{x}{z},k_0^2\right) + \int_x^1 dz P_{gg}(z)\int_{k_0^2}^{k^2}\frac{dk'^2}{k'^2}f\left(\frac{x}{z},k'^2\right) + \int_x^1 dz P_{gq}(z)\Sigma\left(\frac{x}{z},k^2\right)\right] \quad (2.76)$$

where P_{gg} has the usual form

$$P_{gg}(z) = 6\left[\frac{1-z}{z} + z(1-z) + \frac{z}{(1-z)_+} + \frac{11}{12}\delta(1-z)\right] - \frac{N_f}{3}\delta(1-z). \quad (2.77)$$

The comparison of the dashed and dotted curves shows that the differences between the BFKL and DGLAP approaches are not very big, even for the values of x as low as 10^{-3}. The differences become more prominent when one considers smaller values of x, around 10^{-4}. Even then the discrepancies are only visible at lower values of k^2. This effect could at first be quite surprising because we are generally considering two different evolution scenarios. However, this phenomenon can be explained in terms of power series expansion in $\bar{\alpha}_s/\omega$ of the gluon anomalous dimension

$$\gamma^{\mathrm{BFKL}} = \frac{\overline{\alpha}_S}{\omega} + c_4 \left(\frac{\overline{\alpha}_S}{\omega}\right)^4 + \dots$$

see (2.8) and also Figure 2.4, where $c_2 = c_3 = c_5 = 0$. The first term of the expansion, which is common to BFKL and DGLAP, is clearly dominant for the smaller values of $\alpha_S(k^2)$. The rest of the terms are not that big since many of the coefficients c_j are equal to zero and the remaining ones are not numerically big. Thus we confirm the well known result that, in the region of moderately small values of x relevant for the HERA measurements, $\ln(1/x)$ resummation has little effect on the gluon distribution. If the gluon input were adjusted to correspond to the optimum fit with the kinematic constraint imposed, then the continuous curve would be comparable to the other two. However, a common input is used to show the impact of the kinematic constraint. First of all we see that the overall normalisation of the gluon with kinematical constraint is much smaller than without it. We also see that the gluon is growing slower with x which confirms the results for the intercept see Figure 2.5. We also see that the evolution with the momentum k^2 is faster in the case of gluon with kinematical constraint than without it. It should be noted that the very flat behaviour of $f(x, k^2)$ at $x = 10^{-3}$ is because it is proportional to $\alpha_s(k^2)$. This is consistent with our previous result for the anomalous dimension, which is bigger in the case of BFKL + kinematical constraint, see Fig. 2.6. All these features ensure us that the subleading corrections to the $\ln(1/x)$ resummation are extremely important and that the proper treatment of these terms is essential to get physical and reliable results for the description of high energy deep inelastic phenomena.

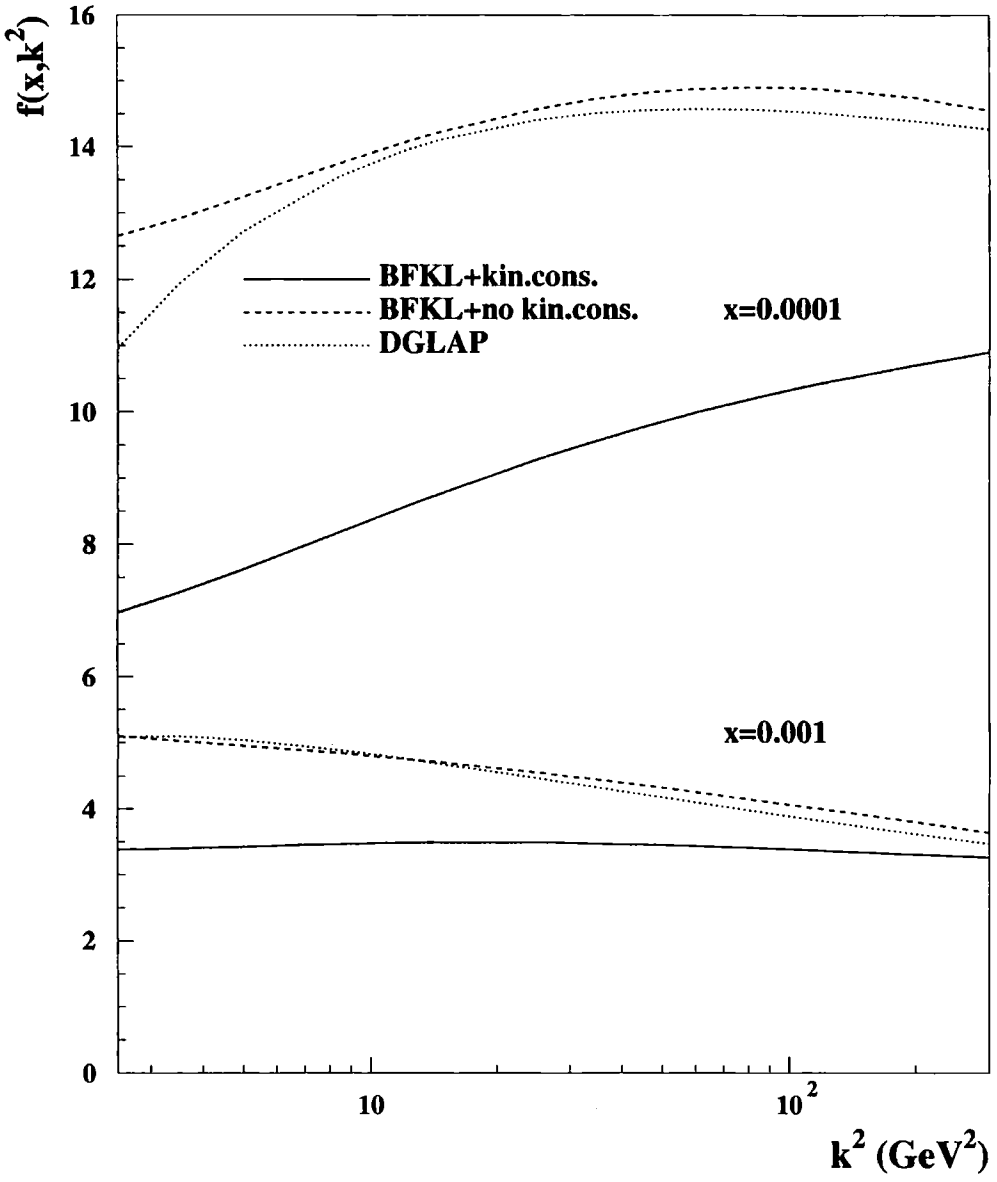

Figure 2.10: The unintegrated gluon distribution $f(x,k^2)$ as a function of k^2 for $x = 10^{-4}$ and 10^{-3} obtained by solving the simultaneous equations for $f(x,k^2)$ and $\Sigma(x,k^2)$. The continuous and dashed curves are obtained by using the unified BFKL/GLAP equation (2.32) for $f(x,k^2)$ with and without the kinematic constraint respectively. The dotted curve corresponds to using GLAP evolution for f, eq. (2.76). In each case the input $xg(x,k_0^2) = 1.57(1-x)^{2.5}$ is used, where $k_0^2 = 1\text{GeV}^2$.

2.4.3 Effect of $\ln(1/x)$ resummation on the structure function F_2

To investigate the various effects of the $\ln(1/x)$ terms in the P_{qg} function we compute $F_2(x,Q^2)$ using four different procedures but with a common input,

$$xg(x,k_0^2) \;=\; 1.57(1-x)^{2.5},$$

correspoding to fit 1. In this calculation we have only included the light quarks u,d,s (which we treat as massless), since we want to avoid any dependence on the choice of scale for the heavy quarks. Such a dependence would spoil the clarity of the explanation of some effects which we want to emphasize. The four different determinations are shown in Fig. 2.11 and correspond to

(i) The full unified BFKL + DGLAP calculation with the kinematic constraint included, eqs.(2.32) and (2.71), shown as a continuous curve.

(ii) Analogous to (i) but without the kinematic constraint (dashed curve).

(iii) Replace (2.32) by the pure DGLAP equation in the gluon sector, eq. (2.76), but keep the full k_T factorization for the quarks (dotted curve).

(iv) Pure DGLAP evolution for both the gluons and the quarks (dot-dashed curve). That is instead of (2.71) we use

$$\Sigma(x,k^2) = S^{(a)}(x) + S^{(b)}(x,k^2) + V(x,k^2) + \int_x^1 dz P_{qg}(z) \int_{k_0^2}^{k^2} \frac{dk'^2}{k'^2} f\left(\frac{x}{z},k'^2\right) \xi(k'^2,k^2) \tag{2.78}$$

where $\xi(k'^2,k^2)$ is the evolution length and is defined by,

$$\xi(k'^2,k^2) = \int_{k'^2}^{k^2} \frac{dq'^2}{q'^2} \alpha_S(q'^2). \tag{2.79}$$

One can again see from Fig. 2.11 that the differences between LO BFKL with running coupling (without kinematical constraint) and DGLAP evolution in the gluon sector are not very big. The calculations start to differ only at $x \simeq 10^{-4}$ (dashed and dotted lines). On the other hand when we compare the pure DGLAP evolution (with the P_{qg} splitting function) with the equations where the entire phase space has been taken into account then the differences are much bigger. This implies that the leading order terms in $\alpha_S \ln 1/x$ present in the gluon off-shell structure function F_2^{box} are much more important than the terms in the gluon anomalous dimension resulting from the BFKL equation. This also shows that one cannot determine the gluon distribution functions unambiguosly. It will depend on the choice of the factorisation scheme and it is not a directly observable quantity. The effect of the kinematic constraint is again evident. It leads to the change from the dashed to the continuous curves. Fig. 2.11 also enables us to see the x values at which the effect of the $\ln(1/x)$ resummation effects become important.

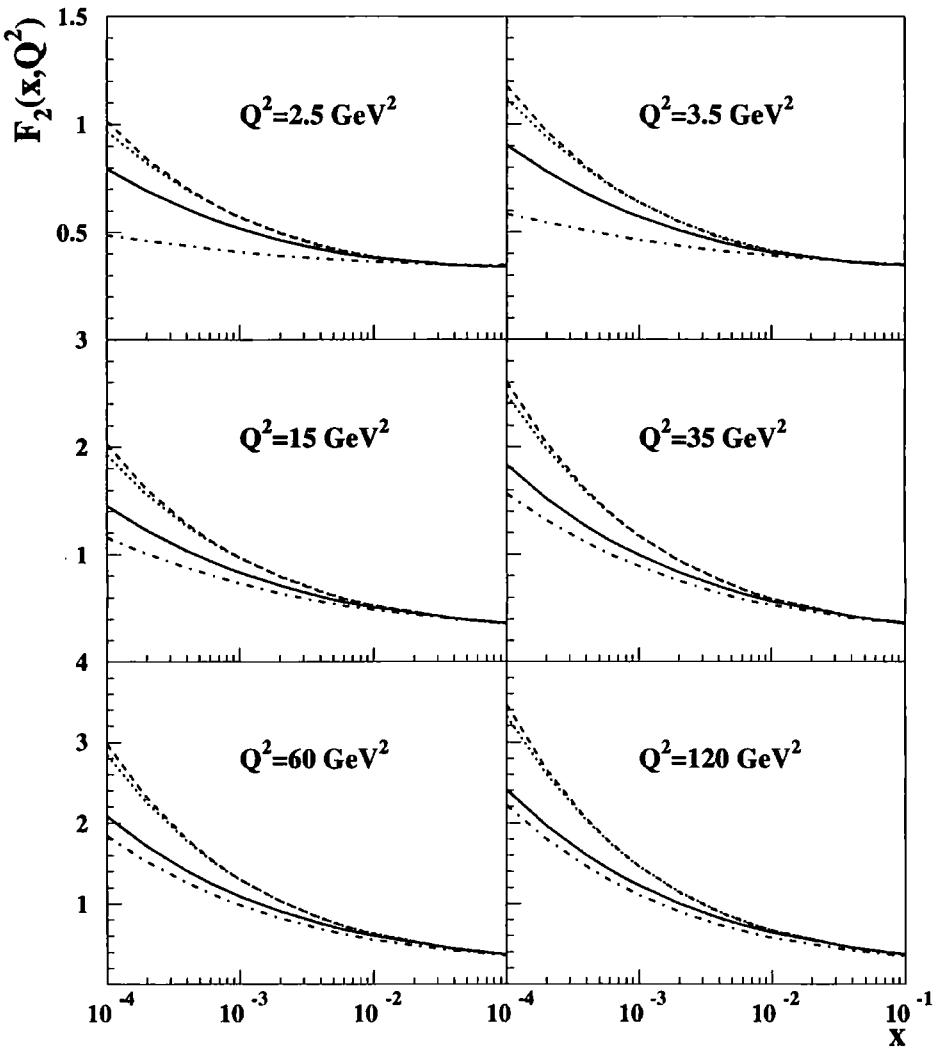

Figure 2.11: The light quark contribution to $F_2(x, Q^2)$ for various Q^2 values obtained from solving different sets of coupled equations for the gluon f and the quark singlet Σ with, in each case, the input $xg(x, k_0^2) = 1.57(1-x)^{2.5}$ where $k_0^2 = 1\text{GeV}^2$. The continuous and dashed curves come from solving (2.32, 2.71) with and without the kinematic constraint. The dotted curve is obtained using DGLAP in the gluon sector, that is (2.76,2.71), whereas the dot-dashed curve corresponds to pure DGLAP evolution, (2.76,2.78).

2.4.4 Predictions for F_2^c and F_L

Once we have determined the parton distributions we can predict the values of other hard scattering observables. At small x we see, via the k_T factorization theorem, that the observables are 'driven' by the unintegrated gluon distribution $f(x,k^2)$. Here we calculate F_2^c and F_L.

The charm component F_2^c of F_2 is given by

$$F_2^c(x,Q^2) \;=\; e_c^2\, S_{q=c}(x,Q^2)$$

where the charm sea $S_{q=c}$ is calculated from (2.65) in terms of the unintegrated gluon $f(x,k^2)$. It is the second term on the right-hand side of (2.65) which drives the small x behaviour. The predictions are compared with the H1 measurements [42] of F_2^c in Fig. 2.12. The percentage of charm in the deep inelastic structure function is shown in Fig. 2.13. At small x we see that F_2^c is an appreciable fraction of F_2. Recall that in the massless charm limit the fraction would be 0.4, provided that we are below the bottom quark threshold. We should stress that this is a prediction, not a fit the to data. Only the total F_2 has been fitted and the resulting charm component compared with F_2^c data. The predictions of the longitudinal structure function F_L are shown in Fig. 2.14. For F_L the k_T factorization formula can be written in the form [38, 43]

$$\begin{aligned} F_L(x,Q^2) \;=\; & \frac{\alpha_s(Q^2)}{\pi}\left[\frac{4}{3}\int_x^1 \frac{dy}{y}\left(\frac{x}{y}\right)^2 F_2(y,Q^2) + \sum_q e_q^2 \int_x^1 \frac{dy}{y}\left(\frac{x}{y}\right)^2\left(1-\frac{x}{y}\right) y g(y,k_0^2)\right] \\ & + \sum_q e_q^2 \frac{Q^4}{\pi^2}\int_{k_0^2}\frac{dk^2}{k^4}\int_0^1 d\beta\beta^2(1-\beta)^2\int d^2\kappa'\alpha_S\left[\frac{1}{D_{1q}}-\frac{1}{D_{2q}}\right]^2 f\left(\frac{x}{z},k^2\right), \end{aligned} \tag{2.80}$$

where the quark box variables D_{iq} and κ' are defined in (2.59). The behaviour of F_L is driven by the gluon through the last term. The argument α_S is taken to be $k^2+\kappa'^2+m_q^2$ as before.

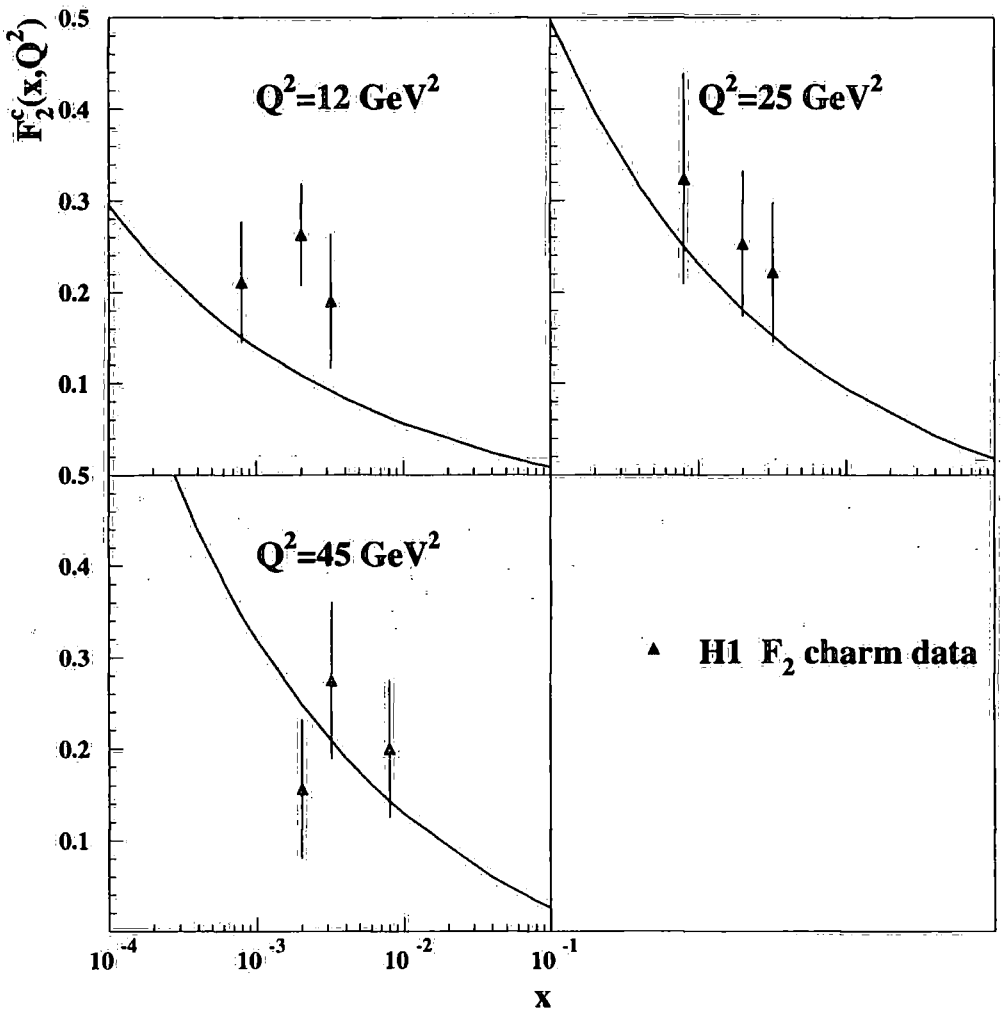

Figure 2.12: The predictions for F_2^c, compared with H1 charm data, obtained from the optimum fit (fit 1).

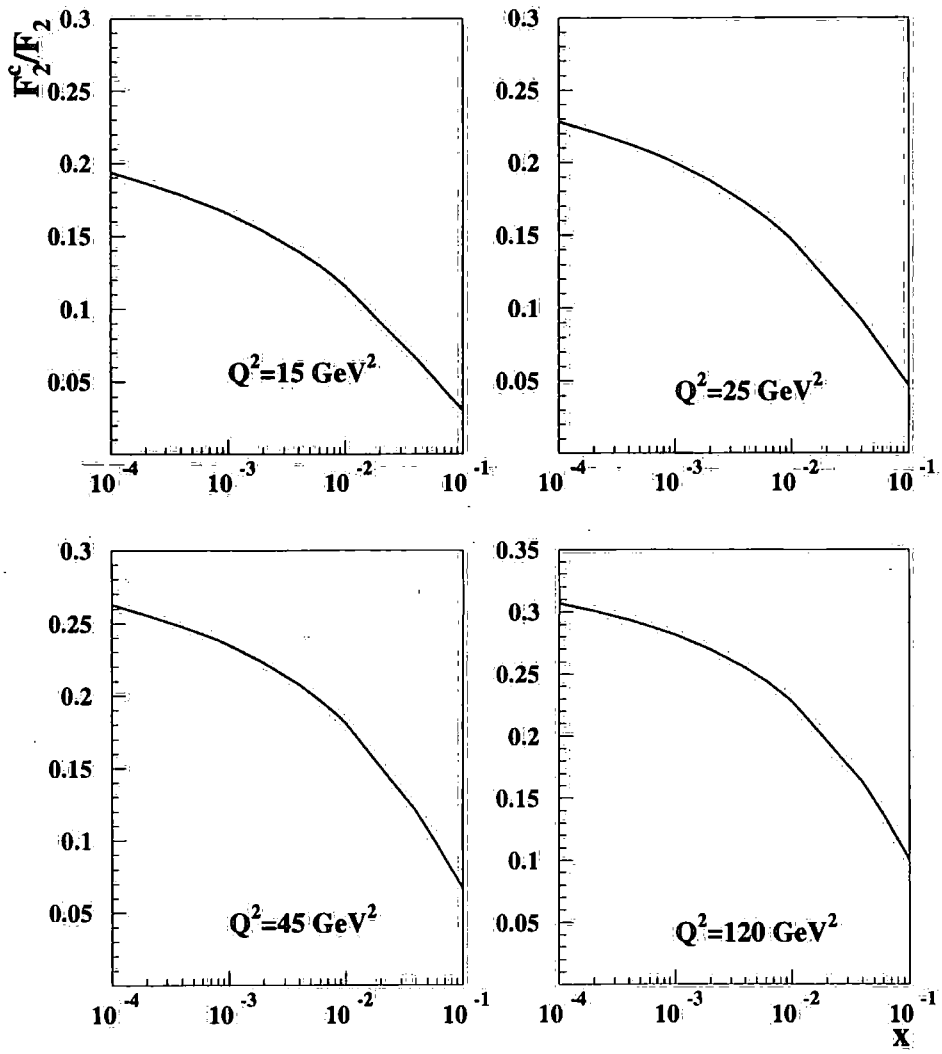

Figure 2.13: Ratio F_2^c/F_2 for different values of Q^2 obtained from fit 1.

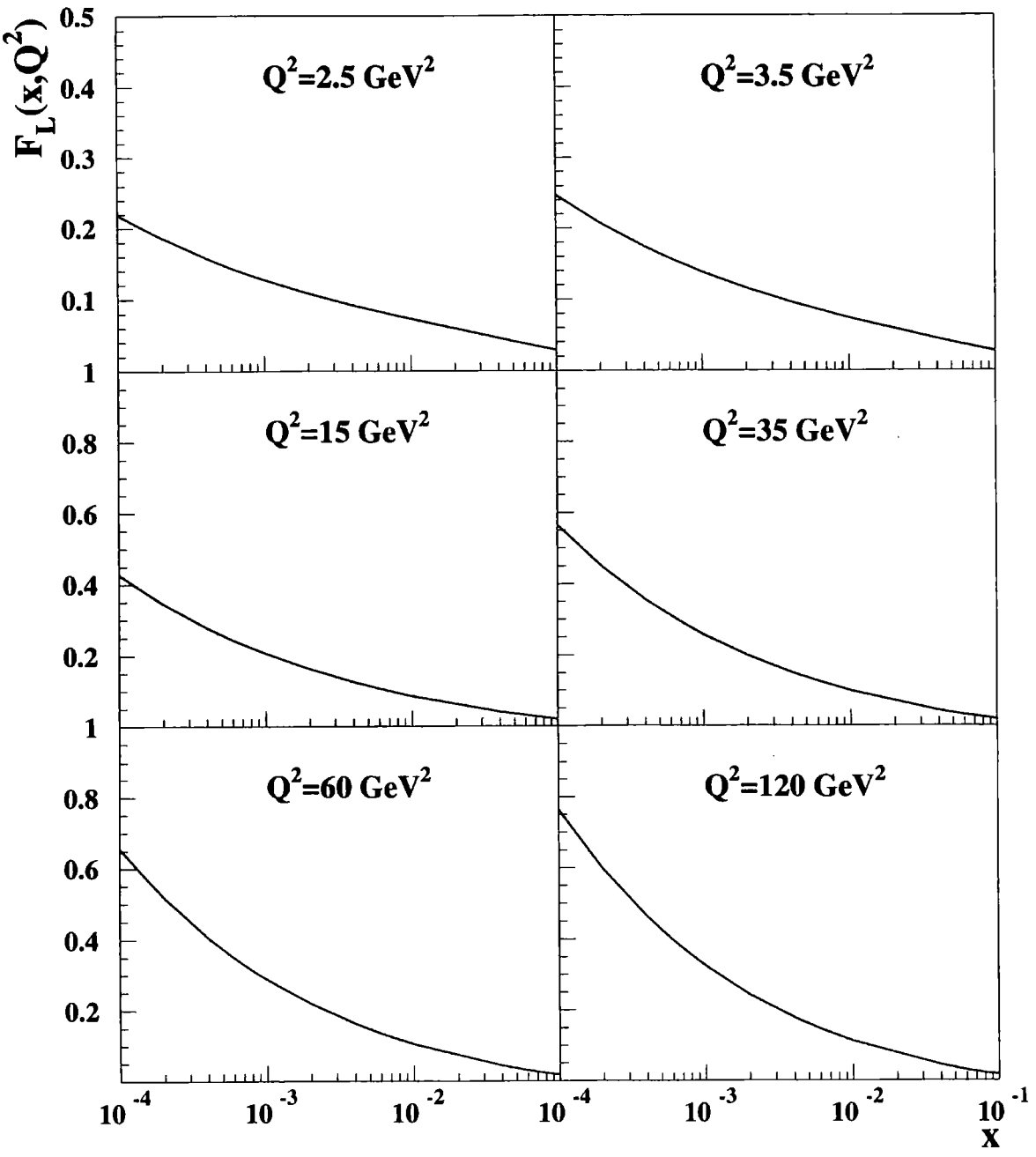

Figure 2.14: The prediction for the structure function F_L as a function of x for different values of Q^2 using the parameters of fit 1.

2.5 Summary

We have obtained a well grounded, consistent formalism of the unifed BFKL-DGLAP equations for the quarks and gluons. Let us remind the basic features of this formalism:

1. We use the natural framework of the unintegrated gluon distribution function $f(x, k^2)$ which is dependent on x, the fraction of proton's momentum and k^2 the momentum of the gluon at the end of the ladder.

2. To calculate the quark distribution and consequently the structure functions we use the high energy factorisation prescription.

3. The gluon $f(x, k^2)$ is calculated from the unifed BFKL-DGLAP system of equations which treats the leading powers of $\ln(1/x)$ and $\ln(Q^2)$ on an equal footing. This equation embodies also very important subleading corrections in $\ln(1/x)$ via consistency constraint.

4. The equation is only solved in the large k^2 region for $k^2 > k_0^2$. We showed that the contribution from the non-perturbative region of low k^2 can be described in terms of the (integrated) gluon and sea quark distributions at the scale k_0^2. The structure of the input is therefore the same as in the case of the pure DGLAP framework. We showed that one can obtain excellent fit using very economical and physically motivated parametrisation of these input distributions.

5. The unifed equation for the unintegrated gluon and the second equation for the singlet quark distribution involving the k_T factorisation prescription form the set of unifed equations which we solve.

6. The few free parameters of the non-perturbative input are adjusted so that the best description of the F_2 data is obtained.

We have therefore obtained a universal unintegrated gluon distribution which can be used to calculate several different quantities in different processes. We have for example calculated the F_L and the charm component of the structure function F_2. In chapter 4 we will show further applications of this formalism.

We shall add to this that the approach presented here is not the only one which has the idea of unification of the BFKL-DGLAP approaches. There exist at least three such attempts. First one was Catani-Ciafaloni-Fiorani-Marchesini equation (CCFM equation) [44, 45, 46] which was the evolution equation for the gluon distribution functions based on the angular ordering constraint. Numerical studies gave quite an interesting results [45]. The second approach has been developed by Thorne [47] using the collinear factorisation. He also proposed the equal treatment of leading $\ln(1/x)$ and $\ln(Q^2)$ powers. However there are certain limitations of this approach namely the reduction only to the leading twist part when going from k_T

factorisation to collinear one. Also in the high energy factorisation there is an easy way to incorporate the running α_s. Last thing we note is that by using the un-integrated gluon distribution function we can clearly control the non-perturbative input. Third approach has been recently proposed by Ciafaloni and collaborators [17] in the context of the resummation of the subleading corrections to BFKL. He has found that by including DGLAP terms into the resummed kernel one gets stable result. This approach is very promising and attracts a lot of attention. It has not however been implemented phenomenologically yet.

The approach which has been presented here although based on the leading order BFKL also performs the resummation of the major part of the subleading corrections in $\ln(1/x)$ via consistency constraint. It is also very easy to apply to phenomenology.

It has however some drawbacks. It is valid only in the perturbative domain, that is for values of $Q^2 > k_0^2 \sim 1\,\mathrm{GeV}^2$. We are going therefore to extend this formalism to be able to describe the low Q^2 deep inelastic data as well as the photoproduction total cross section. This is the topic of the next chapter.

Chapter 3

The description of F_2 at low Q^2

3.1 Short and long distance contributions and the description of F_2 at low Q^2

In the previous chapter we have set up the unifed description of the F_2 data over very wide range of parameter space x, Q^2, namely for $x > 10^{-5}$, $Q^2 > 1\text{GeV}^2$. However we now know that there exist quite a lot of high precision deep inelastic data for F_2 also at very low values of Q^2 [2], as well as measurements of the photoproduction cross section [48, 49]. These results show very interesting features namely the total cross section rises as Q^2 becomes smaller (at fixed values of the energy W) and then from about $Q^2 \sim 0.2$ GeV^2 it flattens and reaches nearly a constant value down to photoproduction point. This transition seems to occur at the border between the perturbative and non-perturbative regimes. This fact highlights the importance of obtaining a complete description which would be valid in the whole region of the kinematical phase space. The framework of unifed equations which we have set up in the previous chapter works very well in the perturbative domain therefore we are tempted to modify it and extend in such a way that it can be used for the description of both perturbative and non-perturbative regions. In order to do this we follow the idea formulated in ref. [50] that is we make a clear separation between short and long distance configurations.
Let $\sigma(s, Q^2)$ be the total cross section for the process $\gamma^* p \to X$ where Q^2 is the virtuality of the photon and $\sqrt{s}$ is the $\gamma^* p$ centre-of-mass energy. It is related to the forward $\gamma^* p$ elastic amplitude A by the optical theorem, Im $A = s\sigma$. We may write a double dispersion relation [51] for A and obtain for fixed s

$$\sigma(s, Q^2) = \sum_q \int \frac{dM^2}{M^2 + Q^2} \int \frac{dM'^2}{M'^2 + Q^2} \rho(M^2, M'^2) \frac{1}{s} \text{ Im } A_{q\bar{q}+p}(s, M^2, M'^2) \quad (3.1)$$

where M and M' are the invariant masses of the incoming and outgoing $q\bar{q}$ pair and $\rho(M^2, M'^2)$ is the double spectral function which is defined by the coupling of the incoming and outgoing $q\bar{q}$ pair to the virtual photon. The relation is shown schematically in Fig. 3.1 .

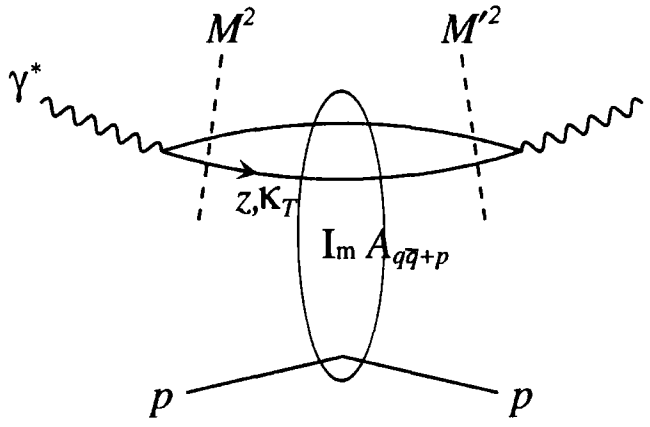

Figure 3.1: The schematic representation of the double dispersion (3.1) for the $\gamma^* p$ total cross section $\sigma(s, Q^2)$ at fixed c.m. energy $\sqrt{s}$. The cut variables, M and M', are the invariant masses of the incoming and outgoing $q\bar{q}$ states in the quasi-elastic forward amplitude, $A_{q\bar{q}+p}$.

If we assume that forward $q\bar{q}+p$ scattering does not change the momenta of the quarks then $A_{q\bar{q}+p}$ is proportional to $\delta(M^2 - M'^2)$, and (3.1) becomes

$$\sigma(s, Q^2) = \sum_q \int_0^\infty \frac{dM^2}{(M^2+Q^2)^2} \rho(M^2)\, \sigma_{q\bar{q}+p}(s, M^2) \tag{3.2}$$

where the spectral function $\rho(M^2)$ is the density of $q\bar{q}$ states in the photon γ^* and $\sigma_{q\bar{q}+p}$ is the total cross section for the interaction between $q\bar{q}$ pairs and the proton.

The original idea by Badelek and Kwiecinski [50] was to divide the integral in (3.2) into two parts by introducing a certain cutoff Q_0^2. In the region of low masses $M^2 < Q_0^2$ it was assumed to be well described by the Vector Meson Dominance Model in which the photon is supposed to form a vector meson rather than a well separated $q\bar{q}$ pair [52, 53]. The region of high masses $M^2 > Q_0^2$ was described by the perturbative QCD. The model worked very well in the region $Q^2 > 1\text{GeV}^2$ but overshoot the data in the region of low Q^2 and the photoproduction points. Nevertheless this idea of separation between perturbative and non-perturbative contributions seems to be very attractive. We are going to exploit it further, and we will achieve a better separation between long and short distance contributions. To do this we take a two-dimensional integral over the longitudinal and transverse momentum components of the quark z and κ_T see Fig. 3.1, rather than simply over the mass M of the $q\bar{q}$ pair. The contribution coming from the small mass region is pure VDM and is given by the following prescription,

$$F_2(\text{VDM}) = \frac{Q^2}{4\pi} \sum_V \frac{M_V^4\, \sigma_V(s)}{\gamma_V^2 (Q^2 + M_V^2)^2} \tag{3.3}$$

where M_V is the mass of vector meson V and where the sum is over the vector mesons which fall in the region $M_V^2 < Q_0^2$. The vector meson-proton cross sections $\sigma_V(s)$ can be determined from the πp and Kp total cross sections using the additive quark model and γ_V^2 from the leptonic width of the vector meson V.

The behaviour of the cross section at large M^2 is a more delicate question. The part which comes from large κ_T of the quark can be calculated by perturbative QCD in terms of the known parton distributions, in this case we will use the framework of unifed DGLAP/BFKL equations presented in the previous chapter. For small κ_T we will use the additive quark model and the impulse approximation. That is we will assume that only one quark interacts with the target and the quark-proton cross section is well approximated by one third of the proton-proton cross section.

3.2 The $\gamma^* p$ cross section

Let us use here the light-cone perturbation theory. We shall choose the photon polarisation vectors to be:

$$\begin{aligned} \varepsilon_T &= \varepsilon_\pm = \frac{1}{\sqrt{2}}(0,\ 0,\ 1,\ \pm i), \\ \varepsilon_L &= (q_+/Q,\ Q/q_+,\ 0,\ 0). \end{aligned} \tag{3.4}$$

We have basically used here the original notation proposed in [54] which was later used also in work [55]. The spectral function ρ occurring in (3.1) may be expressed in terms of the $\gamma^* \to q\bar{q}$ matrix element $\mathcal{M}$. We have $\rho \propto |\mathcal{M}|^2$ which, for transversely polarised photons becomes [55],

$$\begin{aligned} \mathcal{M}_T &= \frac{\sqrt{z(1-z)}}{\overline{Q}^2 + \kappa_T^2}\ \bar{u}_\lambda(\gamma \cdot \varepsilon_\pm)u_{\lambda'} \\ &= \frac{(\varepsilon_\pm \cdot \kappa_T)[(1-2z)\lambda \mp 1]\,\delta_{\lambda,-\lambda'} + \lambda m_q\,\delta_{\lambda\lambda'}}{\overline{Q}^2 + \kappa_T^2}. \end{aligned} \tag{3.5}$$

and $\lambda, \lambda' = \pm 1$ corresponding to $q, \bar{q}$ helicities of $\pm \frac{1}{2}$. Also we introduce

$$\overline{Q}^2 = z(1-z)Q^2 + m_q^2. \tag{3.6}$$

where z and κ_T are the quark momentum variables shown on Figure 3.1. They correspond to the fraction of momentum q_+ and the transverse momentum of the quark. In terms of these variables equations (3.1) and (3.2) become

$$\begin{aligned} \sigma_T &= \sum_q \alpha \frac{e_q^2}{4\pi^2} \sum_{\lambda=\pm 1} \int dz\, d^2\kappa_T\, (\mathcal{M}_T \mathcal{M}_T^*) N_c \frac{1}{s}\, \mathrm{Im}\, A_{q\bar{q}+p} \\ &= \sum_q \alpha \frac{e_q^2}{2\pi} \int dz\, d\kappa_T^2 \frac{[z^2 + (1-z)^2]\kappa_T^2 + m_q^2}{(\overline{Q}^2 + \kappa_T^2)^2}\, N_c\, \sigma_{q\bar{q}+p}(\kappa_T^2) \end{aligned} \tag{3.7}$$

where the number of colours $N_c = 3$, and e_q is the charge of the quark in units of e. We shall give the corresponding cross section σ_L for longitudinal polarised photons in section 3.2.1.

The dispersion relation (3.2) in M^2 has become, in (3.7), a two dimensional integral over z and κ_T^2. The relation between the variables is the following,

$$M^2 = \frac{\kappa_T^2 + m_q^2}{z(1-z)} \tag{3.8}$$

where m_q is the mass of the quark. For massless quarks $z = \frac{1}{2}(1 + \cos\theta)$, where θ is the angle of the outgoing quark with respect to the photon in the $q\bar{q}$ rest frame. The dz integration is implicit in (3.2) as the integration over the quark angular distribution in the spectral function ρ.

To determine $F_2(x, Q^2)$ at low Q^2 we have to evaluate the contributions to σ_T coming from the various kinematic domains. First the contribution from the perturbative domain with $M^2 > Q_0^2$ and large κ_T^2, and second from the non-perturbative or long-distance domains.

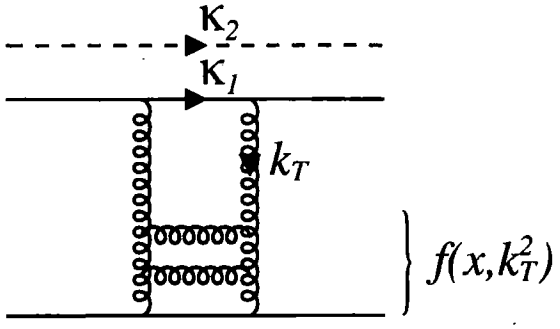

Figure 3.2: The quark-proton interaction via two gluon exchange. The spectator (anti)quark is shown by the dashed line. $f(x, k_T^2)$ is the unintegrated gluon distribution of the proton.

3.2.1 The $\gamma^* p$ in the perturbative domain

We have already used the perturbative expression for the cross section in chapter 2, see eqs. (2.58), (2.59). Expression (2.58) is written as the square of the amplitude for quark-antiquark production, where we integrate over the quark momentum κ_{1T} ($\kappa_{1T} \equiv \kappa_T$, $\kappa_{2T} \equiv k - \kappa$) in the inelastic *intermediate* state, see Fig. 3.2. The first term, proportional to $1/D_{1q}$, corresponds to the amplitude where the gluon couples to the antiquark κ_2, while in the second term, proportional to $1/D_{2q}$, the gluon couples to the quark κ_1. Of course form (2.58) can also be used to calculate the

cross section for high κ_T dijet production ($\gamma^* p \to q\bar{q}p$), where κ_{1T} and κ_{2T} refer to the transverse momenta of the *outgoing* quark jets.

To separate the perturbative and non-perturbative contributions to the cross section (3.7) for our inclusive process we have to introduce a cut on the quark transverse momentum (as well as on the $q\bar{q}$ invariant mass M). At first sight it might appear that in order to obtain the perturbative contribution we simply require $\kappa_{1T} > \kappa_0$. However this implementation of the cut-off would not be correct. For instance if, as in Fig. 3.2, the two exchanged gluons couple to the κ_1 line, then $\boldsymbol{\kappa}_{2T} = \boldsymbol{k}_T - \boldsymbol{\kappa}_{1T}$ may be small and in the limit $m_q \to 0$ and small Q^2 we would have an unphysical infrared singularity in the region of large κ_{1T} and k_T, but small κ_{2T}, coming from the $1/D_2$ term in (2.58). To see better the origin of the infrared singularities we perform the square and write the expression from (2.58) in the form

$$\left\{ \frac{[(1-z)^2+z^2]\kappa_{1T}^2 + m_q^2}{D_1^2} + \frac{[(1-z)^2+z^2](\boldsymbol{k}_T - \boldsymbol{\kappa}_{1T})^2 + m_q^2}{D_2^2} + 2\,\frac{[(1-z)^2+z^2]\boldsymbol{\kappa}_{1T}\cdot(\boldsymbol{k}_T - \boldsymbol{\kappa}_{1T}) - m_q^2}{D_1 D_2} \right\}. \tag{3.9}$$

The potential danger comes from the second term, which corresponds to Fig. 2, whereas the last term, which describes interference, is infrared stable, as we will show later. Our aim is to separate off all the infrared contributions into the non-perturbative part. Therefore to evaluate the perturbative contribution coming from the second term we have to use the cut-off $|\boldsymbol{k}_T - \boldsymbol{\kappa}_{1T}| > \kappa_0$. This is equivalent to changing the variable of integration for the second term from $\boldsymbol{\kappa}_{1T}$ to $\boldsymbol{k}_T - \boldsymbol{\kappa}_{1T}$, and so its contribution is exactly equal to that of the first term.

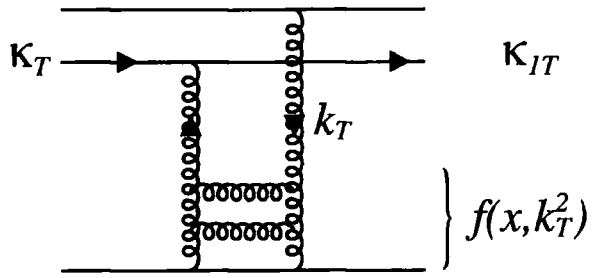

Figure 3.3: A "non-diagonal" $q\bar{q}$ – proton interaction.

An alternative way to introduce the same cut-off is to separate off the incoming $q\bar{q}$ configurations with $\kappa_T < \kappa_0$ so that (3.7) becomes

$$\sigma_T = \sum_q \frac{2\alpha e_q^2}{\pi} \int_{\kappa_0^2} d^2\kappa_T dz d^2 k_T \frac{f(x,k_T^2)}{k_T^4} \alpha_S(k_T^2)$$

$$\times \left\{ \frac{[(1-z)^2+z^2]\kappa_T^2 + m_q^2}{(\bar{Q}^2+\kappa_T^2)^2} - \frac{[(1-z)^2+z^2]\boldsymbol{\kappa}_T\cdot(\boldsymbol{\kappa}_T-\boldsymbol{k}_T)+m_q^2}{(\bar{Q}^2+\kappa_T^2)(\bar{Q}^2+(\boldsymbol{\kappa}_T-\boldsymbol{k}_T)^2)} \right\}. \tag{3.10}$$

Note that the transverse momentum $\boldsymbol{\kappa}_T$ of the incoming quark is equal to $\boldsymbol{\kappa}_{1T}$ when the gluon couples to the antiquark (first term in (3.9)) and is equal to $\boldsymbol{\kappa}_{1T}-\boldsymbol{k}_T$ when the gluon couples to the quark (second term in (3.9)). Working in terms of the variable $\boldsymbol{\kappa}_T$ corresponding to the dispersion cut shown in Fig. 3.1 has the advantage that it is then easy to introduce cut-offs with respect to the invariant $q\bar{q}$ masses M and M', which we need to impose in order to separate off the non-perturbative VDM contribution[1].

Another argument in the favour of the cut written in terms of initial quark momenta κ_T comes from the impact parameter representation. Instead of κ_T we may use the transverse coordinate b and write the cross section (3.10) in the form

$$\sigma_T \propto \int dz d^2b |\Psi_\gamma(b)|^2 \tilde{f}(x,b)\alpha_S(b) \tag{3.11}$$

where the gluon distribution

$$\tilde{f}(x,b) = \int \frac{d^2k_T}{(2\pi)^2}[1-e^{i\boldsymbol{k}_T\cdot\boldsymbol{b}}]\frac{f(x,k_T^2)}{k_T^4}. \tag{3.12}$$

The photon "wave function" is given by [56]

$$|\Psi_\gamma(b)|^2 = \sum_q \alpha e_q^2[z^2+(1-z)^2]\bar{Q}^2K_1^2(\bar{Q}b), \tag{3.13}$$

where for simplicity we have set $m_q=0$. The photon wave function is simply the Fourier transform of the matrix element $\mathcal{M}$ given by (3.10). It is most natural to take the infrared cut-off in coordinate space, say $b<b_0$. The variable which is the Fourier conjugate of b is the *incoming* quark momentum κ_T of Fig. 3.1 (rather than the *intermediate* transverse momentum κ_{1T} of Fig. 3.2). This is further justification for imposing the infrared cut in the form $\kappa_T>\kappa_0$.

Now let us consider the interference contribution, that is the last term in (3.9). It is infrared stable since in the limit $m_q^2\to 0$ and $Q^2\to 0$ it takes the form

$$\int \frac{d^2\kappa_T \boldsymbol{\kappa}_T\cdot(\boldsymbol{\kappa}_T-\boldsymbol{k}_T)}{\kappa_T^2(\boldsymbol{\kappa}_T-\boldsymbol{k}_T)^2} \sim \int \frac{d(|\boldsymbol{\kappa}_T-\boldsymbol{k}_T|)}{\kappa_T} \tag{3.14}$$

when $|\boldsymbol{\kappa}_T-\boldsymbol{k}_T|$ is small. The asymmetric prescription (3.10) has one more advantage over the symmetric one. Namely it allows for inclusion of the non-diagonal terms of

[1]Of course the use of the Feynman rules would yield the same result, but the time-ordered or light cone approach with the incoming q and $\bar{q}$ on-shell is more convenient when we come to separate off the non-perturbative component in terms of $\kappa_T<\kappa_0$ and $M, M'<Q_0$.

different masses M,M'. To see this let us write the symmetric form, see. (2.58) and include the cuts on the invariant masses of the $q\bar{q}$ pairs:

$$\frac{\kappa_T^2}{D_1^2}\Theta(M^2-Q_0^2)+\frac{(\boldsymbol{k}_T-\boldsymbol{\kappa}_T)^2}{D_2^2}\Theta(M'^2-Q_0^2)+\frac{2\boldsymbol{\kappa}_T\cdot(\boldsymbol{k}_T-\boldsymbol{\kappa}_T)}{D_1D_2}\Theta(M^2-Q_0^2)\Theta(M'^2-Q_0^2) \tag{3.15}$$

In this case we only include high mass states for ingoing and outgoing quarks. On the other hand , using asymmetric form of (3.10) we get,

$$\begin{aligned}&\frac{\kappa_T^2}{D_1^2}\Theta(M^2-Q_0^2)+\frac{(\boldsymbol{k}_T-\boldsymbol{\kappa}_T)^2}{D_2^2}\Theta(M'^2-Q_0^2)\\ &+\frac{\boldsymbol{\kappa}_T\cdot(\boldsymbol{k}_T-\boldsymbol{\kappa}_T)}{D_1D_2}\Theta(M^2-Q_0^2)+\frac{\boldsymbol{\kappa}_T\cdot(\boldsymbol{k}_T-\boldsymbol{\kappa}_T)}{D_1D_2}\Theta(M'^2-Q_0^2)\end{aligned} \tag{3.16}$$

Here we have single θ functions accompanying the interference terms and hence we also include the non-diagonal contributions where one mass is large and the other small. There is no double counting because the VDM and AQM contributions contain only diagonal contributions. We will see later when studying numerical results that this interference between $q\bar{q}$ states of different mass has an impact on the overall fit to the data.

So far we have only calculated σ_T. In the same way we may calculate the cross section for longitudinally polarised incident photons. In this case the relation analogous to (3.7) reads

$$\sigma_L=\sum_q\frac{\alpha e_q^2}{2\pi}\int dzd\kappa_T^2\,\frac{4Q^2\,z^2(1-z)^2N_c}{(\overline{Q}^2+\kappa_T^2)^2}\,\sigma_{q\bar{q}+p}(\kappa_T^2), \tag{3.17}$$

which on evaluating $\sigma_{q\bar{q}+p}$ explicitly using matrix element with longitudinally polarized virtual photon γ, gives

$$\begin{aligned}\sigma_L=&\sum_q\frac{2\alpha e_q^2}{\pi}\,Q^2\int_{\kappa_0^2}d^2\kappa_Tdz\,d^2k_T\,\frac{f(x,k_T^2)}{k_T^4}\,\alpha_S(k_T^2)4z^2(1-z)^2\,\times\\ &\left\{\frac{1}{(\bar{Q}^2+\kappa_T^2)^2}-\frac{1}{(\bar{Q}^2+\kappa_T^2)(\bar{Q}^2+(\boldsymbol{\kappa}_T-\boldsymbol{k}_T)^2)}\right\}.\end{aligned} \tag{3.18}$$

We have now ready formulae for the perturbative part. We use them, eq.(3.10) and (3.18) only in strictly perturbative domain that is when $M^2>Q_0^2$ and $\kappa_T^2>\kappa_0^2$. We also introduce the cutoff on the transverse momentum of the gluon k_T^2 as before, see (2.29). We are only going to solve this equation in the perturbative domain of the gluon transeverse momenta.

3.2.2 The γ^*p cross section in the non-perturbative domain

There are two different non-perturbative contributions. First for $M^2<Q_0^2$ we use the conventional vector meson dominance formula (3.3) for $F_2(x,Q^2)$. We also should

include the longitudinal structure function $F_L(x,Q^2)$. F_L is given by a formula just like (3.3) but with the introduction of an extra factor $\xi Q^2/M_V^2$ on the right-hand side. $\xi(Q^2)$ is a phenomenological function which should decrease with increasing Q^2. The data for ρ production indicate that $\xi(m_\rho^2) \lesssim 0.7$ [53], whereas at large Q^2 the usual properties of deep inelastic scattering predict that

$$\frac{F_L}{F_T} \sim \frac{4\kappa_T^2}{Q^2} \lesssim \frac{M_V^2}{Q^2}. \tag{3.19}$$

So throughout the whole Q^2 region the contribution of F_L is less than that of F_T. In order to calculate F_L (VDM) we insert the factor $\xi Q^2/M_V^2$ in (3.3) and use an interpolating formula for ξ:

$$\xi = \xi_0 \left(\frac{M_V^2}{M_V^2+Q^2}\right)^2 \tag{3.20}$$

with $\xi_0 = 0.7$, which accommodates both the ρ meson results and the deep inelastic expectations of (3.19). However the recent ρ electroproduction, $\gamma^* p \to \rho p$, measurements [57] indicate that $\sigma_L(\rho)/\sigma_T(\rho)$ may tend to a constant value for large Q^2. We therefore also show the effect of calculating F_L (VDM) from (3.3) using

$$\xi = \xi_0 \left(\frac{M_V^2}{M_V^2+Q^2}\right), \tag{3.21}$$

see Fig. 3.9 in the section with disscusion.

The second non-perturbative contribution covers the low κ_T part of the $M^2 > Q_0^2$ domain, that is the region with $\kappa_T^2 < \kappa_0^2$. Here we use the additive quark model and the impulse approximation to evaluate the $\sigma_{q\bar{q}+p}$ cross sections in formulas (3.7) and (3.17).

3.3 Final formulae

For completeness we list below the formulae that we use for the non-pQCD contributions coming from the $\kappa_T < \kappa_0$ domain. When $M < Q_0$, with $Q_0^2 \simeq 1 - 1.5\text{GeV}^2$, we use the vector meson dominance model. We have

$$\sigma_T(\text{VDM}) = \pi\alpha \sum_{V=\rho,\omega,\phi} \frac{M_V^4\, \sigma_V(W^2)}{\gamma_V^2 (Q^2+M_V^2)^2} \tag{3.22}$$

$$\sigma_L(\text{VDM}) = \pi\alpha \sum_{V=\rho,\omega,\phi} \frac{Q^2 M_V^2\, \sigma_V(W^2)}{\gamma_V^2 (Q^2+M_V^2)^2}\, \xi_0 \left(\frac{M_V^2}{Q^2+M_V^2}\right)^2 \tag{3.23}$$

with $\xi_0 = 0.7$, see (3.20). For the vector meson-proton cross sections, we take

$$\begin{aligned} \sigma_\rho &= \sigma_\omega = \tfrac{1}{2}\left[\sigma(\pi^+ p) + \sigma(\pi^- p)\right] \\ \sigma_\phi &= \sigma(K^+ p) + \sigma(K^- p) - \tfrac{1}{2}\left[\sigma(\pi^+ p) + \sigma(\pi^- p)\right]. \end{aligned} \tag{3.24}$$

Finally for $M > Q_0$ (and $\kappa_T < \kappa_0$) we use the additive quark model and impulse approximation

$$\sigma_T(\text{AQM}) = \alpha \sum_q \frac{e_q^2}{2\pi} \int dz d\kappa_T^2 \frac{[z^2 + (1-z)^2]\kappa_T^2 + m_q^2}{(\tilde{Q}^2 + \kappa_T^2)^2} N_c \, \sigma_{q\bar{q}+p}(W^2) \quad (3.25)$$

$$\sigma_L(\text{AQM}) = \alpha \sum_q \frac{e_q^2}{2\pi} \int dz d\kappa_T^2 \frac{4Q^2 z^2(1-z)^2}{(\tilde{Q}^2 + \kappa_T^2)^2} N_c \, \sigma_{q\bar{q}+p}(W^2) \quad (3.26)$$

where for $\sigma_{q\bar{q}+p}$ we take, for the light quarks,

$$\sigma_{q\bar{q}+p}(W^2) = \frac{2}{3} \sigma_{p\bar{p}}(s = \tfrac{3}{2}W^2). \quad (3.27)$$

The "photon" wave function contains propagators like $1/(\overline{Q}^2 + \kappa_T^2)$ and in impact parameter b_T space it receives contributions from the whole of the b_T plane extending out to infinity. On the other hand confinement restricts the quarks to have limited separation, say $b_T = |\boldsymbol{b}_{1T} - \boldsymbol{b}_{2T}| \lesssim 1$ fm. To allow for this effect we have replaced $\overline{Q}^2$ by $\tilde{Q}^2 = \overline{Q}^2 + \mu^2$ in (3.25) and (3.26), where μ is typically the inverse pion radius. We therefore take $\mu^2 = 0.1\text{GeV}^2$. This change has no effect for $Q^2 \gg \mu^2$ but for $Q^2 \lesssim \mu^2$ it gives some suppression of the AQM contribution.

3.4 The quark mass

In the perturbative QCD domain we use the (small) current quark mass m_{curr}, while for the long distance contributions it is more natural to use the constituent quark mass M_0. To provide a smooth transition between these values (in both the AQM and perturbative QCD domains) we take the running mass obtained from a QCD-motivated model of the spontaneous chiral symmetry breaking in the instanton vacuum [58]

$$m_q^2 = M_0^2 \left(\frac{\Lambda^2}{\Lambda^2 + 2\eta^2} \right)^6 + m_{\text{curr.}}^2. \quad (3.28)$$

The parameter $\Lambda = 6^{1/3}/\rho = 1.09$ GeV, where $\rho = 1/(0.6 \text{ GeV})$ is the typical size of the instanton. η is the natural scale of the problem, that is $\eta^2 = z(1-z)Q^2 + \kappa_T^2$ or $\eta^2 = z(1-z)Q^2 + (\boldsymbol{k}_T - \boldsymbol{\kappa}_T)^2$ as appropriate. For constituent and current quark masses we take $M_0 = 0.35$ GeV and $m_{\text{curr}} = 0$ for the u and d quarks, and $M_0 = 0.5$ GeV and $m_{\text{curr}} = 0.15$ GeV for the s quarks.

In summary, the q^2 dependence of m_q^2 is obtained from the instanton vacuum model, while the normalisation is fixed by M_0^2. It is interesting to note that this approach gives a value for the quark condensate which is in reasonable agreement with the QCD sum rules originally proposed by Shifman et al.[59]. We will see from Fig. 3.10 that two very different assumptions for the q^2 dependence of the quark mass do not have a large effect on the behaviour of F_2. Indeed we tried several other forms for the q^2 dependence of m_q^2; all gave similar results to the continuous curves shown in Fig. 3.10.

Table 3.1: The values of the gluon parameters of eq. (3.29).

	κ_0^2 (GeV^2)	N	λ	β	χ^2/datapoint [423 points]
Fit A	0.2	0.97	0.16	3.6	1.09
Fit B	0.5	0.42	0.32	3.7	1.70

3.5 The description of the data for F_2 at low Q^2

We have now set up a new framework which is suitable to be used for description of the data at low values of Q^2. We have few free parameters in our fit, κ_0^2, Q_0^2 and the parameters of the input gluon distribution $xg(x,k_0^2)$. Let us remind that κ_0^2 specifes the boundary between the perturbative and non-perturbative components of QCD whereas Q_0^2 is the boundary between the VDM description and the partonic description. The results exhibit very little dependence on the parameter Q_0^2 but they seem to be very dependent on the boundary between perturbative and non-perturbative region, κ_0^2. We therefore choose $Q_0^2 = 1.5$ GeV^2 which corresponds to the inclusion of ρ, ω and ϕ resonances in the VDM contribution. Because of very time-consuming calculation we present here the results for two choices of $\kappa_0^2 = 0.2\,, 0.5$ GeV^2.

We also need to specify the input gluon distribution $xg(x,k_0^2)$ in order to perform the analogous fit as in chapter 2. However because of the cut off κ_0^2 we have chosen slightly different form of input as compared to the previous one, (2.72) namely:

$$xg(x,k_0^2) \;=\; Nx^{-\lambda}(1-x)^{\beta} \tag{3.29}$$

Note that we have included here one more parameter λ which generates a pomeron like behaviour of the structure functions. This is because when introducing a cut-off for the transverse momentum of the quarks κ_T one automatically cuts off part of evolution in x in the unintegrated gluon distribution. Therefore this lack has to be compensated in the initial gluon distribution $xg(x,k_0^2)$. As before in chapter 2, the region where $k_T \ll \kappa_T$ and $k_T < k_0$ is described using the strong ordering approximation. That is we take formulae (3.10) and (3.18) and expand in k_T^2 keeping only linear terms. As will be shown later the vanishing of these contributions as Q^2 goes to zero is crucial in obtaining good description of the data. Exact formulae are given in Appendix A.

We determine the parameters N, λ and β by fitting to the available data for F_2 with $x < 0.05$ and the values of Q^2 extending down to $Q^2 = 0.1$ GeV^2. We present two fits corresponding to a larger perturbative QCD contribution (Fit A with $\kappa_0^2 = 0.2$ GeV^2) and a smaller pQCD component (Fit B with $\kappa_0^2 = 0.5$ GeV^2). The values of the gluon parameters are given in Table 3.1 and the quality of the description of the F_2 data is shown in Fig.3.4. Only a selection of the data fitted are shown in Fig. 3.4. Both descriptions are in general satisfactory, but Fit A is superior

mainly due to Fit B lying below the data for $Q^2 \simeq 1$ GeV^2. This difference is better seen in Fig. 3.5 which shows the fit as a function of Q^2 for various fixed values of W energy. We see that Fit A, with the larger perturbative component is more able to accommodate the charge in slope going from high to low Q^2. It is informative to show the components of the cross section. The breakdown is shown in Figs. 3.6 and 3.7 for Fits A and B respectively for the maximum energy $W = 245$ GeV for which data are available. It appears that the low Q^2 behaviour of the pQCD component with low k_T plays the vital role.

The description of the F_2 data by Fit A is better than that obtained by Badelek and Kwiecinski [50], which is to be expected since we perform a fit to the data, albeit with a very economical parametrization. Fig. 3.5 also shows the HERA photoproduction measurements at $W = 170$ and 210 GeV. These data were not included in the fit. We see that our description overshoots the published H1 [48] and ZEUS [49] measurements, although by a smaller margin than that of ref. [50]. On the other hand our extrapolation is in excellent agreement with a subsequent analysis of ZEUS data performed in ref. [60]. We will return to the comparison with photoproduction data when we study the effects of a different choice of the quark mass.

3.6 Discussion

We have made what appears to be in principle a prediction of F_2, or rather of $\sigma_{\gamma^* p}$, over the entire Q^2 range which relies only on the form of the initial gluon distribution, see (3.29) and the parameter values of Table 3.1. However a comparison of the results of Fits A and B show that in practice the results are dependent on the choice of the boundary $\kappa_T^2 = \kappa_0^2$ between the perturbative and non-perturbative contributions, where $\pm\boldsymbol{\kappa}_T$ are the transverse momenta of the incoming q and $\bar{q}$ which result from the $\gamma^* \to q\bar{q}$ transition.

There are compelling reasons to select Fit A with $\kappa_0^2 = 0.2$ GeV^2, which has the larger perturbative QCD contribution. Fit A is not only preferred by the data, but it also yields an input gluon with a more reasonable small x behaviour. In fact for Fit A ($\kappa_0^2 = 0.2$ GeV^2) the AQM contribution is almost negligible and the fit produces a reasonable λ, namely $\lambda = 0.16$. On the other hand Fit B (with $\kappa_0^2 = 0.5$ GeV^2) requires a larger λ, $\lambda = 0.32$, in order to compensate for the much more flat $x^{-0.08}$ behaviour of the rather large AQM component. Further support for Fit A comes from the predictions for the longitudinal structure function, F_L. Fig. 3.8 shows that the prediction from Fit B is much larger than that of Fit A due mainly to the large AQM contribution. Fig. 3.8 also shows the expectations for F_L from the analysis of ref. [43] and from the MRST partons [61] of the most recent global parton analysis. We see these independent determinations of F_L favour the prediction of Fit A.

For completeness we show by the dashed curve in Fig. 3.9 the predictions of σ_L/σ_T versus Q^2 obtained from Fit A. This figure also shows the effect of replacing (3.20) by (3.21) in the formula for the VDM contribution to F_L. Recall that (3.21)

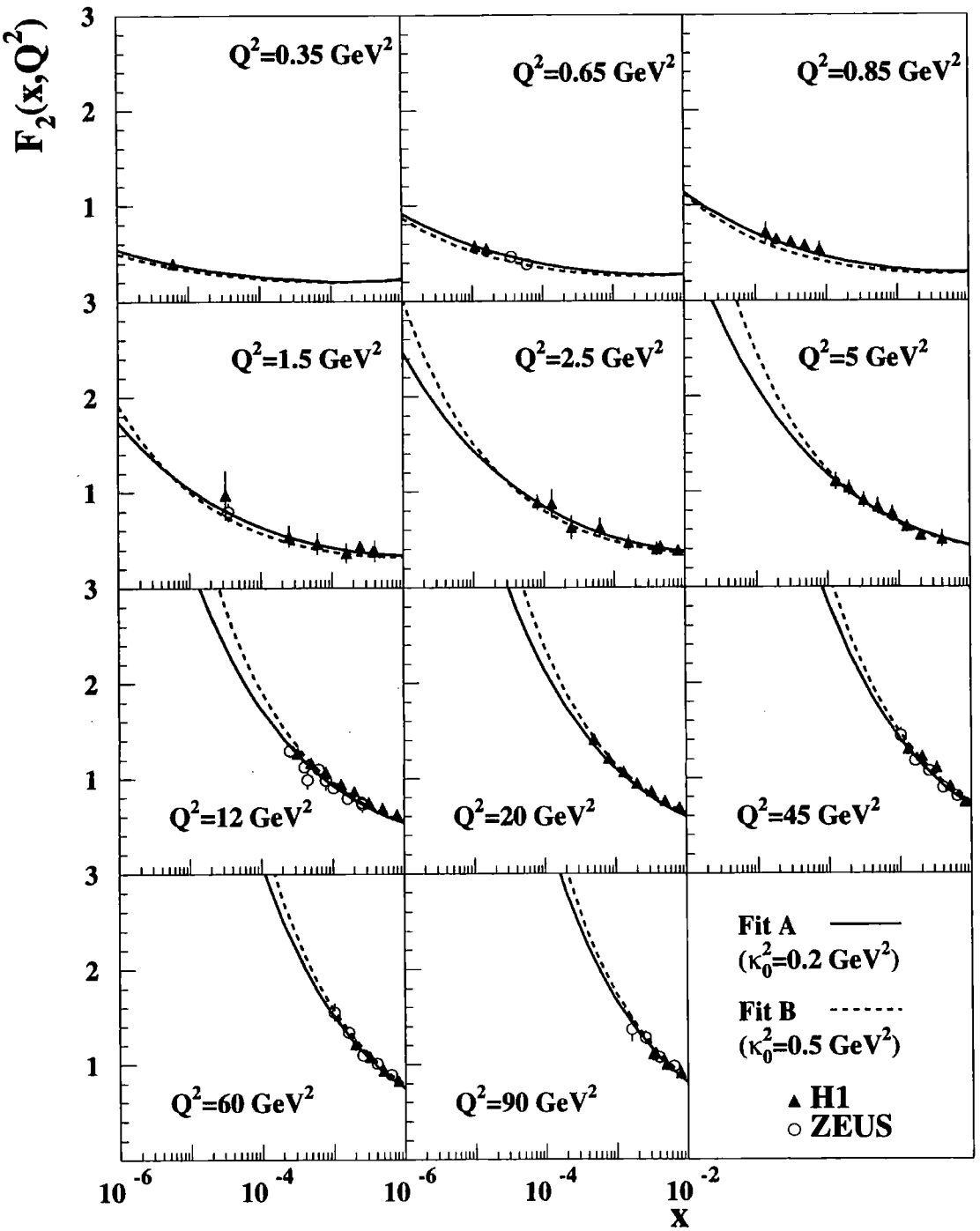

Figure 3.4: The description of the F_2 data obtained in Fits A and B. Only a subset of the data fitted is shown.

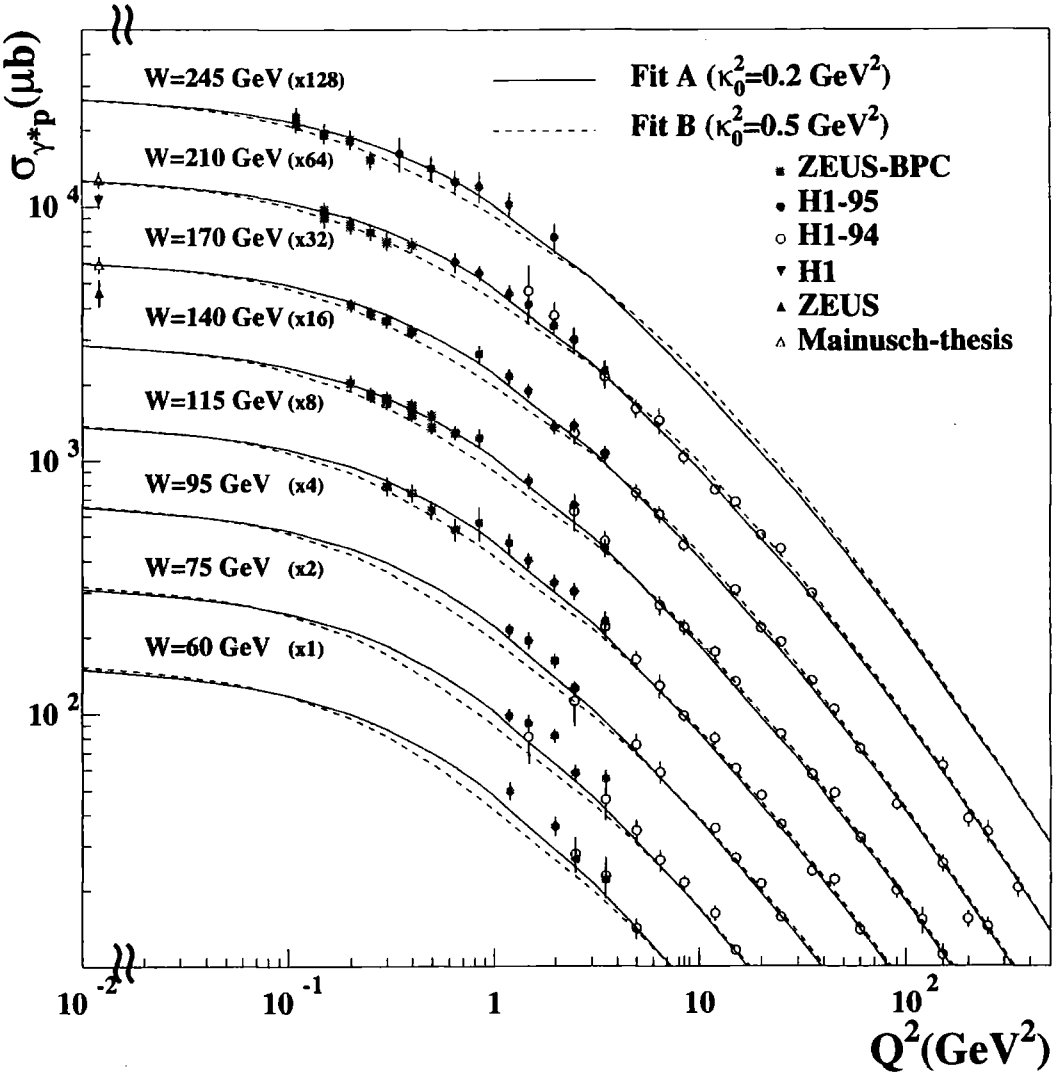

Figure 3.5: The curves are the values of the virtual photon-proton cross section $\sigma_{\gamma^* p}$ of (3.7) as a function of Q^2 for various values of the energy $W = \sqrt{s}$ corresponding to Fits A and B (multiplied by the factor shown in brackets). The data [2] are assigned to the value of W which is closest to the experimental W bin. The upper, lower photoproduction (solid triangular) data points correspond to W = 210, 170 GeV and are from the H1 [48] and ZEUS [49] collaborations respectively. The open triangular points are obtained from an analysis of ZEUS photoproduction data reported in a thesis by Mainusch [60].

was motivated by the possibility that the ratio $\sigma_L(\rho)/\sigma_T(\rho)$ for ρ meson electroproduction tends to a constant value A as $Q^2 \to \infty$. We see from Fig. 3.9 that this change to the VDM contribution affects F_L, and hence σ_L/σ_T, mainly in the interval $0.2 < Q^2 < 10$ GeV^2. It is straightforward to deduce from Fig. 3.9 the effect of changing the value of the parameter ξ_0 of (3.21) to match the constant limit A

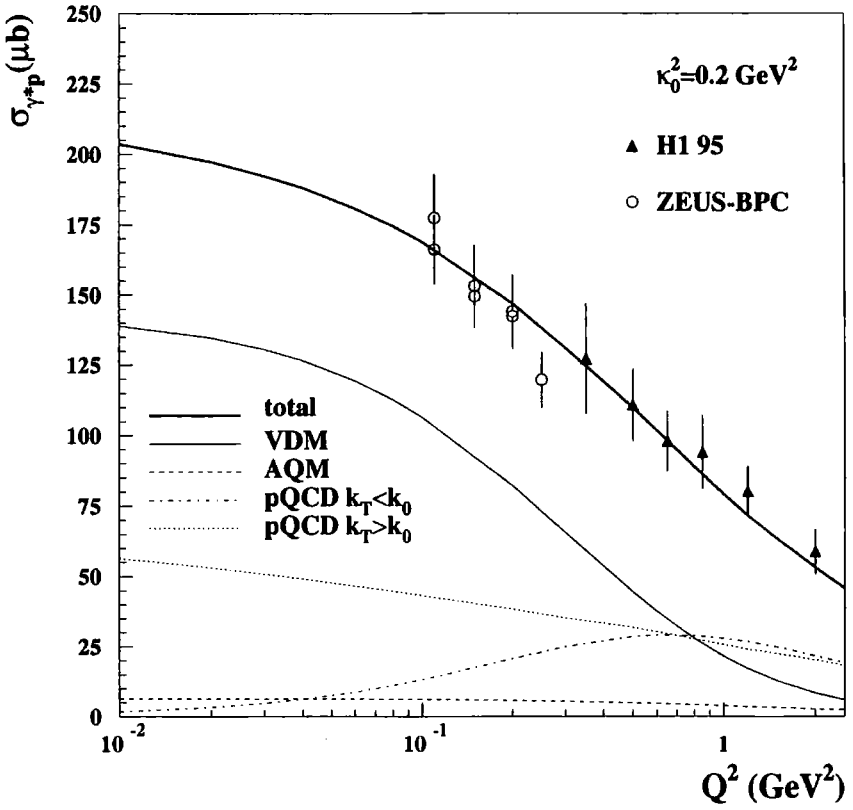

Figure 3.6: The various components of $\sigma_{\gamma^* p}$ (as defined in Section 2.3) shown as a function of Q^2 at $W = 245$ GeV for Fit A (with $\kappa_0^2 = 0.2$ GeV^2). The bold curve shows their sum, $\sigma_{\gamma^* p}$, compared to the HERA measurements.

observed for the ρ ratio.

A remarkable feature of the recent measurements [2] of $\sigma(\gamma^* p) = (4\pi^2\alpha/Q^2)F_2(x, Q^2)$ at fixed W, is the transition from a flat behaviour in the low Q^2 domain to the steep $\sim Q^{-2}$ fall off characteristic of perturbative QCD, see Fig. 3.5. The transition appears to occur at $Q^2 \sim 0.2\text{GeV}^2$. Such a break with decreasing Q^2 may reflect either the saturation due to the onset of absorption corrections or the fact that we are entering the confinement domain. The observed features of the data favour the last possibility, which we allow for through the parameter μ which we introduce below (3.25) and (3.26).

First there is no similar break in the behaviour of F_2 as a function of x at low x which would be expected if absorptive corrections were important. A related observation is that the break, as a function of Q^2, appears to occur at the same value $Q^2 \sim 0.2\text{GeV}^2$ for those W values for which data are available. Moreover we directly estimated the effect of the absorptive corrections in the perturbative QCD component[2] using the eikonal rescattering model and found that they give a

[2]In our approach the main effect of screening is hidden by the fact that we effectively take an

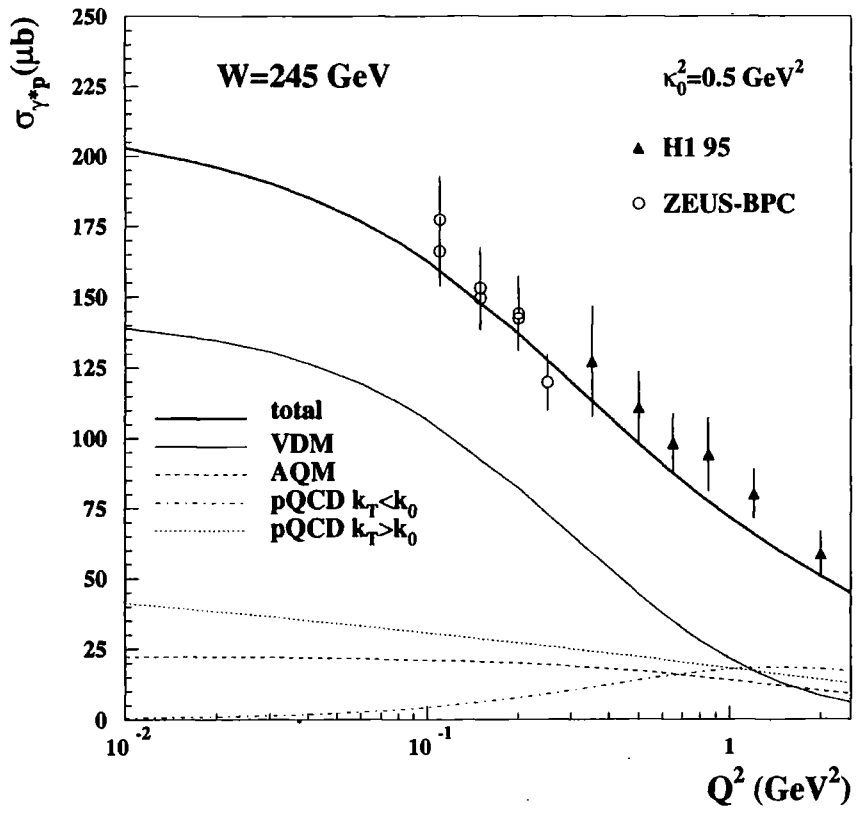

Figure 3.7: The same as Fig. 3.6 but for Fit B (with $\kappa_0^2 = 0.5$ GeV^2). The poorer description of the data in the region $Q^2 \sim 1$ GeV^2, as compared to Fit A, is clearly apparent and can be attributed to the smaller perturbative QCD component at low gluon k_T.

negligibly small effect on the Q^2 behaviour of the cross section and of F_2. On the other hand, if the break is due to confinement then it is expected to occur at a value of $\overline{Q}^2$ which corresponds to the distances of the order of 1 fm, that is

$$z(1-z)\,Q^2 \;\sim\; Q^2/5 \;\sim\; (0.2\text{GeV})^2 \tag{3.30}$$

which gives $Q^2 \sim 0.2\text{GeV}^2$ where the break is observed.

In our calculations we have used a running quark mass which links the current (m_{curr}) to the constituent (M_0) mass. The growth of m_q in the transition region from perturbative QCD to the large distance domain is an important non-perturbative effect, which we find is required by the F_2 data. From the theoretical point of view such a behaviour of m_q may be generated by the spontaneous breakdown of chiral symmetry in the instanton QCD vacuum [58]. The qualitative features are that $m_q \sim M_0$ if the virtuality q^2 of the quark is less or of the order of the

$x^{-0.08}$ behaviour of the "soft" (VDM + AQM) contribution.

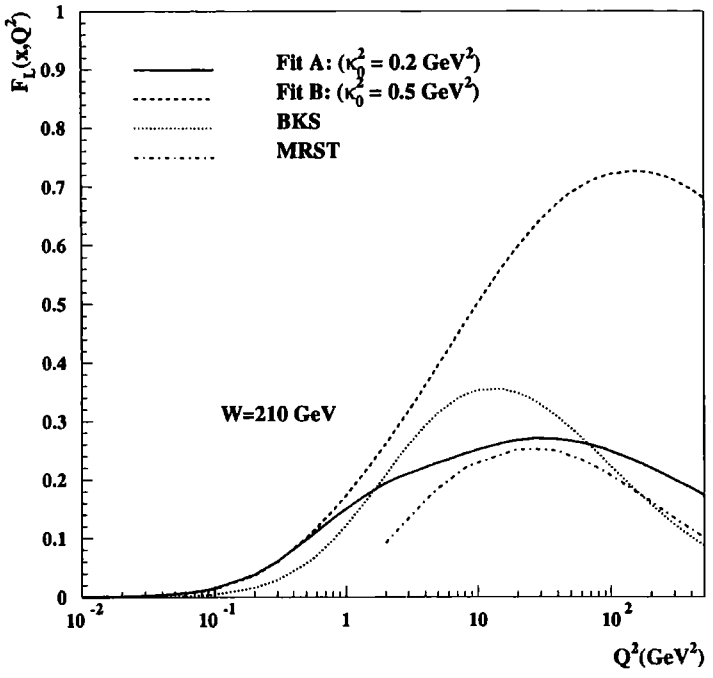

Figure 3.8: The predictions for F_L versus Q^2 at $W = 210$ GeV from Fits A, B (with $\kappa_0^2 = 0.2$ and 0.5 GeV^2 respectively), together with the values obtained by Badelek, Kwiecinski and Stasto [43] and from the MRST set of partons [61].

square of the inverse of the instanton size, but that m_q decreases quickly as q^2 increases. In our analysis we have used a simplified power approximation for m_q, see (3.28). It is interesting to explore the effect of a different choice of quark mass. The dashed curves in Fig. 3.10 show the effect of using the constituent (fixed) mass M_0 of the quarks in all the contributions to F_2 or $\sigma(\gamma^* p)$. As expected in the large $Q^2 \gg M_0^2$ perturbative domain the change has little effect. For small Q^2 it reduces the predictions. The reason why the two predictions are so different is that even for low values of Q^2 the scale η^2 which enters the formula (3.28), can be still large (note that we require $\kappa_T^2 > \kappa_0^2$). Therefore we get quite a small value for m_q as compared to the constituent quark mass M_0. The photoproduction estimates for $W \sim 200$ GeV are reduced by more than 10% and would bring our analysis more into line with the published H1 and ZEUS photoproduction measurements. However our running quark mass predictions (continuous curves) are more physically motivated and should be more reliable. It will be interesting to see if their agreement with the experimental values extracted in ref. [60] is maintained when the new photoproduction measurements are available from the HERA experiments.

A noteworthy point of our description of the F_2 data is the importance of the non-diagonal ($M \neq M'$) perturbative QCD contribution to the double dispersion relation (3.1). The contribution, which comes from the interference terms in (3.10) (and (3.18)), corresponds to the diagram shown in Fig. 3.3. It clearly has a negative

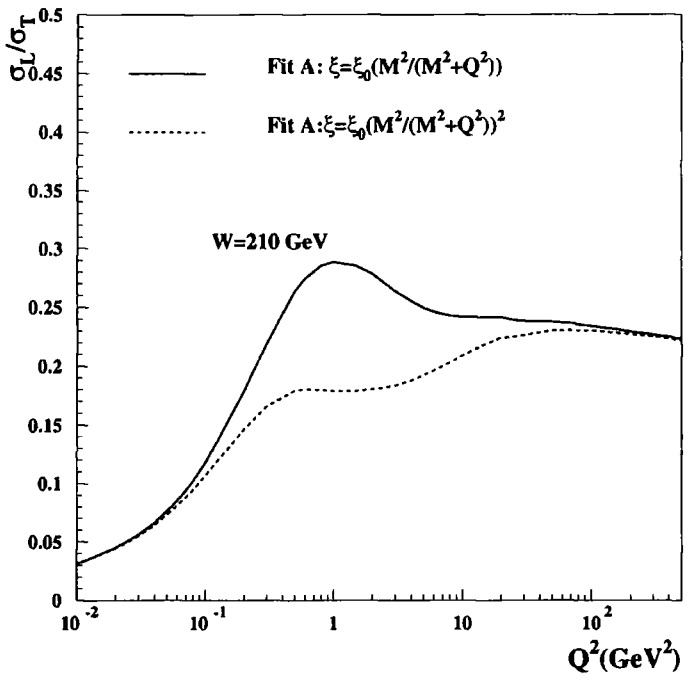

Figure 3.9: The dashed curve is the prediction for σ_L/σ_T versus Q^2 at $W = 210$ GeV from Fit A. For comparison the continuous curve is the prediction obtained using a different choice of the VDM contribution to F_L; namely using (3.21) in the place of (3.20).

sign, and moreover

$$\left\{M^2 = \frac{\kappa_T^2 + m_q^2}{z(1-z)}\right\} \neq \left\{M'^2 = \frac{(\boldsymbol{\kappa}_T + \boldsymbol{k}_T)^2 + m_q^2}{z(1-z)}\right\}. \tag{3.31}$$

After the integration over the azimuthal angle in (3.10), the interference term exactly cancels the diagonal first term for any $k_T < \kappa_T$ in the limit of $Q^2 \to 0$ and $m_q = 0$. As a result the perturbative component of the cross section coming from the region of small k_T essentially vanishes[3] as $Q^2 \to 0$. This property, seen in the $k_T < k_0$ components shown in Figs. 3.6 and 3.7, helps to reproduce the very flat Q^2 behaviour of $\sigma(\gamma^* p)$ observed at low Q^2, $Q^2 \lesssim 0.2\text{GeV}^2$. In fact we cannot achieve a satisfactory description of the F_2 data in the transition region and below without this cancellation. Thus the fact that the low k_T gluon contribution becomes very small as Q^2 decreases (and in fact vanishes for $k_T < \kappa_T$ in the $Q^2 \to 0$ limit) may be considered as a justification of the perturbative QCD contribution to F_2 for low Q^2. The VDM cross section (and other diagonal contributions as well) decrease as $1/(M_V^2 + Q^2)^2$ so we require just such a component which increases with Q^2 in order to compensate the decrease of the diagonal terms. The compensation is well illustrated by Figs. 3.6 and 3.7 which show the behaviour of the various components

[3]Of course there is also a non-negligible contribution coming from the domain $k_T > \kappa_T$ which does not vanish as $Q^2 \to 0$.

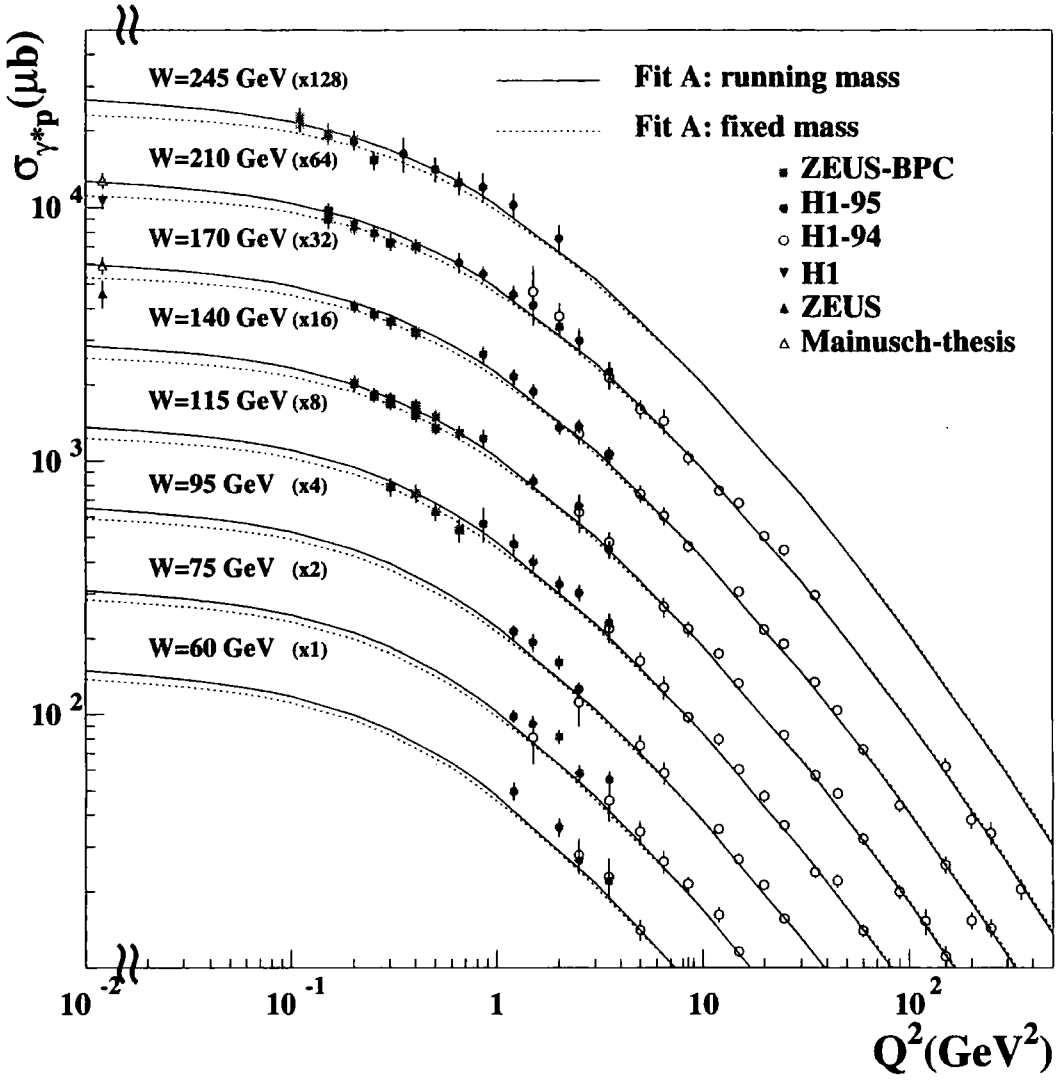

Figure 3.10: The dotted curves show the effect of using a (fixed) constituent mass, M_0, in all contributions. The running mass fit (continuous curves) and the data are those of Fig. 3.5

as a function of Q^2. Of course the compensation (that is the effect of the vanishing of the low k_T^2 contribution as $Q^2 \to 0$) is more manifest in the Fit A where a larger part of the phase space is described in terms of perturbative QCD.

It is interesting to note that in this approach we have included two different types of interference effect. First we have the dominant interference between the large M and M' states which gives rise to the decrease of the pure perturbative small k_T component of the cross section as $Q^2 \to 0$, and which is responsible for the good description of the low Q^2 data. Then there is the interference between the

perturbative and non-perturbative amplitudes which we have modelled using the perturbative formula in the region of small M' and/or small $|\boldsymbol{\kappa}_T - \boldsymbol{k}_T|$. We have noted that this contribution is small due to the infrared stability of the integral, as was shown in (3.14).

In summary we obtain an excellent description of F_2, or rather of $\sigma_{\gamma^* p}$, over the entire Q^2 range (from very low to high values of Q^2) in terms of physically motivated perturbative and non-perturbative contributions. We list some distinctive features of our approach below.

1. Our treatment of the perturbative region is state-of-the-art. We repeat, and extend, the entire numerical analysis of the previous chapter. In this way we are able to work directly in terms of the unintegrated gluon distribution, which is determined by solving coupled integro-differential equations that embody both DGLAP and BFKL evolution. These unified equations are applicable over the entire perturbative region. This is a distinct advantage over other treatments. Remarkably few parameters are required to fully specify the perturbative component.

2. We make a careful treatment of the non-perturbative regime. We use the VDM where it is well-established and for higher masses we use reliable input. No free parameters are introduced. However the results are sensitive to the value of κ_0^2 which separates the perturbative from the non-perturbative domain.

3. We emphasize the importance of the perturbative contribution in the non-perturbative domain. In particular we find that non-diagonal ($M \neq M'$) perturbative QCD contributions play an important role. They cancel the diagonal contributions for $k_T < \kappa_T$ as Q^2 tends to zero. This novel and interesting effect turns out to be required to describe the behaviour of F_2 at low Q^2. Indeed in our physically constrained approach, with very few parameters, we are unable to describe the data in the transition region (and below) without this cancellation.

4. The choice of the boundary between the perturbative and non-perturbative domains which gives an excellent fit to the data, is also found to yield a physically sensible gluon distribution and reasonable predictions for F_L.

It is important to note that there are already many attempts to describe the low Q^2 region. The HERA data initiated many theoretical analysis of this region: [62, 63, 64, 65, 66, 67, 68, 69, 70, 71, 72, 73, 27, 75, 76, 77, 78] (for a review see [79]). These analysis concentrate on the region of small x, there are also other approaches which describe succesfully the region of large values of x [80].

Chapter 4

Dijet production as a probe of BFKL dynamics

In chapters 2 and 3 we have developed a system of unifed BFKL/DGLAP evolution equations. Using the resulting unintegrated gluon distribution $f(x, k^2)$ which is fixed by the fit to the F_2 data we are going to make a predictions for the produced dijet rate. In this way we are testing the universality of approach presented in chapter 2.

Dijet production in high energy deep inelastic electron-proton scattering can expose properties of small x behaviour in QCD, as can be seen from Fig. 4.1. In the dominant $\gamma^* g \to q\bar{q} \to$ dijet subprocess, the incoming gluon can have sizeable transverse momentum accumulated from diffusion in k_T along the gluon chain [81, 82]. The value of the transverse momentum, and hence the azimuthal decorrelation between the jets, increases with decreasing x. That is the jets are no longer back-to-back since they must balance the appreciable transverse momentum k_T of the incoming virtual gluon. The azimuthal decorrelation from the back-to-back configuration $\phi = \pi$ is therefore a measure of k_T and may be expected to be an indicator of the diffusion along the BFKL chain. Clearly to obtain a reliable measure we must avoid the infrared region $k_T \simeq 0$ (that is $\phi \simeq \pi$). However, as will be seen, we are able to make an essentially parameter-free prediction of the integrated dijet production rate (at the parton level).

The description of dijet production is based on the unfolded k_T factorization formula for structure functions [25], which exposes the unintegrated gluon distribution $f(x_g, k_T^2)$ more locally than the structure functions themselves. The calculation goes beyond the conventional (fixed order) QCD-improved parton model, which is known to underestimate the dijet rate [83].

The differential cross section for producing two jets of transverse momenta p_{1T} and p_{2T} in deep inelastic scattering is

$$\frac{d\sigma}{dx dQ^2 d\phi dp_{1T}^2 dp_{2T}^2} = \frac{4\pi\alpha^2}{xQ^2}\left[\left(1-y-\frac{y^2}{2}\right)\frac{dF_T}{d\phi dp_{1T}^2 dp_{2T}^2} + (1-y)\frac{dF_L}{d\phi dp_{1T}^2 dp_{2T}^2}\right] \tag{4.1}$$

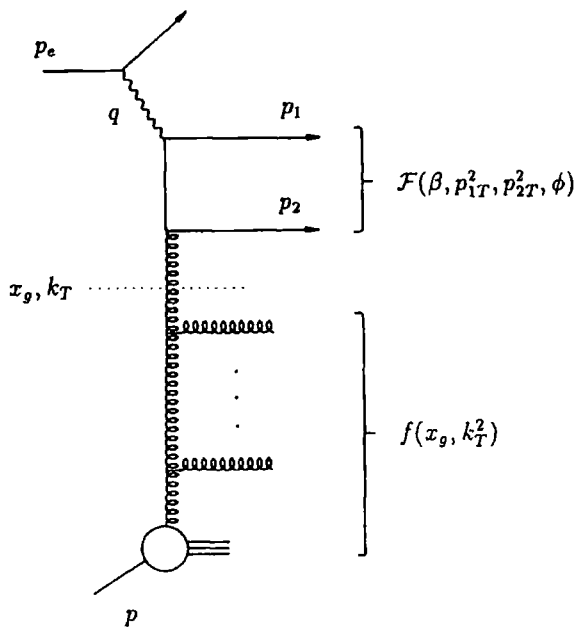

Figure 4.1: Diagrammatic representation of dijet production in deep inelastic scattering via the photon-gluon subprocess. It defines the kinematics and dynamical quantities entering the k_T factorization formula (4.4).

The differential structure functions are obtained from the k_T factorization prescription by unfolding the integrations over p_{1T}^2, p_{2T}^2 and the azimuthal angle ϕ between the q and $\bar{q}$ jets.

It is convenient to use a Sudakov decomposition of the jet four momenta

$$\begin{aligned} p_1 &= (1-\beta)q' + \alpha_1 p + \boldsymbol{p}_{1T} \\ p_2 &= \beta q' + \alpha_2 p + \boldsymbol{p}_{2T} \end{aligned} \tag{4.2}$$

where $q' = q + xp$ and p are the basic lightlike momenta. Since the jets are on-mass-shell

$$\alpha_1 = \left(\frac{p_{1T}^2 + m_q^2}{(1-\beta)Q^2}\right) x, \qquad \alpha_2 = \left(\frac{p_{2T}^2 + m_q^2}{\beta Q^2}\right) x \tag{4.3}$$

where m_q is the mass of the quark. We use again the k_T factorisation formula , see (2.1) but this time for the differential structure functions,

$$\frac{dF_i}{d\phi dp_{1T}^2 dp_{2T}^2} = \sum_q \int_0^1 d\beta\, \mathcal{F}_i^q(\beta, p_{1T}^2, p_{2T}^2, \phi, Q^2)\, \frac{f(x_g, k_T^2)}{k_T^4} \tag{4.4}$$

with $i = T, L$. The variables x_g and k_T are as before the longitudinal momentum fraction and the transverse momentum, relative to the proton, carried by the gluon which couples to the $q\bar{q}$ jet pair. They are given by

$$\begin{aligned} x_g &= x + \alpha_1 + \alpha_2 \qquad (\gtrsim [1 + 4p_{iT}^2/Q^2]x) \\ k_T^2 &= p_{1T}^2 + p_{2T}^2 + 2p_{1T}p_{2T}\cos\phi, \end{aligned} \tag{4.5}$$

see Fig. 4.1.

The functions $\mathcal{F}_i$ have been already used before in eqns. (2.58) and (2.80). For convenience we shall recall their form in jet variables p_{1T} and p_{2T}:

$$\mathcal{F}_T^q = e_q^2\alpha_S(k_T^2)\frac{Q^2}{8\pi^2}\left\{\left[\beta^2 + (1-\beta)^2\right]\left(\frac{p_{1T}^2}{D_1^2} + \frac{p_{2T}^2}{D_2^2} + \frac{2p_{1T}p_{2T}\cos\phi}{D_1 D_2}\right) + m_q^2\left(\frac{1}{D_1} - \frac{1}{D_2}\right)^2\right\} \tag{4.6}$$

$$\mathcal{F}_L^q = e_q^2\,\alpha_S(k_T^2)\,\frac{Q^4}{2\pi^2}\,\beta^2(1-\beta)^2\left(\frac{1}{D_1} - \frac{1}{D_2}\right)^2 \tag{4.7}$$

where the denominators

$$D_i = p_{iT}^2 + m_q^2 + \beta(1-\beta)Q^2. \tag{4.8}$$

As we have already pointed out the gluon $f(x, k^2)$ is taken directly from the fit to F_2 data performed in chapter 2. Formally the integration limits for β in (4.4) are 0 and 1, but they are constrained by the condition $x_g < 1$. Moreover the lower limit on k_T in the determination of the unintegrated gluon means that we cannot predict the azimuthal decorrelation between the jets in the near back-to-back domain $\phi \simeq \pi$. Our decorrelation predictions are limited to the region

$$1 + \cos\phi > k_0^2/2p_0^2 \tag{4.9}$$

where p_0 is the minimal value of the transverse momentum of an outgoing jet in the dijet system.

Predictions for the azimuthal decorrelation are shown in Fig. 4.2. They are compared with the measurements made using the ZEUS detector which so far have been presented in the thesis of Przybycien [83]. We use the parton level data obtained with the k_T jet-finding algorithm. The predictions use the same cuts as the data; that is $Q^2 > 8$ GeV^2, outgoing electron energy < 10 GeV, p_T(jet) < 4 GeV, $-2 < \eta$(lab) < 2.2 and η(HCM) > 0, where the pseudorapidities η refer to the HERA and hadron centre-of-mass frames respectively. In each x bin the data for the ϕ distribution are normalized to unity, and the predictions are normalized to the data point centred at $\phi = 2.55$ radians ($\phi = 146°$). We see that there is satisfactory agreement between the predictions and the shape of the observed ϕ distributions. It should, however, be noted that, due to the cuts, eq. (4.5) implies that $x_g \gtrsim 9x$. Thus the observed x bins do not fully expose the small x_g domain.

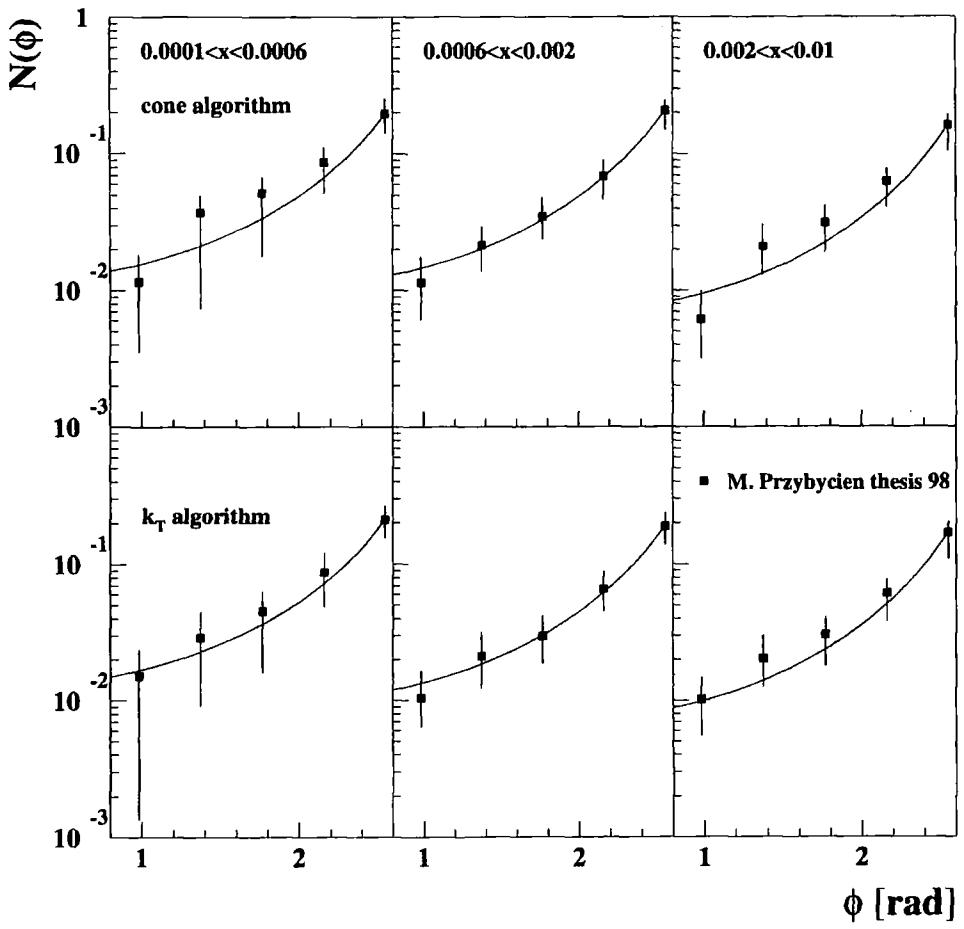

Figure 4.2: Theoretical predictions for the distribution with respect to the azimuthal angle ϕ between the q and $\bar{q}$ jets, compared to the data of ref. [83], for three different intervals of Bjorken x. The data are at the parton level and were obtained using the k_T jet-finding algorithm. The predictions are normalised to the data point at $\phi = 2.55$ radians.

Hence the broadening of the azimuthal decorrelation, although visible in the predictions, is quantitatively marginal. The x_g distribution of the data is compared with the predictions in Fig. 4.3. We see these data sample the gluon in the region $x_g \simeq 10^{-2}$. Not surprisingly, in this x_g domain the ϕ distribution does not give a definitive test of the underlying dynamics. Indeed Monte Carlos, which do not embody BFKL effects, can also describe the ϕ distribution reasonably well [83].

We emphasize that the calculation of dijet production is essentially parameter free. Moreover it applies to the full kinematic domain since it is based on an unintegrated gluon which is obtained from a unified BFKL/DGLAP approach. In this way we are able to test the predictive power of the unifed description. The parameters

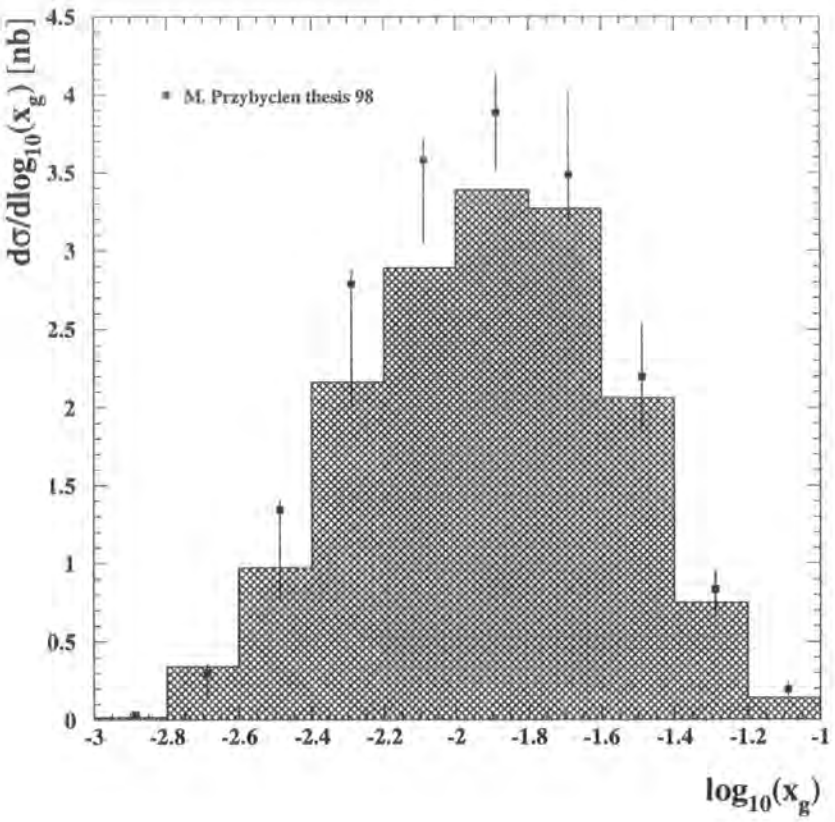

Figure 4.3: Theoretical predictions for (a) the x_g dependence,of the dijet production cross section compared to the parton-level data of ref. [83].

which enter the determination of the unintegrated gluon are completely specified by the fit to the F_2 structure function data, see Chapter 2. Thus we can make an absolute comparison with the measured cross section for dijet production. Fig. 4.4 shows the comparison as a function of Q^2. At large Q^2 there is excellent agreement. However as Q^2 decreases the prediction, with its weaker Q^2 dependence, falls below the data. The reason is that for $Q^2 \ll 4p_{iT}^2$ the denominators D_i of (4.9) are dominated by p_{iT}^2 and hence the calculated cross section depends only weakly on Q^2. There is a natural explanation of the discrepancy in Fig. 4.4. Dijets may also be produced in the photon hemisphere from the higher order contribution in which one of the jets is a gluon emitted from the quark box, that is $\gamma g \to gq(\bar{q})$ or $g\bar{q}(q)$ with a spectator $\bar{q}$ or q of small p_T. We expect a more rapid Q^2 fall-off from such a contribution.

In order to calculate the x_g and Q^2 distributions of Fig. 4.3 and Fig. 4.4 we integrate over the entire k_T^2 range of the gluon. The infrared contribution from $k_T^2 < k_0^2$ is estimated using the strong-ordering approximation $k_T^2 \ll p_T^2$ and expressing the corresponding integrals (2.58,2.59) in terms of the integrated gluon distribution

$g(x_g, k_0^2)$ at scale k_0^2 which we have taken to be exactly as in (2.72).

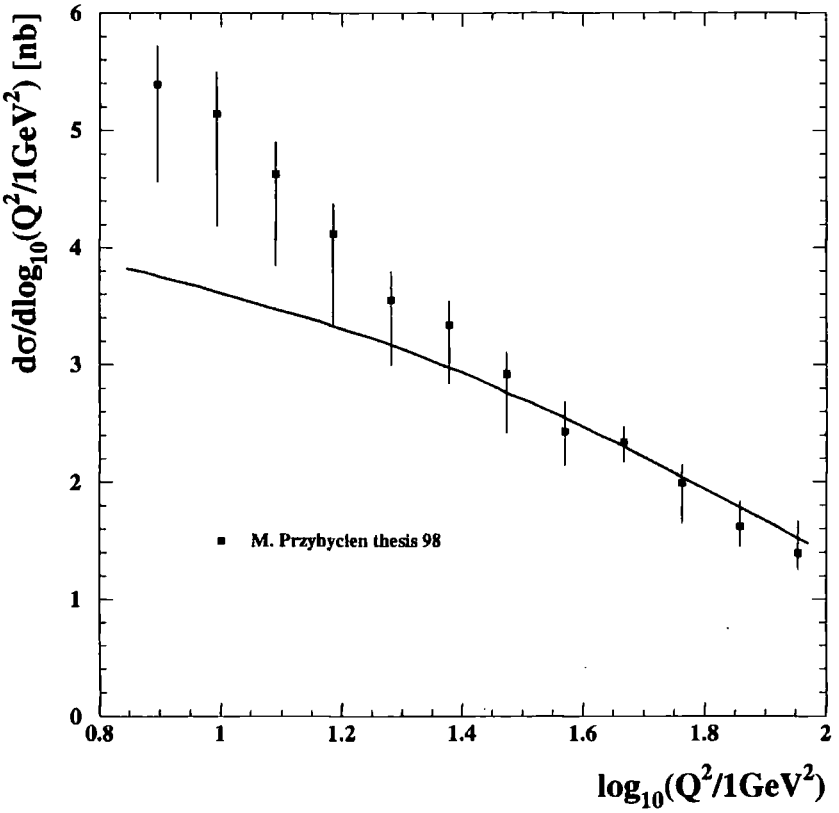

Figure 4.4: Theoretical predictions for and (b) the Q^2 dependence, of the dijet production cross section compared to the parton-level data of ref. [83].

In Table 4.1 we make the comparison of the data and the predictions of the dijet cross section for different values of the minimal p_T of the jets. The calculation reproduces 70–80% of the observed rate. To put this comparison in context, we note that the Mepjet Monte Carlo predicts a dijet cross section for $p_T(\text{jet}) > 4$ GeV of 2.8[1] or 2.6 nb according to whether GRV [13] or MRSA [11] partons were used [83]. The latter set of partons have an integrated gluon more compatible with that used for our analysis. Thus the inclusion of small x contributions are seen to enhance the cross section, although the prediction of 3.2 nb is still below the measured value of 3.9 nb.

In principle dijet production appears to offer an opportunity to study the k_T diffusion property of the BFKL gluon $f(x_g, k_T^2)$. In practice the cuts, necessary on the transverse momentum of the jets, curtail the small x_g "reach" of HERA, see

[1]This number corresponds to Mepjet 2.0 with Q as the scale. If p_T is taken to be the scale the cross section drops to 2.4 nb [83].

p_T in GeV	σ (expt) in nb	σ (theory) in nb
4	3.9	3.2
5	2.6	1.8
6	1.6	1.1
7	1.0	0.7
8	0.6	0.5

Table 4.1: The comparison of the measured [83] and theoretical integrated dijet production cross sections at the parton level for different p_T cuts on the jet transverse momenta in the hadronic centre-of-mass frame.

(4.5). Fortunately our unified BFKL/DGLAP approach is not restricted to small x_g, and gives a satisfactory description of the azimuthal decorrelations of the jets. Not surprisingly, the description is not unique and several standard Monte Carlos are known to also be able to accommodate the decorrelation data. The ϕ distribution, in the presently accessible kinematic domain, cannot therefore be regarded as a discriminator of the underlying small x dynamics. However our BFKL/DGLAP framework (with subleading $\ln(1/x)$ contributions) does give an enhancement of the dijet rate, although the prediction still falls short of the observed cross section. Moreover by comparing the predicted Q^2 dependence of the cross section with the data we are able to reveal the potential source of the remaining discrepancy.

Chapter 5

Summary and outlook

The finitude of philosophy consists not in the fact that it comes up against limits and cannot proceed further. It rather consists in this: in the singleness and simplicity of its central problematic, philosophy conceals a richness that again and again demands a renewed awakening.

- M. Heidegger

In this thesis we have presented a general method of unifying BFKL and DGLAP descriptions of deep inelastic scattering processes. Each of these approaches has different regions of applicability and is only a certain approximation. In this work we wanted to construct formalism which exhausts most of our knowledge of perturbative QCD and which yields phenomenologically acceptable results. By using BFKL and DGLAP equations for the gluon distribution we have been able to accomodate for LO terms in powers of $\ln(1/x)$ and $\ln(Q^2)$ simultaneously. The subleading $\ln(1/x)$ terms have been partially resummed by imposition of consistency constraint. Although this constraint does not reproduce the full NLL corrections it resums their major part and is quite easy to implement in the calculation. The observable structure functions are calculated using high energy factorisation formula which enables us to resum the $\ln(1/x)$ terms in the P_{qg} splitting function. The non-perturbative component is well controlled and parametrised in terms of very few parameters. We have made a fit to the available F_2 data and obtained predictions for the charm component of F_2 as well as the longitudinal structure function F_L.

This formalism has also been extended to describe the low Q^2 data. We have made clear separation of the long and short-distance contributions. For low $q\bar{q}$ states we used VDM model. For high $q\bar{q}$ states but low quark momenta we used additive quark model and the impulse approximation. We have found that the non-diagonal contribution of the perturbative component plays an important role in getting the correct description of the data. The interference term between low and high masses exactly cancels the diagonal contribution for $k_T < \kappa_T$ (where k_T is gluon momentum and κ_T is the quark momentum) as the photon virtuality Q^2 tends to zero. The vanishing of this part of the perturbative contribution helps to reproduce a rapid

flattening of the total $\sigma^{\gamma^* p}$ cross section with decreasing Q^2. We have presented the fit to the low Q^2 data for F_2 as well as the photoproduction cross section. We have also made separate predictions for the longitudinal structure function and the ratio $R = \frac{\sigma_L}{\sigma_T}$.

Using the resulting gluon distribution we have made the prediction for the cross section for produced dijets in deep inelastic scattering. We have compared our calculations with the existing preliminary data for the azimuthal distributions of the outgoing jets and also the distributions in Q^2 and in the longitudinal momentum of the gluon. The predictions are in a quite good agreement with the available data.

The framework presented here can also be used to calculate other oservables, for example the J/Ψ production. It has already been used to calculate the cross section for the ultrahigh energy neutrino interaction [84].

The future of such calculation lies in construction of such an equation which would include the full NLL kernel and the renormalisation group terms at the same time. The biggest uncertainty is to find the proper resummation scheme for the $\ln(1/x)$ terms which would lead to the stable result for the pomeron intercept. First attempts of such calculations have already been made, see [85] and they are quite successfull. They provide bounds on the pomeron intercept and are renormalisation scheme independent. The way to the complete description together with phenomenological applications is still far but we hope that this should be the right direction to follow.

Appendix A

Formulae for the strong ordering approximation

In this appendix we give the exact formulae for the perturbative contributions to the structure functions in strong ordering approximation.

First we provide with the formula for the charm quark distribution in the on-shell approximation used in chapter 2. This formula has been taken directly from [13]. We define following variables:

$$\begin{aligned} xy &= \frac{x}{y} \\ \beta &= \sqrt{1-\frac{4m_c^2}{Q^2}\frac{xy}{(1-xy)}} \end{aligned} \tag{A.1}$$

The coefficient function in the case of the massive charm quark reads:

$$\begin{aligned} S_c^{\rm box} &= \log(\frac{1+\beta}{1-\beta})(xy^2+(1-xy)^2+xy(1-3xy)\frac{4m_c^2}{Q^2}-xy^2\frac{8m_c^4}{Q^4}) + \\ &+ \beta(-1+8xy(1-xy)-xy(1-xy)4m_c^2/Q^2) \end{aligned} \tag{A.2}$$

The final formula for the quark sea reads:

$$S_c(x,Q^2) = \alpha_s \int_{ax}^1 dy\, \frac{x}{y}\, g(y,Q^2) S_c^{\rm box}(Q^2, m_c^2, xy) \tag{A.3}$$

where $a = 1 + \frac{4m_c^2}{Q^2}$ is a threshold factor.

In chapter 3 we used strong ordering approximation to evaluate the contributions when $k_T \ll \kappa_T$. The formula for σ_T reads as follows:

$$\sigma_T = \sum_q \frac{2\alpha e_q^2}{\pi} \int_{\kappa_0^2} d\kappa_T^2\, dz\, xg(x,k_0^2)\alpha_s(\kappa_T^2)\frac{\bar{Q}^2}{(\bar{Q}^2+\kappa_T^2)^4}\left\{[z^2+(1-z)^2]\kappa_T^2+m_q^2\right\} \tag{A.4}$$

and the formula for the longitudinal cross section:

$$\bar{\sigma}_L = \sum_q \frac{2\alpha e_q^2}{\pi} Q^2 \int_{\kappa_0^2} d\kappa_T^2 \, dz \, xg(x, k_0^2)\alpha_s(\kappa_T^2)\frac{\bar{Q}^2}{(\bar{Q}^2 + \kappa_T^2)^4} \tag{A.5}$$

where $\bar{Q}^2 = Q^2 z(1-z) + m_q^2$.

Appendix B

Method of solution to the unifed system

We would like to present here in more detail the method which incorporates a projection of the unifed integral equations presented in chapter 2 onto a set of linear algebraical equations. We have chosen to use the Tchebyshev orthogonal polynomials:

$$T_n(x) = \cos(n \arccos x) \tag{B.1}$$

Each polynomial $T_n(x)$ has n zeros at points,

$$x_k = \cos \frac{\pi(k-\frac{1}{2})}{n} \quad k = 1, 2, \ldots, n \tag{B.2}$$

We interpolate the two unknown functions $f(x, k^2)$ and $\Sigma(x, k^2)$ see eqns. (2.32) and (2.71), using the following prescription:

$$f(x, k^2) = \sum_{m,l=1}^{N} f(x_l, k_m^2)\, c_l(x) c_m(k^2) \tag{B.3}$$

where

$$\begin{aligned} c_m(k^2) &= \frac{2}{N} \sum_{i=1}^{N} v_i T_{i-1}(k_m^2) T_{i-1}(k^2) \\ c_l(x) &= \frac{2}{N} \sum_{i=1}^{N} v_i T_{i-1}(x_l) T_{i-1}(x) \end{aligned} \tag{B.4}$$

with coefficients $v_1 = \frac{1}{2}$, $v_i = 1$ for $i > 1$. N is the number of interpolating polynomials. Of course we have to transform the variables x and k^2 into the variables which can be used as arguments of the Tchebyshev polynomials. We choose:

$$\omega = \frac{\ln \frac{k^2}{\Lambda^2} - \frac{1}{2}(\ln \frac{Q_F^2}{\Lambda^2} + \ln \frac{k_0^2}{\Lambda^2})}{\frac{1}{2}(\ln \frac{Q_F^2}{\Lambda^2} - \ln \frac{k_0^2}{\Lambda^2})} \tag{B.5}$$

If $k^2 \in [k_0^2, Q_F^2]$ then $\omega \in [-1,1]$.

$$\psi = \frac{\ln\frac{1}{x} - \frac{1}{2}\ln\frac{1}{x_{min}}}{\frac{1}{2}\ln\frac{1}{x_{min}}} \tag{B.6}$$

Here $x \in [x_{min}, 1]$ and $\psi \in [-1,1]$. Therefore instead of (B.3) and (B.4) we should write,

$$f(\psi,\omega) = \sum_{m,l=1}^{N} f(\psi_l,\omega_m)c_l(\psi)c_m(\omega) \tag{B.7}$$

and

$$\begin{aligned} c_m(\omega) &= \frac{2}{N}\sum_{i=1}^{N} v_i T_{i-1}(\omega_m)T_{i-1}(\omega) \\ c_l(\psi) &= \frac{2}{N}\sum_{j=1}^{N} v_j T_{j-1}(\psi_l)T_{j-1}(\psi) \end{aligned} \tag{B.8}$$

Using this we are now ready to rewrite our integral equations for $f(x,k^2)$ and $\Sigma(x,k^2)$ into the algebraic equations for the vectors $f(\psi_k,\omega_l)$ and $\Sigma(\psi_k,\omega_l)$. Let us consider equation for $f(x,k^2)$ (2.32), we have then:

$$f(x,Q^2) = f^{(0)}(x,Q^2) + \int dk^2 \int dz A(x,Q^2;z,k^2)\, f(\frac{x}{z},k^2) + \int dz B(x,Q^2;z)\,\Sigma(\frac{x}{z},Q^2) \tag{B.9}$$

Functions A and B are easily deduced from equations (2.32) and (2.71). We have also included in them the information about the limits of integrations over x and k^2. Using the decomposition (B.7) and (B.9), and changing the variables (B.5) and (B.6) we get,

$$\begin{aligned} f(\psi_k,\omega_l) &= f^{(0)}(\psi_k,\omega_l) + \eta\xi \int d\psi \int d\omega \sum_{m,n=1}^{N} A(\psi_k,\omega_l;\psi,\omega) f(\psi_m,\omega_n)c_m(\psi)c_n(\omega) \\ &+ \eta \int d\psi \sum_{m}^{N} B(\psi_k,\omega_l;\psi)\Sigma(\psi_m,\omega_l)c_m(\psi) \end{aligned} \tag{B.10}$$

η and ξ are two Jacobi determinants which come from variable transformation (B.5) and (B.6). We can now define the following matrices and vectors,

$$\begin{aligned} f_{kl} &\equiv f(\psi_k,\omega_l) \\ f^{(0)}_{kl} &\equiv f^{(0)}(\psi_k,\omega_l) \\ H_{kl,mn} &\equiv \eta\xi \int d\psi \int d\omega\, A(\psi_k,\omega_l;\psi,\omega)c_m(\psi)c_n(\omega) \\ K_{kl,m} &\equiv \eta \int d\psi\, B(\psi_k,\omega_l;\psi)c_m(\psi) \end{aligned} \tag{B.11}$$

Using these definitions we get the following equation:

$$f_{kl} = f^{(0)}_{kl} + \sum_{m,n=1}^{N} H_{kl,mn} f_{mn} + \sum_{m,n=1}^{N} K_{kl,mn}\Sigma_{mn}\delta_{nl} \tag{B.12}$$

Similiar equation we get for the quarks, from eq. (2.71),

$$\Sigma_{kl} = \Sigma^{(0)}_{kl} + \sum_{m,n=1}^{N} P^{(1)}_{kl,mn} f_{mn} + \sum_{m,n=1}^{N} P^{(2)}_{kl,mn} \Sigma_{mn} \tag{B.13}$$

Equations (B.12) and (B.13) form a set of algebraic linear equations for two vectors f_{kl} and Σ_{kl}. We can rewrite it in a symbolic way as a matrix equation:

$$\begin{bmatrix} f \\ \Sigma \end{bmatrix} = \begin{bmatrix} f^{(0)} \\ \Sigma^{(0)} \end{bmatrix} + \begin{bmatrix} H & K \\ P^{(1)} & P^{(2)} \end{bmatrix} \begin{bmatrix} f \\ \Sigma \end{bmatrix}$$

The dimension of this system is equal to $2N^2 \times 2N^2$ therefore a choice of N must be a compromise between accuracy and time of calculation. We have chosen to use $N = 15$.
In fact we simplify our calculations by taking out two summations outside the integrations over ψ and ω. That is,

$$\begin{aligned} H_{kl,mn} &= \eta\xi \int d\psi \int d\omega \; A(\psi_k, \omega_l; \psi, \omega) c_m(\psi) c_n(\omega) \\ &= \eta\xi \int d\psi \int d\omega \; A(\psi_k, \omega_l; \psi, \omega) \sum_{i=1}^{N} \frac{2}{N} v_i T_{i-1}(\psi_m) T_{i-1}(\psi) \sum_{j=1}^{N} \frac{2}{N} v_j T_{j-1}(\omega_n) T_{j-1}(\omega) \\ &= \sum_{i,j=1}^{N} \frac{4}{N^2} v_i v_j T_{i-1}(\psi_m) T_{j-1}(\omega_n) \; \eta\xi \int d\psi \int d\omega A(\psi_k, \omega_l; \psi, \omega) T_{i-1}(\psi) T_{j-1}(\omega) \\ &= \sum_{i,j=1}^{N} \frac{4}{N^2} v_i v_j T_{i-1}(\psi_m) T_{j-1}(\omega_n) G_{kl,ij} \end{aligned} \tag{B.14}$$

where

$$G_{kl,ij} = \eta\xi \int d\psi \int d\omega \; A(\psi_k, \omega_l; \psi, \omega) T_{i-1}(\psi) T_{j-1}(\omega) \tag{B.15}$$

We therefore first perform integration over ψ and ω and get matrix $G_{kl,ij}$ and then do summation over indices i and j to get final matrix $H_{kl,mn}$. Of course the same procdure we utilise for matrices $K, P^{(1)}$ and $P^{(2)}$.

Bibliography

[1] R. G. Roberts, *The structure of the proton: Deep inelastic scattering*, Cambridge University Press, Cambridge, 1990.

[2] H1 Collab., S. Aid et al., *Nucl. Phys.* **B470** (1996) 3;
H1 collab. C. Adloff et al., *Nucl. Phys.* **B497** (1997) 3;
ZEUS Collab. J. Breitweg et al., *Phys. Lett.* **B407** (1997) 432.
ZEUS Collab., M. Derrick et al., *Z. Phys.* **C69** (1996) 607; *Z. Phys.* **C72** (1996) 399.

[3] V.N. Gribov and L.N. Lipatov, *Sov. J. Nucl. Phys.* **15** (1972) 438;
Yu.L. Dokshitzer, *Sov. Phys. JETP* **46** (1977) 641;
G. Altarelli and G. Parisi, *Nucl. Phys.* **B126** (1977) 298.

[4] E.A. Kuraev, L.N. Lipatov and V.S. Fadin, *Sh. Eksp. Teor. Fiz.* **72** (1977) 373, (*Sov. Phys. JETP* **45** (1977) 199); Ya. Ya. Balitzkij and L.N. Lipatov, *Yad. Fiz.* **28** (1978) 1597 (*Sov. J. Nucl. Phys.* **28** (1978) 822), J.B. Bronzan and R.L. Sugar, *Phys. Rev.* **D17** (1978) 585; T. Jaroszewicz, *Acta. Phys. Polon.* **B11** (1980) 965.

[5] R.K. Ellis, W.J. Stirling and B.R. Webber, *QCD and Collider Physics*, Cambridge University Press, Cambridge, 1996.

[6] F. Halzen and A. D. Martin, *Quarks and Leptons: An introductory course in modern Particle Physics*, John Wiley and Sons, 1984.

[7] Tai-Pei Cheng and Ling-Fong Li, *Gauge theory of elementary particle physics*, Oxford University Press, 1994.

[8] P.V. Landshoff, J.C. Polkinghorne, K.D. Short, *Nucl. Phys.* **B28** (1971) 225;
P.V. Landshoff and J.C. Polkinghorne, *Phys. Rep.* **5C** (1972) 1.

[9] E. Leader and E. Predazzi, *An Introduction to Gauge Theories and the "New Physics"*, Cambridge University Press, 1982.

[10] Taizo Muta, *Foundations of Quantum Chromodynamics*, World Scientific Singapore, 1987.

[11] A.D. Martin, R.G. Roberts, W.J. Stirling and R.S. Thorne, *Eur. Phys. J.* **C4** (1998) 463; A.D. Martin, R.G. Roberts, W.J. Stirling, *Phys. Lett.* **B387** (1996) 419; A.D. Martin, W.J. Stirling, R.G. Roberts, *Phys. Lett.* **B356** (1995) 89; A.D. Martin, W.J. Stirling, R.G. Roberts, *Int. J. Mod. Phys.* **A10** (1995) 2885; A.D. Martin, W.J. Stirling, R.G. Roberts, *Phys. Lett.* **B354** (1995) 155.

[12] H.L. Lai et al. (CTEQ collaboration), `hep-ph/9903282`; H.L. Lai et al. (CTEQ collaboration), *Phys. Rev.* **D55**, (1997) 1280.

[13] M. Gluck, E. Reya, A. Vogt, *Eur. Phys. J.* **C5** (1998) 461; M. Gluck, E. Reya, A. Vogt, *Z. Phys.* **C67** (1995) 433;

[14] A. Donnachie and P.V. Landshoff, *Phys. Lett.* **B296** (1992) 227; *Z. Phys.* **C61** (1994) 139.

[15] L. N. Lipatov and V. S. Fadin, *Sov. J. Nucl. Phys.* **50** (1989) 712;
V.S. Fadin, R. Fiore and M.I. Kotsky, *Phys. Lett.* **B339** (1995) 181; *Phys. Lett.* **B387** (1996) 593; *Phys. Lett.* **B389** (1996) 737;
V. S. Fadin and L. N. Lipatov, *Nucl. Phys.* **B406** (1993) 259; *Nucl. Phys.* **B477** (1996) 767; *Phys. Lett.* **B429** (1998) 127;
V. S. Fadin, R. Fiore and A. Quartarolo, *Phys. Rev.* **D50** (1994) 5893;
V. S. Fadin, M. I. Kotsky and L. N. Lipatov, *Phys. Lett.* **B415** (1997) 97;
V. Del Duca, *Phys. Rev.* **D54** (1996) 989; *Phys. Rev.* **D54** (1996) 4474;
V. Del Duca and C. R. Schmidt, *Phys. Rev.* **D57** (1998) 4069; *Phys. Rev.* **D59** (1999) 074004;
V. S. Fadin, R. Fiore, A. Flashi and M. I. Kotsky, *Phys. Lett.* **B422** (1998) 287;
M. Ciafaloni, *Phys. Lett.* **B429** (1998) 363;
G. Camici and M. Ciafaloni, *Phys. Lett.* **B386** (1996) 341; *Phys. Lett.* **B395** (1997) 118; *Phys. Lett.* **B412** (1997) 396, *Erratum-ibid.* **B417** 390; *Phys. Lett.* **B430** (1998) 349; *Nucl. Phys.* **B496** (1997) 305;
M. Ciafaloni and D. Colferai , *Nucl. Phys.* **B538** (1999) 187;
D. A. Ross, *Phys. Lett.* **B431** (1998) 161.

[16] G.P. Salam, *J. High Energy Phys.* **9807** (1998) 019.

[17] M. Ciafaloni, D. Colferai, *Phys. Lett.* **B452** (1999) 372;
M. Ciafaloni, G. Camici , *Phys. Lett.* **B430** (1998) 349;
M. Ciafaloni, *Phys. Lett.* **B429** (1998) 363.

[18] A.H. Mueller, *Nucl. Phys.* **B415** (1994) 373; A.H. Mueller and B. Patel, *ibid.* **B425** (1994) 471; A.H. Mueller, *ibid.* **B437** (1995) 107.

[19] N.N. Nikolaev and B.G. Zakharov, *Z. Phys.* **C49** (1991) 607; *ibid.* **C53** (1992) 331; *ibid.* **C64** (1994) 651; *JETP* **78** (1994) 598.

[20] G.P. Salam, *Nucl. Phys.* **B449** (1995) 589; G.P. Salam, *ibid.* **B461** (1996) 512; G.P. Salam, *Comput. Phys. Commun.* **105** (1997) 62; A.H. Mueller and G.P. Salam, *Nucl. Phys.* **B475** (1996) 293.

[21] A. Bialas , W. Czyz and W. Florkowski, *Eur. Phys. J.* **C2** (1998) 683;

[22] A. Bialas, R. Peschanski and C. Royon, *Phys. Rev.* **D57** (1998) 6899; A. Bialas, H. Navelet, R. Peschanski, *Phys. Lett.* **B427** (1998) 147; A. Bialas and R. Peschanski, *ibid.* **B387** (1996) 405;A. Bialas and R. Peschanski, *ibid.* **B378** (1996) 302;

[23] H. Navelet, R. Peschanski, C. Royon and S. Wallon, *Phys. Lett.* **B385** (1996) 357; H. Navelet, R. Peschanski and C. Royon, *ibid.* **B366** (1996) 329.

[24] I. Bojak and M. Ernst, *Nucl. Phys.* **B508** (1997) 731.

[25] S. Catani, M. Ciafaloni and F. Hautmann, *Phys. Lett.* **B242** (1990) 97; *Nucl. Phys.* **366** (1991) 657;
J.C. Collins and R.K. Ellis, *Nucl. Phys.* **B360** (1991) 3;
S. Catani and F. Hautmann, *Nucl. Phys.* **B427** (1994) 475;
M. Ciafaloni, *Phys. Lett.* **B356** (1995) 74.

[26] A.J. Askew, J. Kwieciński, A.D. Martin and P.J. Sutton, *Phys. Rev.* **D47** (1993) 3775.

[27] J. Kwieciński and A.D. Martin, *Phys. Lett.* **B353** (1995) 123.

[28] *Handbook of Mathematical Functions*, ed. by Milton Abramowitz and Irene Stegun, Dover Publications, INC., New York.

[29] T. Jaroszewicz, *Phys. Lett.* **B116** (1982) 291.

[30] R.K. Ellis, Z. Kunszt and E.M. Levin, *Nucl. Phys.* **B420** (1994) 517; *erratum-ibid.* **B433** (1995) 498.

[31] R.K. Ellis, F. Hautmann and B.R. Webber, *Phys. Lett.* **B348** (1995) 582.

[32] R.D. Ball and S. Forte, *Phys. Lett.* **B351** (1995) 313.

[33] J.R. Forshaw, R.G. Roberts and R.S. Thorne, *Phys. Lett.* **B356** (1995) 79.

[34] J. Blümlein, S. Riemersma and A. Vogt, Proceedings of the International Workshop on Deep Inelastic Scattering and Related Phenomena (DIS 96), Rome, Italy, 15-19 Apr 1996, DIS (1996) 572.

[35] J. Kwieciński, A.D. Martin and P.J. Sutton, *Z. Phys.* **C71** (1996) 585.

[36] B. Andersson, G. Gustafson and J. Samuelsson, *Nucl.Phys.* **B467** (1996) 443, Lund preprint, LU-TP 95-13; B. Andersson, G. Gustafson, H. Kharraziha and J. Samuelsson, *Z. Phys.* **C71** (1996) 613.

[37] K. Charchula, M. Krawczyk, DESY-90-122; M. Krawczyk, *Nucl. Phys.* B (Proc. Suppl.) **18C** (1990) 64.

[38] J. Blümlein, *J. Phys.* **G19** (1993) 1623; *Nucl. Phys. B* (Proc. Suppl.) **39B,C** (1995) 22.

[39] J. Kwieciński and D. Strozik-Kotlorz, *Z. Phys.* **C48** (1990) 315.

[40] BCDMS collaboration: A.C. Benvenuti et al., *Phys. Lett.* **B223** (1989) 485; New Muon collaboration (NMC): M. Arneodo et al., *Nucl. Phys.* **B483** (1997) 3;
E665 collaboration: M.R. Adams et al., *Phys. Rev.* **D54** (1996) 3006.

[41] WA70 collaboration: M. Bonesini et al., *Z. Phys.* **C38** (1988) 371.

[42] H1 collaboration: C. Adloff et al., *Z. Phys.* **C72** (1996) 593.

[43] B. Badelek, J. Kwiecinski and A. Stasto, *Z. Phys.* **C74** (1997) 297.
A. Stasto, *Acta Phys. Polon.* **B27**, (1996) 1353.

[44] M. Ciafaloni, *Nucl. Phys.* **B296** (1988) 49; S. Catani, F. Fiorani and G. Marchesini, *Phys. Lett.* **B234** (1990) 339; *Nucl. Phys.* **B336** (1990) 18; G. Marchesini in Proceedings of the Workshop "QCD at 200 TeV", Erice, Italy, (1990) eds. L. Cifarelli and Yu. L. Dokshitzer (Plenum Press, New York, 1992); G. Marchesini, *Nucl. Phys.* **B445** (1995) 49.

[45] J. Kwieciński, A.D. Martin and P.J. Sutton, *Phys. Rev.* **D52** (1995) 1445.

[46] Yu. L. Dokshitzer et al., *Rev. Mod. Phys.* **60** (1988) 373.

[47] R.S. Thorne, RAL-96-065, `hep-ph/9701241`; *Phys. Lett.* **B392** (1997) 463; *Nucl. Phys.* **B512** (1998) 323.

[48] H1 collaboration: S. Aid et al., *Z. Phys.* **C69** (1995) 27.

[49] ZEUS collaboration: M. Derrick et al., *Z. Phys.* **C63** (1994) 408.

[50] B. Badelek and J. Kwiecinski, *Phys. Lett.* **B295** (1992) 263.

[51] V.N. Gribov, *Sov. Phys. JETP* **30** (1970) 709;
J.J. Sakurai and D. Schildknecht, *Phys. Lett.* **40B** (1972) 121;
B. Gorczyca and D. Schildknecht, *Phys. Lett.* **47B** (1973) 71.

[52] J.J. Sakurai, *Ann. Phys. (NY)* **11** (1960) 1.

[53] T.H. Bauer, R.D. Spital, D.R. Yennie and F.M. Pipkin, *Rev. Mod. Phys.* **50** (1978) 261.

[54] S. Brodsky and P. Lepage, *Phys. Rev.* **D22** (1980) 2157.

[55] E.M. Levin, A.D. Martin, M.G. Ryskin and T. Teubner, *Z. Phys.* **C74** (1997) 671.

[56] N.N. Nikolaev and B.G. Zakharov, *Z. Phys.* **C49** (1991) 607.

[57] ZEUS collaboration: contribution to the 6th International Workshop on "Deep Inelastic Scattering and QCD" (DIS98), Brussels, April 1998.

[58] V.Yu. Petrov et al., *Phys. Rev.* **D57** (1998) 4325.

[59] M. Shifman, A. Vainshtein and V. Zakharov, *Nucl. Phys.* **B147** (1979) 385,488,519.

[60] J. Mainusch, Measurement of the total photon-proton cross section at HERA energies, University of Hamburg, Ph.D. thesis (1995), DESY *F35D-95- 14.*

[61] A.D. Martin, R.G. Roberts, W.J. Stirling and R.S. Thorne, *Eur. Phys. J.* **C4** (1998) 463.

[62] D. Schildknecht and H. Spiesberger, Bielefeld preprint `BI-TP 97/25, hep-ph/9707447`;
D. Schildknecht, *Acta Phys. Pol.* **B28** (1997) 2453.

[63] G. Kerley and G. Shaw, *Phys. Rev.* **D56** (1997) 7291.

[64] K. Adel, F. Barreiro and F.J. Yndurain, *Nucl. Phys.* **B495** (1997) 221 .
K. Adel and F.J. Yndurain, FTUAM-96-44, `hep-ph/9612469`.

[65] A. Capella, A. Kaidalov, C. Merino and J. Tran Thanh Van, *Phys. Lett.* **B337** (1994) 358.

[66] H. Abramowicz, E.M. Levin, A. Levy and U. Maor, *Phys. Lett.* **B269** (1991) 465.

[67] K.J. Golec-Biernat and M. Wusthoff, *Phys. Rev.* **D59** (1999) 014017.

[68] H. Abramowicz and A. Levy, DESY preprint-97-251 (1997).

[69] E. Gotsman, E.M. Levin and U. Maor, *Eur. Phys. J.* **C5** (1998) 303.

[70] A. Rostovtsev, M. G. Ryskin, R. Engel, *Phys. Rev.* **D59** (1999) 014021.

[71] U. D'Alesio, A. Metz, H. J. Pirner,HD-TVP-98-10, `hep-ph/9811349`.

[72] P. Desgrolard, L. Jenkovszky and F. Paccanoni, Eur. Phys. J. **C7**, 263 (1999).

[73] P. Desgrolard, A. Lengyel and E. Martinov, Eur. Phys. J. **C7**, 655 (1999).

[74] A.B. Kaidalov and C. Merino, hep-ph/9806367 (1998).

[75] E. Gotsman, E. Levin, U. Maor and E. Naftali, Nucl. Phys. **B539**, 535 (1999).

[76] W. Buchmueller, T. Gehrmann and A. Hebecker, Nucl. Phys. **B537**, 477 (1999).

[77] N.N. Nikolaev, B.G. Zakharov and V.R. Zoller, JETP Lett. **66**, 138 (1997).

[78] A. Donnachie and P.V. Landshoff, Phys. Lett **B437**, 408 (1998).

[79] A.M. Cooper-Sarkar, R.C.E. Devenish and A. De Roeck, Int. J. Mod. Phys. **A13** (1998) 3385.

[80] A. Szczurek and V. Uleshchenko, hep-ph/9904288.

[81] A.J. Askew, D. Graudenz, J. Kwiecinski and A.D. Martin, *Phys. Lett.* **B338** (1994) 92.

[82] J.R. Forshaw and R.G. Roberts, *Phys. Lett.* **B335** (1994) 494.

[83] M. Przybycien, Ph.D. thesis "Two jets production in neutral current deep inelastic e^+p interactions at 300 GeV c.m.s. energy", Krakow, Dec. 1998.

[84] J. Kwiecinski, A.D. Martin, A.M. Stasto, *Phys. Rev.* **D59** (1999) 093002.

[85] M. Ciafaloni, D. Colferai, G.P. Salam, DFF-338-5-99, hep-ph/9905566.